Integrated Fluorescence Spectroscopy for FRET Analysis of Novel Ionic Strength Sensors in the Presence of a Hofmeister Series of Salts

A Thesis

SUBMITTED TO THE FACULTY OF

UNIVERSITY OF MINNESOTA

BY

Robert C. Miller

IN PARTIAL FULFILLMENT OF THE REQUIREMENTS

FOR THE DEGREE OF

MASTER OF SCIENCE

Dr. Erin D. Sheets

Dr. Ahmed Heikal

July 2019

Acknowledgements

I would like to acknowledge Dr. Arnold J. Boersma for providing the genetically encoded hetero-FRET biosensors used to pursue this project. I would also like to acknowledge the financial support provided by the University of Minnesota Duluth, the Minnesota Supercomputing Institute, the Siders Family Grant, the Department of Chemistry and Biochemistry, and the Swenson College of Science and Engineering.

I would like to express gratitude and appreciation to both Dr. Erin Sheets and Dr. Ahmed Heikal for their mentorship, patience, and kindness. You have provided me with an excellent example for how to carry out scientific research, and I hope one day to pay forward the kindness and generosity you both extended to me. I would also like to thank Dr. Jacob Wainman and Dr. Alessandro Cembran for their patience and willingness to help me throughout my graduation school experience.

I would like to thank and acknowledge previous graduate students, Hannah Leopold and Jake Schwarz. Their foundational work provided me the opportunity to explore and develop new ideas related to FRET biosensors and the biophysical characterization of protein-based systems with integrated fluorescence spectroscopy. I would also like to thank Anh Cong, whose friendship I'm extremely grateful for. I would like to thank Cody Aplin, who suffered with me through many long days in the lab and who is an amazing colleague and friend to learn alongside with. To Chris Coffman, whose passion for physical chemistry inspired my own. I would like to thank all of the great faculty, staff, and students within the Chemistry and Biochemistry Department, and lastly to my family and fiancé whose constant support was invaluable during the toughest times of graduate school.

Dedication

To Alexis, who helped me through it all.

Abstract

Living eukaryotic cells are complex, crowded, and dynamic organisms that continually respond to environmental and intracellular stimuli. In addition, these cells have heterogeneous ionic strength with compartmentalized variation of both intracellular concentrations and types of ions. The underlying mechanisms associated with ionic strength variations that trigger different biological functions and response to environmental cues remain largely unknown. Therefore, there is a need to develop a quantitative method for mapping the compartmentalized ionic strength and their temporal fluctuations within living cells. In this Thesis, we investigate a class of novel ionic strength sensors that consists of tethered mCerulean3 (a cyan fluorescent protein) and mCitrine (a yellow fluorescent protein) via a linker of varied amino acids. In these protein constructs, mCerulean3 and mCitrine act as a donor-acceptor pair undergoing fluorescence resonance energy transfer (FRET) based on both the linker amino acids and the environmental ionic strength. The energy transfer efficiency and the donor-acceptor distance of these sensors can be quantified noninvasively using integrated fluorescence methods in response to intracellular ionic strength in living eukaryotic cells. In this work, we employed time-resolved fluorescence methods to monitor the excited-state dynamics of the donor in the presence and absence of the acceptor as a function of the environmental ionic strength using potassium chloride (0–500 mM). Towards mapping out the response to of these sensors towards biologically relevant salts, we carried out time-resolved fluorescence for FRET analysis of these sensors as a function of the Hofmeister series of salts (KCl, LiCl, NaCl, NaBr, NaI, Na_2SO_4). We also used these results towards technique development for FRET analysis based on time-resolved fluorescence polarization anisotropy. Our results show that the energy transfer efficiency of these sensors is sensitive to both the linker amino acid sequence and the environmental ionic strength. These studies in a controlled environment complement previous steady-state spectroscopy analysis of these sensors in a cuvette with the advantage of the compatibility of our approach with fluorescence lifetime imaging microscopy on living cells.

Table of Contents

List of Tables

List of Figures

List of Abbreviations

AMP	Amplifier
DM	Dichroic mirror
EDTA	Ethylenediaminetetraacetic acid
F	Filter
FRET	Förster Resonance Energy Transfer
FWHM	Full width half maximum
G-factor	Geometrical factor
IPTG	Isopropyl β-D-thiogalactopyranoside
L	Lens
LB	Luria Bertani
MA	Magic angle
PBS	Phosphate-buffered saline
PMSF	Phenylmethylsulfonyl fluoride
PD	Photodiode
RhG110	Rhodamine green, hydrochloride (5(6)-CR 110, SE)
SDS-PAGE	Sodium dodecyl sulfate-polyacrylamide gel electrophoresis
TB	Terrific broth
TCSPC	Time-correlated single photon counting

List of Symbols

D_R	Rotational diffusion coefficient
E	Energy transfer efficiency of a FRET pair
G	Anisotropy geometrical factor
$I_{\parallel}$	Parallel polarized fluorescence intensity
$I_{\perp}$	Perpendicularly polarized fluorescence intensity
k_{ET}	Energy transfer rate of a FRET pair
k_{fl}	Rate of fluorescence
f_i	Fractional population
R_o	Förster distance at which energy transfer efficiency is 50%
r_o	Initial anisotropy
R_{DA}	Average donor-acceptor distance in a FRET pair
p	Polarization
V_i	Hydrodynamic volume
α_i	Fractional amplitude fraction of TCSPC decay
β_i	Fractional amplitude fraction of anisotropy decay
η	Viscosity
θ	Angle between absorbing and emitting dipoles
κ^2	Orientation parameter between donor-acceptor dipole moments
λ	Wavelength

Chapter 1

Introduction

1.1 Overview

Living eukaryotic cells are complex mixtures of various different organelles and contain heterogeneous levels of viscosity and ionic strength (1, 2). The effects of macromolecular crowding, viscosity, and ionic strength are known to play important and significant roles in biological function, such as enzymatic activity, protein folding, and energy production; however well-established explanations describing these roles are not yet known. Therefore, there is a need to develop a method for investigating these relationships and providing a means for replicating these conditions in an experimental setting. In this Thesis, a novel family of genetically encoded protein-based hetero-FRET sensors designed to be sensitive to ionic strength are investigated using a series of integrated fluorescence spectroscopy techniques.

1.2 Theoretical and experimental studies of compartmentalized and fluctuating ionic strength

It has long been known that a simplistic model of eukaryotic cells cannot accurately describe observed biological function and that the dynamic and complex intracellular conditions of these cells play a critical role in allowing for and regulating cellular responses. Due to the presence of large biomolecules such as DNA, proteins, and membranes approximately 20–30% of the total cell volume is occupied and the concentrations and localization of different salts and solutes are constantly fluctuating (3-8). The differences in macromolecular crowding, ionic strength, and the time scales under which these conditions fluctuate between cells leads to distinct morphological and physiological behaviors in eukaryotic cells but the role of these intracellular conditions is merely appreciated without a detailed understanding of the mechanism used to put forth a cellular response (3, 9). The lack of a detailed mechanistic understanding is largely caused by the complexity of the molecular systems to be studied, with commonly an unknown number of components and processes affecting the overall cellular response, as well as the conditions under which eukaryotic cells are studied. Common methods for

measuring the intracellular conditions of living cells requires the use of inorganic or physiologically toxic dyes (10) and various other methods that give rise to insight that is abstracted and complicated by the quantification of the impact of the experimental approach and measurement on the perceived final result (11, 12).

The utility and application of protein-based hetero-FRET sensors for measuring intracellular conditions of living cells in a physiologically relevant context has been previously shown by both Biemans-Oldehinkel et al. and Syeda et al. where naturally occurring protein-based ionic strength sensors were investigated and characterized (13, 14). Specifically, Biemans-Oldehinkel et al. investigated a family of proteins known as cystathionine-β-synthase domains which are present in a large number of biological organisms across a wide array of life domains yet their biological role remained largely unknown (13). In their work, they demonstrated the sensitivity and tunability of naturally occurring ionic strength sensors, in which modifying anionic residues resulted in an increased or diminished sensitivity to ionic strength (13). Syeda et al. showed the sensitivity of the LRRC8 protein family to activation by low ionic strength, representing another class of naturally occurring ionic strength protein-based biosensors (14).

1.3 The impact of differential salt concentrations in living cells

Although the profound impact of varying and dynamic levels of ionic strength in living cells has long been known, an analytical and noninvasive technique and theory for the quantitative assessment of the ionic strength in living cells is still not established. Traditional experimental approaches rely on studying proteins, membranes, and other biomolecules in dilute, well-buffered solutions that do not accurately mimic intracellular conditions. These studies give great insight into biological systems but the significance of the results in undermined by the simplistic environment in which the biomolecules are investigated (15). The inability to properly mimic the intracellular conditions of living cells may have major impacts on the understanding and assessment of the kinetic and thermodynamic stability of biomolecules, particularly in a dynamic system such as a living cell (16, 17). Thus, the use of time-resolved methods that allow for the extraction of temporal and spatial information in living cells under conditions that best mimic

physiological conditions is needed, such that other experimental studies may be more accurately and precisely designed to provide improved insight into important biological systems (11, 12).

1.4 The role of protein-based hetero-FRET sensors to precisely quantify differential intracellular conditions

Förster resonance energy transfer (FRET) is a widely used and powerful tool used to quantify and assess protein-protein interactions, binding interactions, conformational changes, and molecular distances which is why it is commonly referred to as a "molecular ruler" (18, 19). FRET is a phenomenon involving the nonradiative energy transfer of a fluorescent donor molecule in an excited electronic state to another fluorescent acceptor molecule in the ground state within close proximity (<10 nm), where the physically linked donor and acceptor molecule are considered a FRET pair (20). The extent of energy transfer from the donor to the acceptor molecule in the FRET pair is dependent on the spectral overlap between the donor's fluorescence emission and the acceptor's absorption, the distance between the donor and acceptor, the relative orientation of the donor's emission dipole and the acceptor's absorption dipole, and the refractive index of the solution (21). The upper limit of distances between the donor and acceptor molecule is approximately 10 nm which allows FRET to measure small conformational changes with nanometer resolution (21, 22).

Due to the conformation sensitivity of FRET (23), a novel family of genetically encoded protein-based hetero-FRET proteins were developed by Boersma et al., which were comprised of green fluorescent protein (GFP) mutants that can be specifically expressed in different organelles within eukaryotic cells (24). More specifically, these FRET sensors were comprised of a donor molecule (mCerulean3), a cyan fluorescent protein, and an acceptor molecule (mCitrine), a yellow fluorescent protein, tethered together with an amino acid linker consisting of two α-helices of variable sequence designed for sensitivity to ionic strength (24-26). As shown in Table 1 and Figure 1.1, the linker region contains flexible regions represented by $(GSG)_X$ and rigid helices represented by $(ZAAAX)_Y$ (12, 24), where three of the four FRET sensors investigated in

this work were designed with α-helices of opposite charge and the fourth with two neutral α-helices such that they were sensitive and insensitive to ionic strength, respectively. It was hypothesized that, due to the electrostatic attraction of the α-helical linker regions, upon increased ionic strength and electrostatic screening the donor-acceptor distance would increase leading to a decrease in the energy transfer efficiency. Therefore, changes in the energy transfer efficiency may be used to quantitatively assess changes in ionic strength.

Table 1.1: Amino acid sequence and designed expected sensitivity to ionic strength of the four hetero-FRET sensors investigated in this thesis.

Acronym	**Sequence**	**Sensitivity to Ionic Strength**
RD	–A$(AAAAR)_6$A$(GSG)_6$$(DAAAA)_6$A–	Yes
RE	–A$(AAAAR)_6$A$(GSG)_6$$(EAAAA)_6$A–	Yes
KE	–A$(AAAAK)_6$A$(GSG)_6$$(EAAAA)_6$A–	Yes
E6G2	–A$(EAAAK)_6$A$(GSG)_2$$(EAAAK)_6$A–	No

Using steady-state spectroscopy techniques, Boersma et al. (24) demonstrated the sensitivity of these ionic strength hetero-FRET probes to increased ionic strength in a variety of salt types using the qualitative FRET assessment of the intensity ratios of mCerulean3 and mCitrine (27, 28). This qualitative assessment is complicated by the spectral overlap between the donor and acceptor molecules and lacks the ability to distinguish between an increase in the energy transfer efficiency and the population of FRET pairs undergoing FRET. Furthermore, the consequences associated with the steady-state FRET assessment, such as a lack of capability with deconvoluting subpopulations undergoing and not undergoing FRET, would greatly impact the ability to perform live cell studies and evaluate fluctuations of levels of ionic strength on molecular time scale (11).

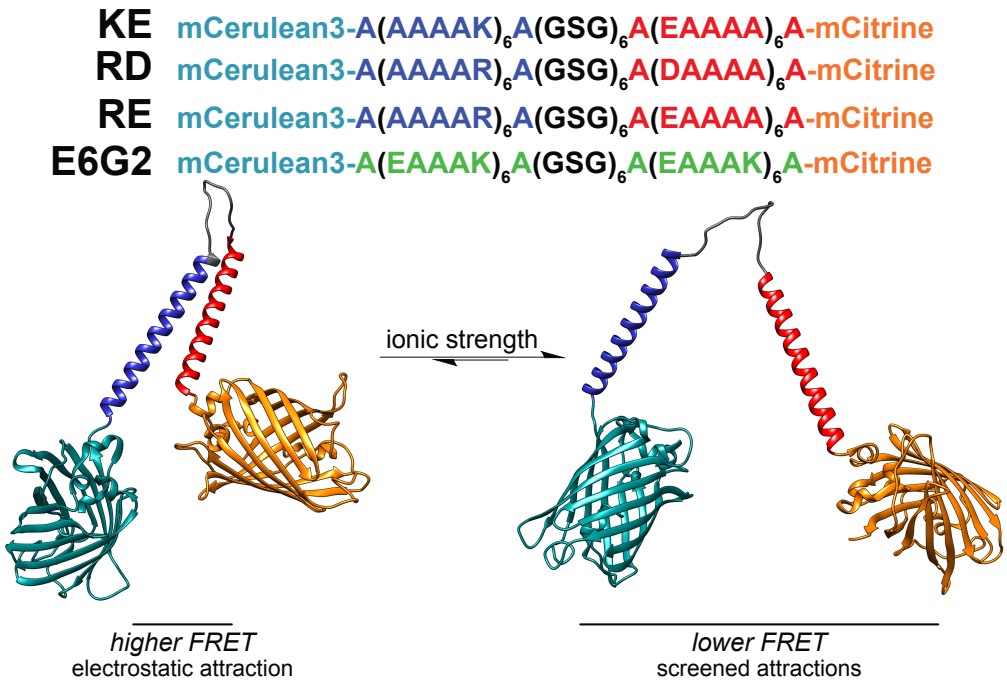

Figure 1.1: Representative structure for the four ionic strength FRET sensors investigated as well as the predicted physical impact of increase ionic strength on the FRET sensor. Importantly, this schematic is simply a representation and does not use actual crystal structures of these biosensors in the presence and absence of salt.

1.5 Quantitative, noninvasive methods for investigating in vitro levels and fluctuations of ionic strength

The analysis of FRET biosensors has been traditionally performed using steady-state spectroscopy methods, commonly using continuous-wave excitation and lacking the ability to extract any structural or temporal information (18, 29, 30). These methods have been historically relied upon due to their ease of accessibility, cost, and simplified analysis process in comparison to time-resolved techniques. Although these techniques offer excellent and fiscally available opportunities for FRET analysis, they lack the ability to probe the excited state dynamics of these fluorophores (11, 12).

More specifically, these approaches also suffer due to spectral overlap, represented by the term $J(\lambda)$, of the donor and acceptor fluorophore, determinations of the concentration of the donor and donor-acceptor pairs due to the inherent complexity and reproducibility associated with proteolytic cleavage, as well as the inherent ensemble averaging of these steady-state approaches (31). In addition, the impact of the A206K

mutation on the excited-state dynamics of both mCerulean3 (donor) and mCitrine (acceptor), particularly under the varying experimental conditions discussed in later Chapters of this Thesis, is unknown and therefore there exists a need for a more sensitive approach that provides spatial and temporal information (24, 28, 30). In this Thesis, time-correlated single photon counting (TCSPC) and time-resolved polarized fluorescence anisotropy were used to map the excited-state dynamics and FRET efficiencies of a series of biosensors which are discussed in greater detail in this Chapter as well as Chapters 3–5.

Chapter 2

Materials and Methods

2.1 Overview

This Chapter describes the purification of the FRET probes, preparation of ionic strength test samples, and the theory of time-correlated single photon counting and time-resolved polarized fluorescence anisotropy. Here, both time-correlated single photon counting (TCSPC) and time-resolved polarized fluorescence anisotropy were used for the FRET analysis of genetically encoded protein-based hetero-FRET sensors. In addition, a novel approach for FRET analysis at the single molecule level using molecular brightness as determined from fluorescence correlation spectroscopy (FCS) was rigorously assessed using a representative FRET biosensor, namely RD.

2.2 FRET probe purification

The development and purification of the genetically encoded ionic strength hetero-FRET probes RD, RE, KE, and E6G2 have been described in detail elsewhere (11, 12). Briefly, the FRET sensors (~60 kDa) are comprised of mCerulean3 (a fluorescent cyan protein donor, ~27 kDa) and mCitrine (yellow fluorescent protein acceptor, ~27 kDa) to form a hetero-FRET pair. Each fluorescent protein contained an A206K mutation to minimize self-association or aggregation (32-34). Each FRET sensor also consists of an identical linker region except for a variable amino acid in both the basic and acidic α-helical regions (Fig. 1.1) (24).

Plasmids of the five constructs in the pRSET A host vector were a generous gift from Dr. Arnold J. Boersma (24). They were transformed into the *E. coli* strain BL21(DE)pLysS (Invitrogen), and plated on LB-agar plates containing 100 μg/mL ampicillin. Successfully transformed colonies were selected and inoculated into 2 mL of LB (100 μg/mL ampicillin) and shaken overnight at 37°C. Half of the overnight culture was used to conduct an alkaline lysis mini prep and an analytical restriction digest to confirm the correct plasmid DNA. Following confirmation, a glycerol stock of the transformed *E. coli* was prepared and stored at –80°C for all future cultures.

The following approach was used to purify and isolate the four FRET sensors. A small sample of the frozen glycerol stock was inoculated into 2 mL of TB medium (1.2% bactotryptone, 2.4% yeast extract, 0.4% glycerol, 1.4% (w/v) potassium phosphate, pH 7.5) with 1 mg/mL ampicillin and shaken overnight at 37°C. One mL of overnight culture was placed into two baffled flasks containing 25 mL of TB medium each and grown at 30°C to the equivalent of OD 0.6, (0.06 as measured by a NanoDrop 2000 spectrophotometer). The cells were induced overnight with 0.1 mM isopropyl-β-D-thiogalactoside (IPTG) at 25°C. The cells were centrifuged at 5,000 rpm (Beckman J25.5, 3000 × g) for five minutes at 4°C and resuspended with 8 mL of lysis buffer (10 mM sodium phosphate, 100 mM sodium chloride, 0.1 mM phenylmethylsulfonyl fluoride [PMSF], 1 mg/mL lysozyme, pH 7.4) and incubated on ice for 30 minutes. The lysate was sonicated on ice and drawn up with an 18.5 gauge needle five times to shear DNA and other debris and incubated on ice for a minimum of one hour. The lysate was clarified at 5,000 rpm (Beckman J25.5, 3000 × g) for 15 minutes at 4°C and imidazole was added to the supernatant to a final concentration of 10 mM. A column of ProBond^{TM} nickel-chelating resin (Life Technologies) was equilibrated four times with binding buffer (10 mM sodium phosphate, 100 mM sodium chloride, 10 mM imidazole, pH 7.4). The lysate was then loaded onto the equilibrated column and rocked for one hour at room temperature. The column was washed four times with wash buffer (50 mM sodium phosphate, 300 mM sodium chloride, 20 mM imidazole, pH 8.0). The protein was eluted with 8 mL of elution buffer (50 mM sodium phosphate, 300 mM sodium chloride, 250 mM imidazole, pH 8.0). The peak fraction was dialyzed against 10 mM sodium phosphate, pH 7.4 (10 mM NaPi; pH 7.4) at 4°C using a Slide-A-Lyzer (ThermoScientific, MWCO 3.5 kDa). The purified protein was aliquoted in to 100 µL aliquots, flash frozen in liquid nitrogen, and stored at –80°C until use. After thawing an aliquot, it was stored at 4°C. The purified protein was analyzed using 12% SDS-PAGE gel and visualized using Coomassie staining (Figure 2.1). The absorption and emission spectra were determined using a Beckman Coulter DU800 spectrophotometer and a Horiba Jobin Yvon Fluorolog, respectively. In Figure 2.2 the absorption band at 280 nm (ε = 54,000 $M^{-1}cm^{-1}$) was used to calculate the concentration of the purified FRET probe

following each purification.

To disrupt FRET between the donor (mCerulean3) and the acceptor (mCitrine) as a control, the flexible linker region (GSG_X) of the FRET probe was digested using the serine protease, proteinase K. This cleavage serves as a control for energy transfer analysis between mCerulean3 and mCitrine. For this cleavage reaction, 0.56 ng of proteinase K (Sigma-Aldrich) was added per μmol of the purified probe. After 1 minute incubation at 25°C, 20 μmol of PMSF per mg of proteinase K was added to terminate the cleavage reaction. SDS-PAGE analysis was used to determine the extent of the proteolytic cleavage as compared with the control, a completely intact FRET-capable protein, for which no proteinase K was added (Figure 2.1).

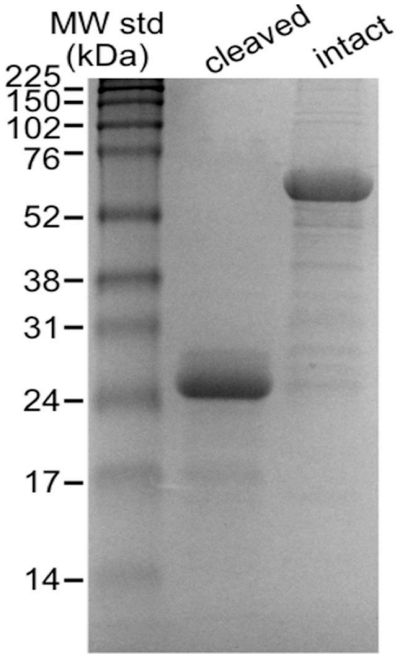

Figure 2.1: Representative SDS-PAGE image of the proteinase K enzymatic cleavage of the flexible linker in the FRET pair RD (cleaved, lane 2) with a final molecular weight of ~27 kDa (mCerulean3 and mCitrine) used for TCSPC measurements. As a control, an identical sample is tested in the absence of proteinase K and the possibility of enzymatic cleavage (intact, lane 3) with an approximate molecular weight of ~61 kDa (RD).

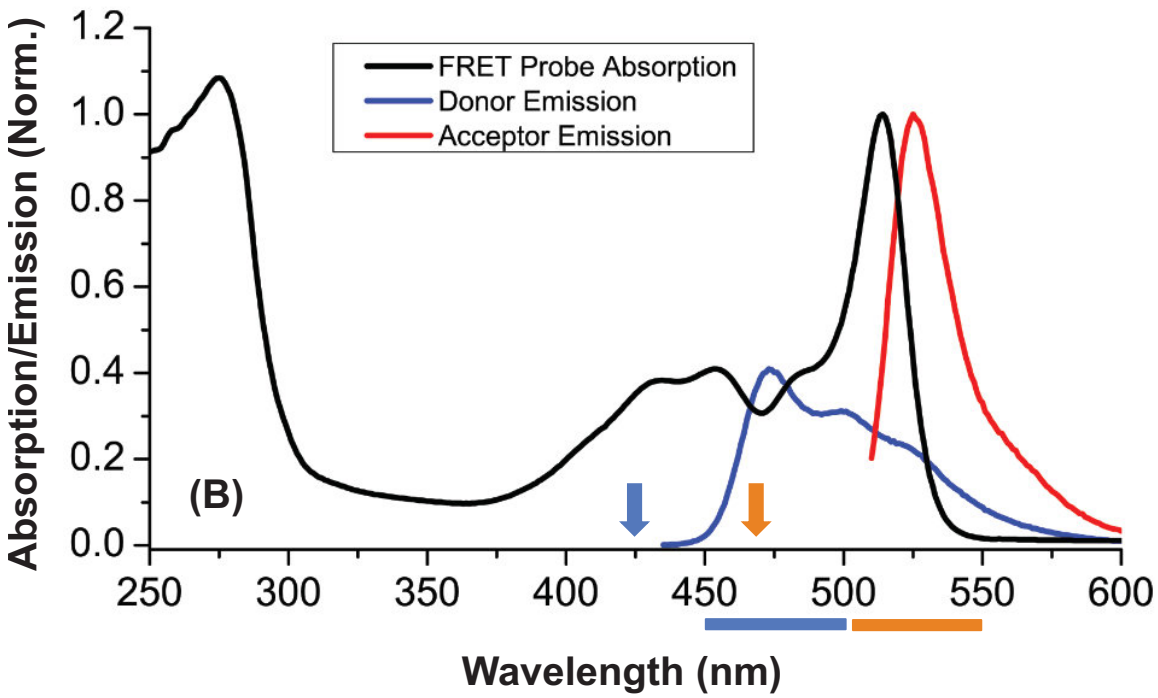

Figure 2.2: Absorption and emission spectra of GE biosensor (black curve) of both the donor (mCerulean3) (excited at 425 nm) and acceptor (mCitrine) (excited at 465 nm). The arrows indicate the excitation wavelengths used in the TCSPC fluorescence lifetime and anisotropy measurements. The horizontal lines indicate the bandwidth emissions filters for the donor (blue curve) and acceptor (red curve) fluorescent detections. The absorption and emission bands are normalized for both the donor and acceptor.

2.3 Sample Preparation

10 mM sodium phosphate , pH 7.4 solutions were used and various salts were supplemented to this buffer as indicated. To evaluate the range of sensitivities of the FRET probes, we used a common salt, potassium chloride (KCl), for the ionic strengths (0, 100, 200, 300, 400, and 500 mM) on all FRET sensors (RD, RE, KE, and E6G2). When evaluating the sensitivities to the type of salt, six salts from the Hofmeister series were selected, KCl, NaCl, LiCl, NaBr, NaI, Na_2SO_4 at the ionic strengths (0, 25, 50, 100, 200, 300 mM) (35-37). For both TCSPC and anisotropy measurements, the FRET probes were prepared to a final concentration of approximately 2 μM, adjusting the concentration for daily fluctuations in the laser and optical system (11, 12).

For all fluorescence correlation spectroscopy (FCS) samples and molecular brightness measurements the FRET probe, RD, was prepared in 10 mM NaPi, pH 7.4 at

an approximate concentration of 10 nM, adjusting the concentration for daily fluctuations in the laser and optical system.

2.4 Time-correlated single photon counting (TCSPC) for fluorescence lifetime measurements

2.4.1 Overview

Time-correlated single photon counting (TCSPC) measures the excited state dynamics of a fluorophore by generating a probability histogram of detecting a single photon per each excitation-detection cycle. These photon counts are stored into 1024 time bins with approximately 24.2 ps/bin, which are equally and uniformly binned through the acquisition time. TCSPC is an extremely sensitive technique, absent from large signal-to-noise acquisition issues, that is compatible with live cell imaging techniques such as fluorescence lifetime imaging microscopy (FLIM) (38, 39). The acute sensitivity of TCSPC allows for the monitoring of the fluorescence lifetime with picosecond-resolution for quantitative assessment of environmental and conformational effects on the excited-state dynamics of a given fluorophore (20).

For selective detection of fluorescence signals, a constant fraction discriminator is used to distinguish the signal from the background noise of the sample prior to using a time amplitude converter, where the detected photons are stored in time bins, according to their detection time. A computer generated system response function was calculated and used for deconvolution of the measured fluorescence decay to obtain the true decay. The excitation wavelength (λ_{ex}) used in all fluorescence lifetime measurements was 425 nm, generated from the second harmonic of the 850 nm IR fempto-second laser pulse generated from the titanium-sapphire laser, and the fluorescence emission (λ_{em}) was monitored at 475/50 nm (11, 12).

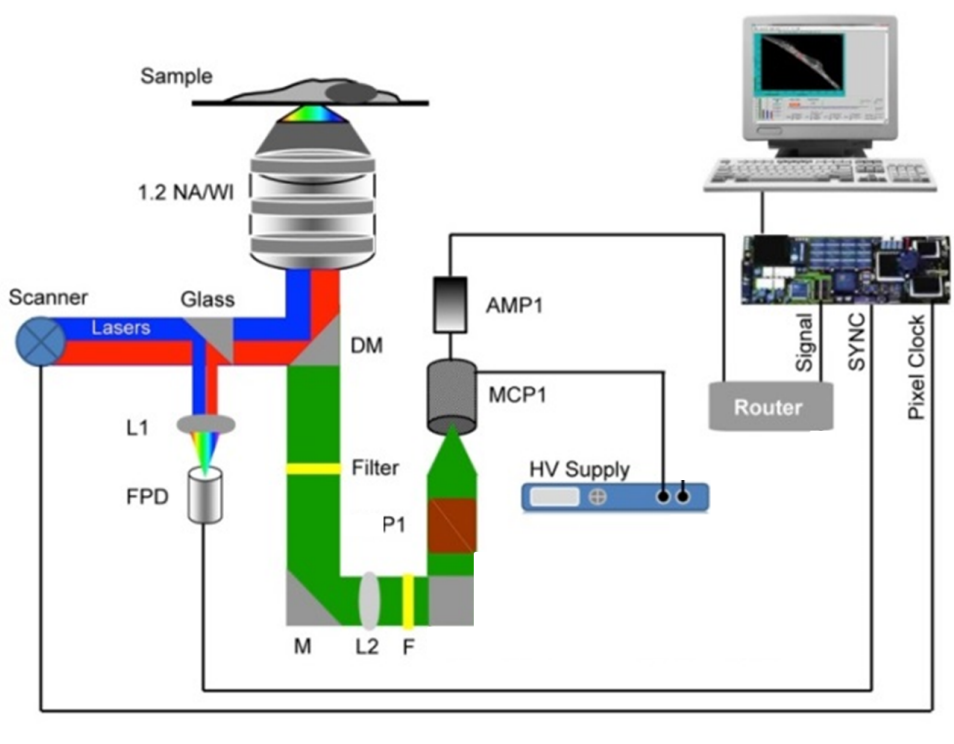

Figure 2.3: Representative diagram of the optical system used for the TCSPC technique used in this Thesis. M: mirror, L:lens, FPD: fast photodiode, NA/WI: numerical aperture/water immersion, DM: dichroic, F: Filter, P1: polarizer, MCP1: microchannel plate, AMP: amplifier.

2.4.2 Experimental setup and calibration

For fluorescence lifetime measurements using TCSPC techniques, the excitation laser pulses (425 nm, 4.2 MHz, 120 fs) were steered towards dichroic mirrors (x396rdc) prior to band pass filters 475/50 (fluorescence lifetime) and 531/40 (anisotropy) for detecting donor and acceptor emission, respectively. IR laser pulses were generated at 76 MHz, using a titanium-sapphire crystal (Mira 900-F, Coherent). A Russian blue filter was also used to prevent direct laser detection. The average power for the two-photon laser ranged between 480–800 mW, with a pump laser setting of 6.5–7 W, depending upon the laser wavelength used in the experiment. The fluorescence emission was detected using a microscope objective (1.2 NA, Olympus UPlanApo IR, water immersion, 60×), and analyzed using a magic angle (54.7°) polarizer prior to detection using a micro-channel plate photomultiplier tube (R3809U, Hamamatsu). The photon probability histograms

were then collected using SPC-830 software (Becker & Hickl). The signal-to-noise ratio and optical setup were verified using the well-characterized dye Coumarin-1 (11, 12).

2.4.3 Data analysis of fluorescence lifetime measurements

The photon probability histograms acquired using SPC-830 module was then deconvoluted using a computer generated system response function to obtain fluorescence lifetime decays. Fluorescence, F(*t*), decays were modeled using a multi-exponential function such that (11, 12):

$$F(t) = \alpha_f e^{-(t/\tau_D)} + \alpha_{FRET} e^{-t(1/\tau_D + k_{ET})} \quad (2.1)$$

The α_f term represents the fractional amplitude (or population) of molecules that do not undergo FRET (cleaved biosensor), τ_D represents the fluorescence lifetime of an intact FRET pair that do not undergo FRET, and k_{ET} represents the rate of energy transfer in the intact FRET pair. In this Thesis, all TCSPC measurements and nonlinear regression analysis was performed on a truncated data set, ~0.2–17 ns, as approximately 0-200 ps of the initial signal is solely due to the computer generated system response function.

Following the nonlinear regression analysis, the energy transfer efficiency (*E*) and corresponding donor-acceptor distance (R_{DA}) were calculated using two different methods, referenced as ensemble averaged and rate-determined energy transfer efficiencies and donor-acceptor distances (2.2 and 2.3, respectively) (11, 12).

$$E = 1 - \frac{\langle \tau_{DA} \rangle}{\tau_D} \quad (2.2)$$

$$E = \left(\frac{k_{ET}}{k_{ET} + 1/\tau_D}\right)\left(\frac{\alpha_{FRET}}{\alpha_{FRET} + \alpha_f}\right) \quad (2.3)$$

$$E = \left(\frac{k_{ET}}{k_{ET} + 1/\tau_D}\right) \quad (2.4)$$

The ensemble averaged approached to calculating the energy transfer efficiency relies on the ratio of averaged fluorescence lifetime of the donor in the presence of the acceptor (τ_{DA}) to the fluorescence lifetime of the donor alone (τ_D), where the donor alone is incapable of undergoing FRET. The average fluorescence lifetime of the donor in the presence of the acceptor is calculated using Equations 2.2 and 2.5, where α_i and τ_i represent the fractional amplitudes and exponential decay constants of the biexponential model shown in Equation 2.1.

$$\langle \tau_{DA} \rangle = \frac{\alpha_1\tau_1+\alpha_2\tau_2}{\alpha_1+\alpha_2} \tag{2.5}$$

Note that the rate-determined energy transfer efficiency does not require a cleaved, FRET incapable counterpart because it relies only on the rate of energy transfer and as a control fluorescence lifetime of the donor in the presence of an acceptor (τ_{DA}), which greatly reduces both the number experimental samples needed and the possibility of experimental sample preparation error.

The relative donor-acceptor distance under varying experimental conditions is then calculated using a known Förster distance (R_o) of 5.3 nm (Equation 2.6) (24). It is important to note that under all experimental conditions tested in this Thesis, the Förster distance (R_o) for these FRET pairs did not change more then 1% upon increased ionic strength of any salt and therefore these changes in the Förster (R_o) distance were considered negligible.

$$\mathrm{R_{DA}} = \sqrt[6]{\mathrm{R_0^6}(\frac{1}{E} - 1)} \tag{2.6}$$

2.5 Time-resolved polarized fluorescence anisotropy

2.5.1 Theory

Time-resolved polarized fluorescence anisotropy allows for the polarization

analysis of the rotational dynamics of fluorophores during their excited-state lifetime. Using a polarized femtosecond laser pulse, fluorophores with dipoles oriented parallel to the electric field of the incoming laser pulse will be preferentially selected and therefore excited from their ground state to the fast excited electronic state. Due to the selective excitation of molecules aligned with the polarized laser pulse, the emission of the excited fluorophores will be partially polarized at time-zero (t_o). The probability of the photoselective excitation (p) at time-zero is proportional to the cosine of the angle (θ) between the absorbing and emitting dipole:

$$p_{\text{excitation}} \propto \cos(\theta) \tag{2.7}$$

After the electronic-excitation from the polarized laser pulse ($t > 0$) the fluorescence photons become depolarized due to the rotational motion of the excited fluorophores. By detecting the parallel ($I_{\parallel}$) and perpendicularly ($I_{\perp}$) polarized components of the fluorescence emission, the rotational dynamics and nonradiative energy transfer of a donor to an acceptor fluorophore can be monitored. Other processes that may lead to fluorescence emission depolarization are conformation changes within the fluorophore, ultrafast nonradiative photophysical processes, and multiple populations undergoing FRET at a different rates of energy transfer.

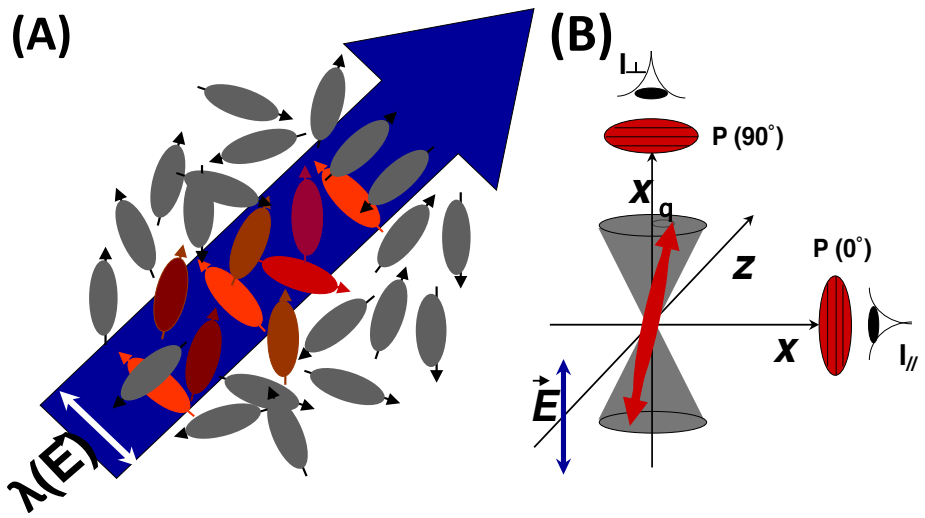

Figure 2.4: Illustration of fluorophore selective excitation and fluorescence emission depolarization. (A) Selective photoexcitation of fluorophores, into an excited electronic state, with absorption dipoles parallel to the incoming excitation laser pulse (B) Radial probability of photoselection and subsequent detection of the depolarizing fluorescence emission in both the parallel and perpendicular component.

The additional depolarization of the hetero-FRET pairs due to the nonradiative energy transfer from the fluorescent donor molecule to the acceptor may be deconvoluted from the molecular rotation, where the depolarization due to FRET is assumed to be ultrafast (k_{ET}) in comparison to the molecular rotation of the protein-based FRET probes. This ultrafast photophysical observation is inherent in FRET studies (40-44) and the more random orientation of the acceptor molecules dipole moment, in comparison to the initial orientation of the dipole moment of the donor, contributes to the increased rate of fluorescence depolarization. Thus, photoselecting the fluorescent donor molecule and measuring the fluorescence depolarization of the acceptor molecule allows for the FRET analysis of these protein-based hetero-FRET probes. It is important to note that due to the experimental approach there exists no need to perform experiments on FRET incapable (donor alone) samples (11, 12), when anisotropy measurements are acquired in conjunction with fluorescence lifetime measurements (Equation 2.3-2.4).

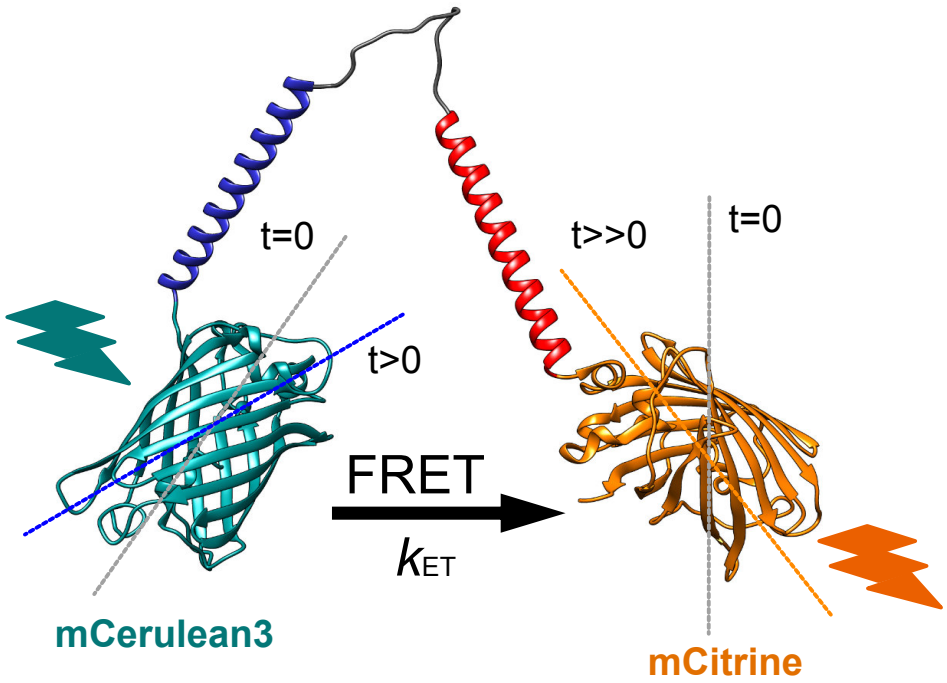

Figure 2.5: Illustration of the ionic strength protein-based hetero-FRET sensors and schematic of the time-resolved polarized fluorescence anisotropy detection and excitation conditions where one-photon laser pulses (425 nm) were generated to excite the donor fluorophore and the polarization analysis was performed on the acceptor's fluorescence emission using a 530/40 nm band pass filter. Importantly, this illustrates the rapid depolarization of the fluorescence emission, in comparison to the polarized laser excitation pulse, due to the ability of the donor and acceptor fluorophores to rotate freely from one another.

The rate of energy transfer (k_{ET}) and the rotational constant (ϕ_{DA}) of the donor-acceptor FRET pair, determined from the depolarization analysis and discussed in detail in Section 2.5.3, are used to calculate the energy transfer efficiency (E), a measure of how efficiently the excited donor fluorophore excites the corresponding acceptor fluorophore in the FRET pair (11, 12).

$$E = \frac{k_{ET}}{k_{ET} + \phi_{DA}^{-1}} \tag{2.8}$$

The average energy transfer efficiency (E) is then weighted by the population of undergoing FRET in the measured sample as previously described by (11, 12).

$$E = \left(\frac{k_{ET}}{k_{ET}+\phi_{DA}^{-1}}\right)\times\left(\frac{\beta_{FRET}}{\beta_{FRET}+\beta_{rot}}\right) \quad (2.9)$$

The rotational constant (ϕ_{DA}) and rate of energy transfer (k_{ET}) were determined simultaneously from the anisotropy decay analysis, where the rotational constant (ϕ_{DA}) describes the average molecular rotation time of the excited hetero-FRET pair (45). The distance between the donor and acceptor molecules (R_{DA}) in samples of varying ionic strength were calculated using the known Förster distance (R_o) and weighted energy transfer efficiency (*E)* with the relationship shown in Equation 2.6.

The Förster distance (R_o) was determined using steady-state spectroscopy as described in Boersma et al. (24). Briefly, the Förster distance depends on the spectral overlap, J(λ), between the donor and acceptor molecules (Fig 2.1), the refractive index (η) of the sample solution, the quantum yield (Φ) of the fluorescent molecules, and the relative orientation (κ^2) of the dipoles of both the donor and acceptor molecules. The orientation parameter was assumed to be equal to 2/3, the result of assuming randomly oriented dipoles (46).

2.5.2 Experimental setup and calibration

The rotational dynamics and energy transfer efficiency of each FRET pair was characterized using time-resolved polarized fluorescence anisotropy, where the experimental approach and optical system are shown in Figures 2.3 and 2.4, respectively. Femtosecond infrared laser pulses (850 or 930 nm) were generated using a titanium-sapphire solid-state laser system (Mira 900-F, Coherent). A 50 μL droplet of sample was positioned on a coverslip on a 1.2 NA water immersion microscope objective (Olympus UPlanApo/IR). One-photon laser pulses (425 and 465 nm) were generated to excite the sample at a 4.2 MHz repetition rate. A 475 filter with a FWHM of 50 nm was used for detecting the donor. For detection of the acceptor a 531 filter with a FWHM of 40 nm was used. From here on, the convention maximum/FWHM will be used to identify the bandpass filters (e.g. 531/40). The filtered wavelength-dependent fluorescence was

polarization-analyzed, detected, amplified, and routed to a synchronized SPC-830 module (Becker & Hickl) for data acquisition. A polarizing beam splitter was used to isolate the parallel and perpendicular fluorescence polarizations (with respect to the laser polarization), which were detected simultaneously using two microchannel plate (MCP) photomultiplier tubes (R3809U, Hamamatsu). The laser was calibrated using the anisotropy of rhodamine 110 (Rh110; rotational time of ~140 ps) and coumarin (rotational time of ~98 ps) to assess the wavelength dependence of the *G*-factor. Standards were carried out at the start and end of each experiment to validate the stability of the laser during data collected (11, 12).

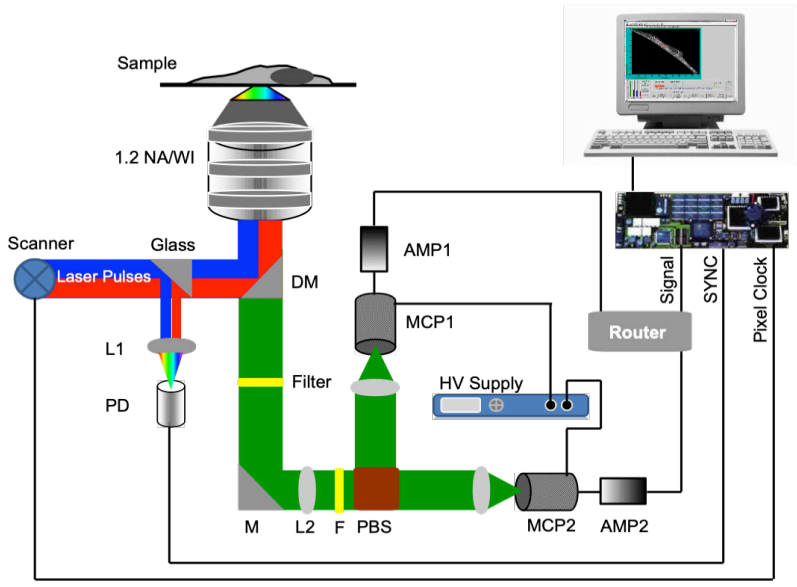

Figure 2.6: Schematic diagram of the optical system used to acquire the time-resolved polarized fluorescence anisotropy signal. PD: fast photodiode, L: lens, DM: dichroic mirror, F: filter, PBS: polarizing beam splitter, MCP: microchannel plate, AMP: amplifier.

2.5.3 Data analysis of time-resolved polarized fluorescence anisotropy

The time-resolved polarized fluorescence anisotropy signal was generated from the separately collected parallel and perpendicularly polarized fluorescence emission of the acceptor molecule (Fig 2.4), where the anisotropy signal was adjusted for daily

fluctuations in the optical system using a geometric factor (*G*-factor, *G*). The *G*-factor accounts for a potential bias of the multichannel plates in detecting parallel and perpendicular polarization and is experimentally determined from our optical setup on a daily basis using a tail-matching approach (47, 48).

$$r(t) = \frac{I_{\parallel}(t) - GI_{\perp}(t)}{I_{\parallel}(t) + 2GI_{\perp}(t)} \tag{2.10}$$

The constant factor of 2 shown in the denominator is used to account for the depolarization measured due to the high numerical aperture of the microscope objective (48). The decay in the anisotropy signal is represented by an n-term exponential function as shown below (2.11) but upon the addition of a FRET component this decay becomes dependent on the sum of the rates of both the molecular rotation (ϕ_{DA}) and rate of energy transfer (2.12):

$$r(t) = \sum_i^n \beta_i e^{-t/\phi_{DA}} \tag{2.11}$$

$$r(t) = \beta_{rot,i} e^{-t/\phi_{DA}} + \beta_{FRET} e^{-t(1/\phi_{DA} + k_{ET})} \tag{2.12}$$

The initial anisotropy, $r_o(t)$, is the sum of the fractional amplitudes of the exponential decay (β_i), equivalent to the theoretical maximum anisotropy of a fluorophore fixed in a viscous media such as a gel or the maximum anisotropy in a given system (39, 48, 49). In a system absent of any molecular rotation, such a fluorophore frozen in both space and time, the maximum initial anisotropy is equal to 0.4, which corresponds to collinear parallel ($I_{\parallel}$) and perpendicular ($I_{\perp}$) decay components, but this is rarely observed in experimentation due to the use of computer generated system response functions (SRF) (50). If the effects of this computer-generated system response function are assumed to be negligible, the magnitude of the initial anisotropy, $r_o(t)$, may be used to evaluate the extent of additional fluorescence depolarization mechanisms such as FRET.

The rotational diffusion decay constant of the donor-acceptor FRET pair is modeled and represented by (ϕ_{DA}) but this FRET approach is unable to distinguish

between pure rotational diffusion and intramolecular conformational and rotational fluctuations and therefore the proposed model (2.13) may not describe all physical and photophysical processes the FRET pair undergo (11, 12). The *G*-factor was determined daily using a common tail-matching approach that removes any polarization bias in the system detector (Fig 2.4) (51). Due to the large numerical aperture of the microscope objective, and the lack of an impact this increased depolarization has on the measured decay constants (rotational motion, FRET), the traditional anisotropy model shown in Equations 2.10–2.12 were used for all nonlinear regression analysis of the fluorescence depolarization. The quality of the fit of each model was evaluated using both an adjusted chi-squared and Akaike information criterion score, which allowed for the verification of the biexponential model. The mechanics of the analysis and results of these statistical tests are discussed in the next Section, and all anisotropy data analyses were carried out in the statistical programming software R (52).

Following the determination of the rotational decay constant and rate of energy transfer efficiency from the nonlinear regression, as described in the next Section, the anisotropy signal was used to obtain additional system information such as rotational diffusion coefficients using several models. Specifically, the Stokes-Einstein model for spherical models was applied to the anisotropy analysis to extract the approximate hydrodynamic radius (R) and volume (V) using the known refractive index (η) of the solution and rotational diffusion constant (ϕ_{DA}) and coefficient (D_R) of the FRET pair (53).

$$\mathrm{D_R} = \frac{\mathrm{k_B T}}{6\eta V} \tag{2.13}$$

Where k_B represents the Boltzman constant, T represents the temperature of the sample (25 °C). The diffusion coefficient used in Equation 2.13 was calculated using the known rotational constant as shown below:

$$\phi_{DA} = \frac{\eta V}{\mathrm{k_B T}} = \frac{1}{6\mathrm{D_R}} \tag{2.14}$$

To approximate the validity of the spherical molecule assumption the rotational constant was calculated using the known molecular weight (MW), where deviations between the two constants were assumed to be proportional to deviations for the spherical structure in the FRET pairs.

$$\phi_{DA} = \frac{\eta MW}{\mathrm{k_B T}} (v_o + h) \tag{2.15}$$

The sum of the parameters (v_o) and (h) represent the partial specific volume sampled by the FRET pair to account for deviations for spherical structure and varying levels of hydration by the surround local water environment. For most proteins, this value is approximately 0.96 mL/g (54).

Chapter 3

FRET Analysis of the Ionic-Strength (KCl) Sensors using Fluorescence-Lifetime Approaches

3.1 Rationale

We hypothesized that as the environmental ionic strength increases, the two oppositely charged α-helical regions of the linker, which are expected to be electrostatically attracted to one another, would be electrostatically screened leading to an increase in the donor-acceptor distance and therefore a reduced energy transfer efficiency due to the enhanced donor-acceptor distance in a manner that is dependent on both the linker's amino acid sequence and the type of salt present in solution. To test this hypothesis, we used time-correlated single photon counting (TCSPC) for fluorescence lifetime measurements to investigate the sensitivity of the genetically encoded protein-based hetero-FRET sensors (namely, RD, RE, and KE) to increased ionic strength (μ) in a commonly used salt, potassium chloride (KCl) (35). Prior to using these protein biosensors to investigate the biocomplexity associated with living cells (13, 14), we must first understand how these proteins respond in well-controlled environment with a representative salt such as potassium chloride at concentrations up to 500 mM, which is beyond eukaryotic physiologically relevant levels of ionic strength (13, 14, 55).

To this end, we used the TCSPC technique to measure the fluorescence lifetime of the first excited electronic state of these biosensors as a function of the KCl concentration (or the ionic strength). Here, the epifluorescence was detected at magic-angle polarization (54.7°) to remove any depolarization effect due to the rotational mobility of the fluorescent proteins. The measured fluorescence lifetime of both the intact and cleaved sensors are then used to calculate the energy transfer efficiency (E) and donor-acceptor distance (R_{DA}) as a function of the ionic strength (see Chapter 2 for more details on the materials and methods used here). These measurements were carried out under 425-nm excitation while detecting the donor's emission at 475/50 nm at room temperature in 10 mM NaPi buffer as a function of KCl concentration.

As a control, we also performed similar measurements on E6G2, a FRET probe with a flexible linker made of neutrally charged α-helices in the linker, and therefore insensitive to the environmental ionic strength. In addition, this control, E6G2, enabled us to assess any possible adverse impacts of ions of the conformational structure and dipole orientation of the biosensors (22). A range of KCl concentrations (0–500 mM) was used in these studies, which corresponds to the upper limit or beyond of projected intracellular salt concentrations in most prokaryotic and eukaryotic cell types (1, 2, 9) and allows for the determination of the range of ionic strengths the biosensors are sensitive too. For the FRET-incapable control using the cleaved FRET sensors, we examined the extent of the enzymatic cleavage daily using an SDS-PAGE gel analysis (Figure 2.1) and comparisons with the free mCerulean3 fluorescence lifetime (τ_{fl}) from literature (56, 57).

3.2 Results and discussion

3.2.1 Cleaved and intact FRET sensors have distinct excited-state fluorescence lifetime when exciting and detecting the donor

To explore the dynamic range and sensitivity of these protein-based hetero-FRET sensors to the environmental ionic strength (KCl), we measured time-resolved fluorescence using the TCSPC technique to quantify the fluorescence lifetime of the FRET-capable (intact) and FRET-incapable (cleaved) biosensor. The results are summarized in Table S2 and Figures S1–2.

Figure 3.1 shows representative fluorescence decays of the donor in cleaved and intact RD sensor in a sodium phosphate (NaPi) buffer. Our results show that the fluorescence emission of the donor in the FRET-incapable (cleaved) biosensor decays as a single exponential decay with an estimated fluorescence lifetime of ~4 ns at pH 7.4. The observed excited-state lifetime of the cleaved probe is consistent with literature values for the free mCerulean3 (11, 12, 58). In contrast, the fluorescence emission of the FRET-capable (intact) biosensor decays as a double exponential (see Table S1 for fitting parameters), which we attribute to the presence of two populations of molecules; one population undergoing FRET, the other not undergoing FRET (Chapter 2, Equation 2.1).

It is worth noting that the average fluorescence lifetime of the donor in intact RD is smaller than that of the cleaved counterpart due to the energy transfer from the donor to the acceptor in the former (see below for the estimated energy transfer efficiency of RD).

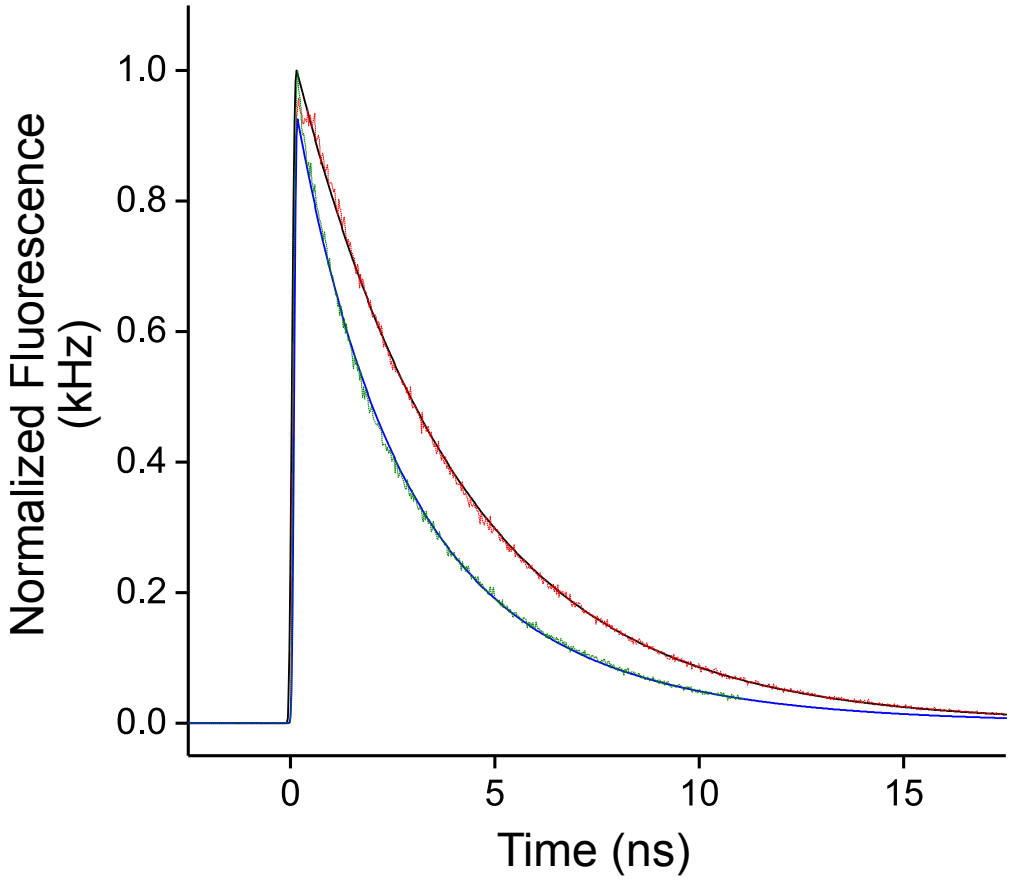

Figure 3.1: Representative excited-state fluorescence lifetime decays of the FRET-capable (intact, blue/green) and FRET-incapable (cleaved, black/red) biosensor, RD, in a 10 mM sodium phosphate buffer at room temperature. The fluorescence emission intensity (kHz) was normalized (shown here in arbitrary units) for visual comparison between the excited-state lifetime of donor in RD with and without the presence of the acceptor.

We have shown that exciting (425 nm) and detecting (475/50 nm) the fluorescence emission of the donor in these FRET sensors is sensitive to the proximity of the acceptor and therefore the energy transfer from mCerulean3 to mCitrine. When exciting (465 nm) and detecting (530/40 nm) the acceptor, however, the fluorescence

lifetime of the acceptor in intact and cleaved sensors is basically the same due to the absence of FRET (energy does not flow from low-energy to high-energy transition).

In addition, we compared the fluorescence decay of the intact and cleaved biosensor, RD, in the presence and absence of KCl (500 and 0 mM, respectively) to gain perspective on the sensitivity of our experimental signal to the presence and varying levels of FRET. As shown in Figure 3.2, the intact and cleaved biosensors display distinct fluorescence emission decays and the difference in the intact species is attributed to varying levels of energy transfer.

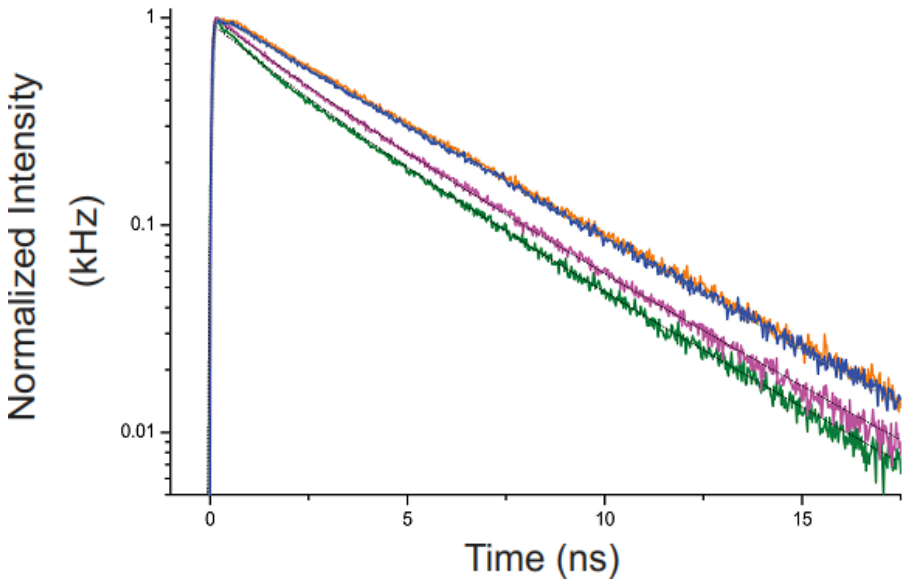

Figure 3.2: Representative time-correlated single photon counting (TCSPC) fluorescence decays of the protein-based hetero-FRET biosensor, RD, in the FRET-capable (green/pink) and FRET-incapable (orange/blue) species in the presence (pink/blue) and absence (green/orange) of KCl (0/500 mM). The intensity of the measurement (kHz) was normalized and displayed on a log base 10 scale for visual evaluation. The fluorescence decay of both FRET-incapable (cleaved) is statistical the same whereas there exists a statistical difference between the FRET-incapable and -capable species as well as in between the FRET-capable (intact) at both 0 and 500 mM KCl.

3.2.2 The excited-state fluorescence lifetime the hetero-FRET sensors is sensitive to the amino acid sequence of the linker

To examine the effect of the amino acid sequence of the linker, we carried out comparative studies on the fluorescence lifetime of the donor in intact and enzymatic

cleaved FRET sensors (RD, RE, and KE). These measurements were conducted in a sodium phosphate buffer in the absence of any additional ions (i.e., no additional ionic strength). The FRET pairs are comprised of stable fluorophores embedded within the large β-barrel secondary protein structure (57) and therefore the design of the linker was assumed to have negligible impacts on the fluorescence lifetime of either the donor (mCerulean3) or the acceptor (mCitrine) as shown in Figure 3.2. Specifically, we found there was no statistically significant difference between the average fluorescence lifetime of the cleaved biosensors RD, RE, and KE as well as the control E6G2. In contrast, significant difference in the average fluorescence lifetime of the donor in intact RD, RE, and KE sensors was observed (Figure 3.3). In addition, we have demonstrated that the average fluorescence lifetime of the intact E6G2 (a control with neutral amino acid residues of the linker) is significantly longer than those of RD, RE, and KE with charged α-helices. This increase in the fluorescence lifetime of the control biosensor, E6G2, likely arises from the inherently low energy transfer efficiency of this intact FRET sensor of approximately 8–20%, where the magnitude is dependent on the mode of calculation. Due to the relatively low level of energy transfer from the donor to the acceptor fluorophore it is to be expected that the average fluorescence lifetime more closely resembles the cleaved sample (donor alone).

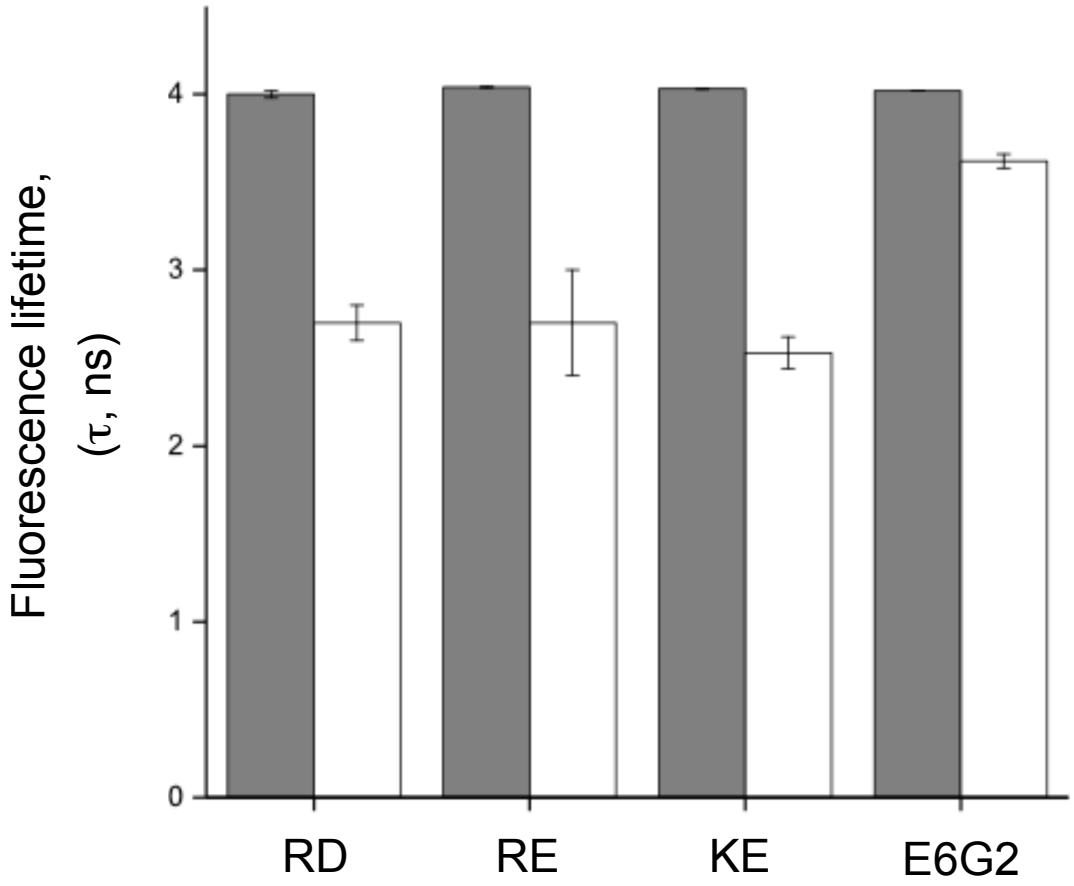

Figure 3.3: Linker effects on the average fluorescence lifetime of intact and leaved RD, RE, KE and E6G2 (control) in sodium phosphate buffer. Bar plot diagram of all four ionic strength biosensors (RD, RE, KE, and E6G2) average fluorescence lifetime in the intact (solid, dark gray) and cleaved (clear, white) species in 10 mM sodium phosphate. The lack of a statistical difference in the fluorescence lifetime of the cleaved species for all biosensors indicates that the excited-state dynamics of the mCerulean3 donor fluorophore are not affected by the linker in these biosensor design post-enzymatic cleavage.

The fluorescence lifetime measurements on these ionic strength sensors will be used to calculate the energy transfer efficiency and the donor-acceptor distance as a function of the environmental ionic strength (see below) as described in Chapter 2 (Materials and Methods).

3.2.3 The sensitivity of the fluorescence lifetime of cleaved and intact RD to the environmental KCl concentration is distinct

As a first step towards the characterization of the sensitivity of these FRET sensors to the environmental ionic strength, we carried out time-resolved fluorescence measurements on these sensors as a function of KCl concentration at room temperature. As a control, similar measurements were carried out on E6G2 under the same experimental conditions.

Figure 3.3 shows representative measurements on intact and cleaved RD sensor as a function of the KCl concentration (0–500 mM) at room temperature. These results show that the average fluorescence lifetime of the intact, FRET-capable FRET sensor, RD, increases upon increased ionic strength (0–300 mM). Above 300 mM, the average fluorescence lifetime of intact RD reaches a plateau. In contrast, the average fluorescence lifetime of the control E6G2 biosensor is insensitive to the environment ionic strength (0–500 mM) over the same range, which is attributed to the neutral amino acid residues of the linker region (data not shown). The fitting parameters of the time-resolved fluorescence of RD and E6G2 are summarized in Table S1.1.

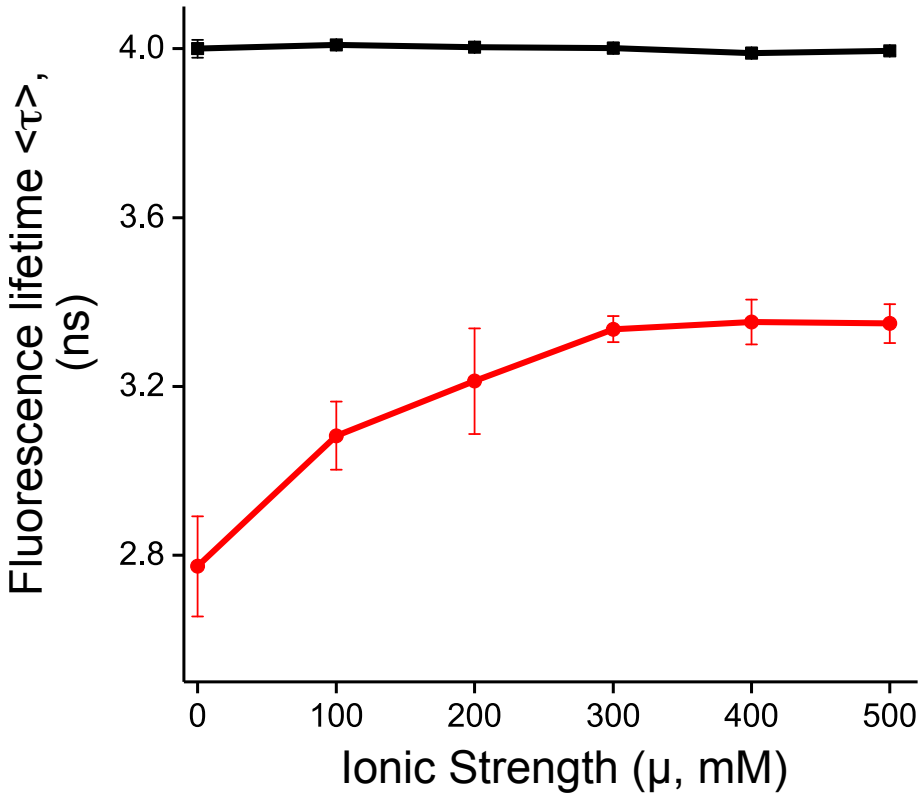

Figure 3.4: Illustration of the biosensor (RD) sensitivity to increased ionic strength (μ) in the intact species (red), where the excited-state fluorescence lifetime shows dependency in the concentration range (0–300 mM) and the cleaved species (mCerulean3, black) shows a complete lack of sensitivity indicating changes in the fluorescence lifetime are due to changes in the rate of energy transfer (k_{ET}) from the donor to the acceptor fluorophore.

Similar fluorescence lifetime measurements were carried out on the other ionic strength sensors (RE and KE), where the donor of intact and cleaved counterpart was excited and detected. These measurements were then used to calculate the energy transfer efficiency and donor-acceptor distance as a function of the KCl ionic strength (see below). See the fitting parameters of these fluorescence decays on intact and cleaved RD, RE, and KE along with E6G2 as summarized in Table S1.1.

3.2.4 Different approaches for calculating the energy transfer efficiency of the ionic-strength sensors based on time-resolved fluorescence measurements

We hypothesize that as the environmental ionic strength increases, the two charged α-helical regions of the linker would be electrostatically screened leading to an

increased donor-acceptor distance and therefore reduced energy transfer efficiency due to the enhanced donor-acceptor distance in a manner that is dependent on both the linker's amino acid sequence and identity of the ions in solution.

To test this hypothesis, we carried out time-resolved fluorescence measurements on the ionic-strength sensors (RD, RE, and KE) and E6G2 (as a control) as a function of the KCl concentration at room temperature. In addition, these time-resolved fluorescence measurements were analyzed using three different models as described in Chapter 2 (Materials and Methods; Section 2.4.3) to determine the energy transfer efficiency (E%) of each sensor at each environmental ionic strength (Figure 3.5).

The first approach for data analysis of the measured fluorescence decays of the donor in intact and cleaved biosensors is based on the traditional, ensemble averaging approaches (11, 12) following Equation 2.2 (Figure 3.5, Top). The results show that the energy transfer efficiency (E) decreases as the ionic strength of KCl increases. Overall, the energy transfer efficiency of RE is larger than that of KE and RD in a given environment. Importantly, KE exhibits the largest dynamic range among these sensors' with respect to sensitivity to environmental ionic strength (Table S1.3). In contrast, E6G2 exhibits negligible sensitivity to the environmental ionic strength (Figure 3.5, Top).

Ensemble averaging is inherently incapable of probing sub-populations that may undergo different FRET at different rates due to distinct structural conformations. To overcome this ensemble-based challenge, we have developed a model (59) in which the energy transfer rate constant (k_{ET}) can be determined directly from the measured fluorescence decays of each sensor. In this model, we assumed two populations of intact FRET pairs where on undergo energy transfer and the other does not, which also explain our observed time-resolved fluorescence under 425-nm illumination. The second and third approaches on FRET analysis are described in Section 2.4.3.

In the second approach for FRET analysis, the energy transfer rate of each sensor in a given environmental ionic strength was calculated from the observed biexponential fluorescence decays of intact sensors. The estimated energy transfer rate (k_{ET}) was then used to calculate the corresponding energy transfer efficiency (E) of each sensor as

described in Equations 2.1 and 2.3. For these measurements, the fluorescence decay constant of the donor alone was either measured using the time-resolved fluorescence of the cleaved sensor or the second slow decay component of each fluorescence decay of the intact probe. Both approaches gave fairly similar FRET efficiencies. To reproduce the energy transfer efficiencies of the ensemble average, we then weighted the k_{ET}-based energy transfer efficiency by the population fraction undergoing FRET and the results are shown in Figure 3.4(Middle). These analyses yield similar trend concerning the sensitivity of the energy transfer efficiency (E) to the ionic strength of KCl-containing buffer.

The third approach for FRET analysis using time-resolved fluorescence of the donor in both intact and cleaved sensors is essentially the same as the second approach above but without the weighting factor. In this approach, we calculate the energy transfer efficiency of these sensors that only undergo FRET. Once we removed the ensemble averaging, we observed an enhanced energy transfer efficiency that is almost twice that calculated using the first and second averaging approaches (Figure 3.5, Bottom) in sodium phosphate buffer. However, the observed trend using this third approach is fairly similar to the previous methods, where we observed a reduction of the energy transfer efficiency of these FRET sensors as the ionic strength increases (Figure 3.5, Bottom). This trend was attributed to the electrostatic screening of the two charged α-helices on the linker, which leads to relatively larger donor-acceptor distance.

All three models of data analysis also agree on the negligible sensitivity of E6G2 to the environmental ionic strength due to its electrostatically neutral linker. In addition, although the ensemble averaging method is most commonly used and therefore most comparable, the rate determined approach offers the possibility of a lack of need of a cleaved counterpart and is more comparable to anisotropy measurements (Chapter 5).

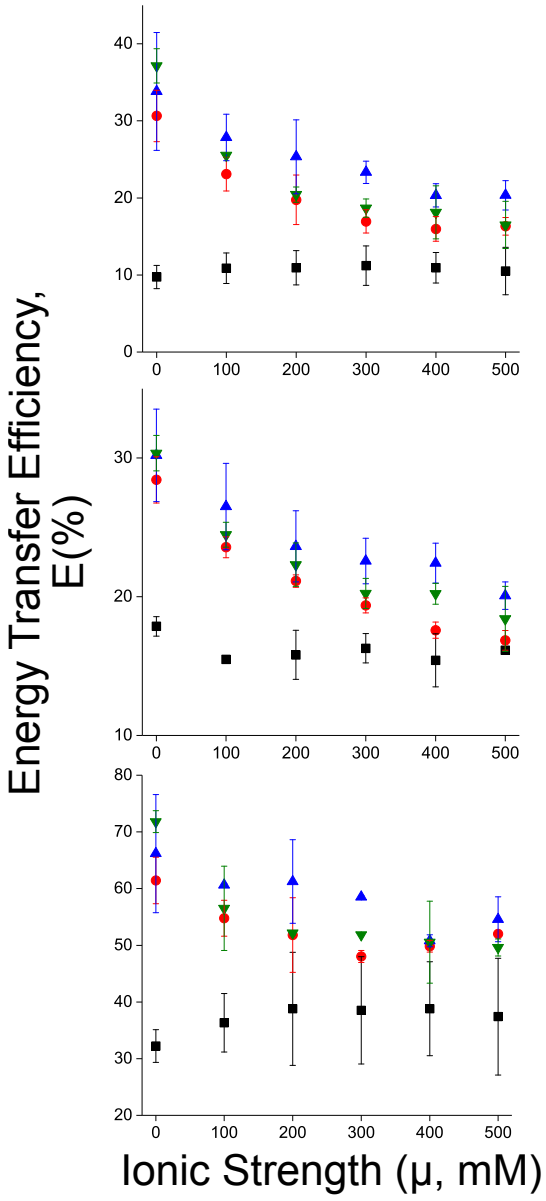

Figure 3.5: Different approaches for FRET analysis using time-resolved fluorescence measurements of the ionic strength sensors. The energy transfer efficiency, *E*(%), as a function of increasing ionic strength (μ, KCl) of all four biosensors (RD-red circle, RE-upright blue triangle, KE-downright green triangle, E6G2-black square) calculated using three methods: an ensemble averaging approach (Top, Equation 2.2), and a weighted and non-weighted rate determined approach (Middle/Bottom and Equations 2.3–2.4, respectively). All measurements were acquired in sodium phosphate buffer, pH 7.4 and all error represents the standard deviation between replicate measurements taken on different days.

3.2.5 The donor-acceptor distance of the ionic-strength sensors is sensitive to both the salt concentration and the linker sequence

To test the hypothesis that the two charged α-helical regions of the linker region would be electrostatically screened in an environment with larger ionic strength leading to an increase in the donor-acceptor distance, we used the estimated energy transfer efficiency (*E*) of each sensor (Section 3.2.4) to calculate the corresponding donor-acceptor distance as a function of both the ionic strength of KCl-containing solution and the linker's amino acid sequence.

As we described in Section 2.4.3, we used the literature value for the Förster distance of the mCerulean3-mCitrine FRET pair of 5.3 nm (24), which is dependent upon the spectral overlap of the donor emission and the acceptor absorption, the relative orientation of their respective dipole moments, the donor's fluorescence quantum yield, and the environmental refractive index. Here, we also assume a random dipole moments orientation with an orientation parameter (κ^2) of 2/3 (22). In addition, we calculate the corresponding donor-acceptor distance in each sensor as a function of the ionic strength of the KCl-containing buffer using three models, which we used to calculate the energy transfer efficiency (Section 3.2.4). This approach allows us to examine the sensitivity of these calculations to how the time-resolved fluorescence measurements are being analyzed.

Figure 3.5 summarizes the calculated donor-acceptor distance (R_{DA}) of the ionic strength sensors (RD, RE, KE) as well as E6G2, with electrostatically neutral amino acids in the linker region as a control in the KCl-supplemented buffer (μ = 0–500 mM). The three models used to calculate *E* and therefore R_{DA} provide a consistent trend where the donor-acceptor distances for RE, KE, and RD increase as the ionic strength of the KCl-containing buffer increases, which we attributed to ionic screening of the two charged α-helices of the linker. This observation supports our stated hypothesis that the two charged α-helical regions of the linker region would be electrostatically screened in an environment with larger ionic strength leading to an increase in the donor-acceptor distance. In addition, the donor-acceptor distance displays an apparent minor sensitivity

to the amino acid sequence of the linker in each sensor (RD, RE, and KE). In contrast, the donor-acceptor distance of E6G2 with neutral amino acids in the linker regions exhibit a negligible sensitivity to the environmental ionic strength of the KCl-containing buffer.

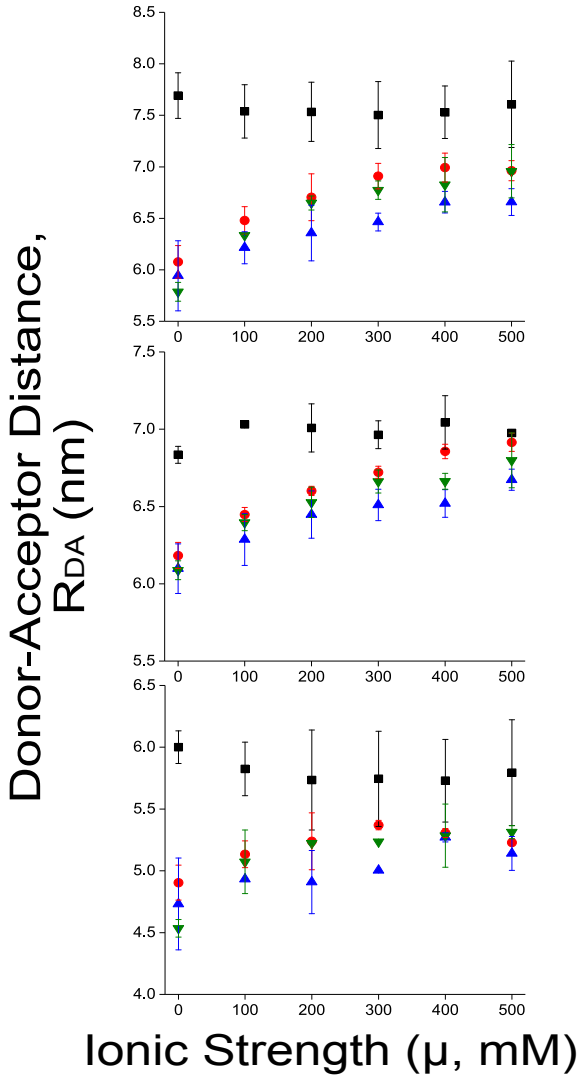

Figure 3.6: The donor-acceptor distances, R_{DA}, as a function of increasing ionic strength (μ, KCl) of all four biosensors (RD-red circle, RE-upright blue triangle, KE-downright green triangle, E6G2-black square) calculated using three methods: an ensemble averaging approach (Top, Equations 2.2, 2.6), and a weighted and non-weighted rate determined approach (Middle/Bottom and Equations 2.3–2.4 and 2.6, respectively). All measurements were acquired in sodium phosphate buffer, pH 7.4, and all error represents the standard deviation between replicate measurements taken on different days. The Förster distance used was 5.3 nm as determined in Boersma et al. (24) was assumed to be constant under all experimental conditions.

These comparative studies also show that the ensemble-averaged determined donor-acceptor distance (Figure 3.6, Top and Middle) is significantly larger than that of the population of sensors that undergo FRET (Figure 3.6, Bottom). It is also worth noting that the standard deviation of these donor-acceptor distance using a given set of experimental data (same day and sample preparation) is significantly smaller than that averaged on a number of trials on different days. Because the temporal resolution of our TCSPC is ~50 ps, such observations can be attributed to the efficiency of the cleavage reaction using the proteinase K enzyme (24, 60). In other words, any changes in the yield of the cleavage reaction would influence the fluorescence lifetime of the cleaved sample and therefore the corresponding energy transfer efficiency and the donor-acceptor distance. More specifically, if there exists a small population of biosensor that remains intact (i.e. not proteolytically digested) the measured fluorescence lifetime would be decreased due to the presence of FRET.

3.3 Conclusions

We measured the time-resolved fluorescence of a set of ionic strength sensors (RD, RE, and KE), both cleaved and intact, as a function of the ionic strength of the KCl-containing buffer. In these measurements, the donor (mCerulean3) in each sensor was excited (at 425 nm) and the corresponding fluorescence emission was detected at 475/50 nm.

Our results indicate that the fluorescence lifetime of the donor in these sensors is sensitive to the presence of the acceptor in close proximity (<10 nm). In addition, the fluorescence lifetime of the donor in the intact sensors (RD, RE, and KE) is sensitive to both the amino acid sequence of the linker region as well as the environmental ionic strength of the KCl-containing buffer.

In contrast, the fluorescence lifetime of E6G2 with the neutral amino acids in the linker region exhibit negligible sensitivity to the environmental ionic strength. In addition, the fluorescence lifetime of the donor in the cleaved sensors is also constant and independent of the environmental ionic strength.

Our results also support our hypothesis that as the ionic strength (μ) of the KCl-containing buffer increases (0–500 mM KCl), the energy transfer efficiency, E(%), decreases and the donor-acceptor distance, R_{DA}, increases, regardless of the model used for FRET analysis using these fluorescence lifetime measurements. These observations are attributed to ionic screening of the charged α-helices in the linker region in the KCl-containing buffer with larger ionic strength, which leads to a reduced electrostatic interaction and thus an enhanced donor-acceptor distance. While the trends are relatively the same in the three models used for FRET analysis, the estimated energy transfer efficiency and donor-acceptor distance of each sensor population that undergoes FRET was significantly different than the ensemble-averaged estimates. Because the intercellular ionic strength contains different types of ions, it is important to examine the sensitivity of these sensors to different types of ions or salts. Towards this goal, we extended these measurements in the KCl-containing buffer to the Hofmeister salt series (Chapter 4) using the same experimental approach and FRET analysis.

Chapter 4

Examining the Ion-Specific Sensitivity of the FRET Sensors to the Hofmeister Series of Salts

4.1 Rationale

We have demonstrated the sensitivity of the FRET sensors to the ionic strength of KCl solution (K^+ and Cl^- ions) using time-resolved fluorescence of the donor in the presence and the absence of the acceptor. However, the intracellular ionic strength contains different concentrations and types of ions such as H^+, Li^+, Na^+, Mg^{2+}, Ca^{2+}, Br^-, I^-, and SO_4^{2-}) (35-37, 61). As a result, it is critical to examine the sensitivity of these sensors (RD, RE, and KE) to different types of salts, which are strong electrolytes that dissociate to ions in water.

We hypothesize that the sensitivity of the RD, RE, and KE sensors will be sensitive to both the type of ions as well as the ionic strength of the Hofmeister series (KCl, LiCl, NaCl, NaBr, NaI, and Na_2SO_4). Our rationale is that the electrostatic interaction between the charged α-helices and the dissolved ions may depend on both the type of ions (size) and the charge they carry. Such electrostatic interactions are likely to influence the electrostatic screening between the two charged α-helices and therefore the donor-acceptor distance and the energy transfer efficiency.

To test this hypothesis, we carried out time-resolved fluorescence measurements of the donor in intact and cleaved FRET probes in buffer supplemented with the Hofmeister salt series at variable ionic strength. The results are analyzed using the same approach as described in Chapters 2 and 3. Our previous results (discussed in Chapter 3) suggested a lack of sensitivity (reaching a plateau) of these protein-based hetero-FRET biosensors at ionic strengths exceeding 300 mM, which represents an upper limit of physiologically relevant concentrations. Therefore, we tested the sensitivity of these biosensors in the Hofmeister salt series at concentrations ranging from 0 to 300 mM (13, 14). The buffer used in these experiments was 10 mM NaPi at room temperature to minimize the impact of additional levels of ionic strength due to the composition of the buffer.

4.2 Results and discussion

4.2.1 Ensemble averaging approach for calculating the energy transfer efficiency and donor-acceptor distance of the ionic-strength sensors to the Hofmeister series

To test the hypothesis that the sensitivity of the RD, RE, and KE sensors will be sensitive to both the type of ions as well as the ionic strength of the Hofmeister series, we carried out time-resolved fluorescence measurements on the ionic-strength sensors (RD, RE, and KE) and E6G2 (as a control) as a function of the corresponding ionic strength (μ) at room temperature. As previously discussed in Chapter 3, the time-resolved fluorescence measurements of the donor in these sensors were carried out using 425-nm excitation and 475/50 nm detection at room temperature. These time-resolved fluorescence measurements were analyzed using two different models as described in Section 2.4.3 to determine the energy transfer efficiency (*E*%) of each sensor at each level of ionic strength.

Prior to evaluating the energy transfer efficiency and donor-acceptor distances of the biosensors in the presence of the Hofmeister salts, the fluorescence lifetime decay of the model sensor, KE, was compared across all six salts in both an intact and cleaved species. In disagreement with our hypothesis, the acquired fluorescence decay of each salt is almost perfectly overlapping for each respective species although a decrease in the fluorescence lifetime is observed between the cleaved and intact KE (Figure 4.1), which is attributed to FRET and in agreement with the results discussed in Chapter 3.

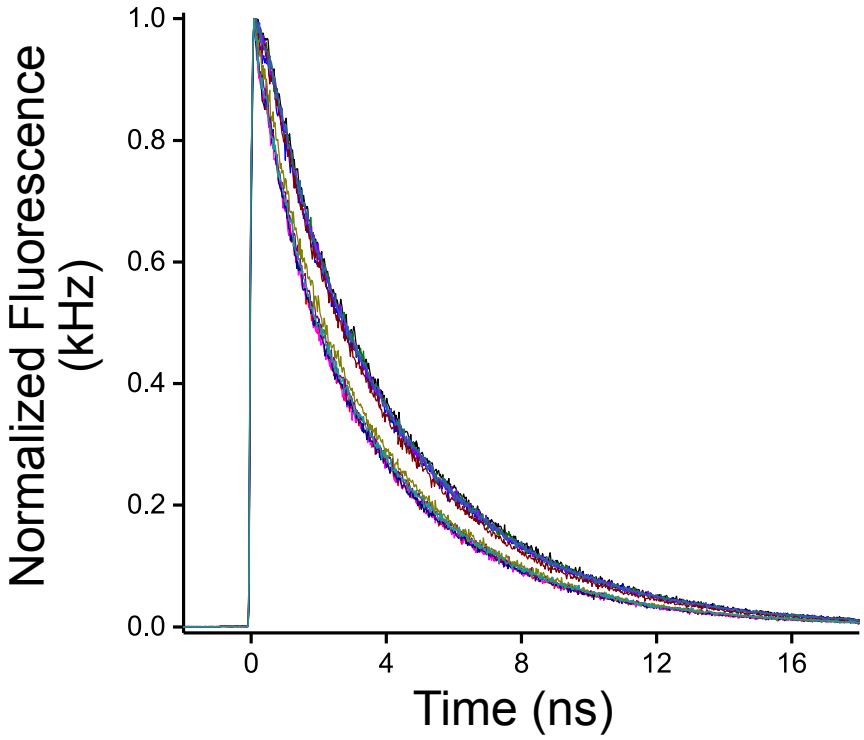

Figure 4.1: Representative TCSPC fluorescence decays of the FRET-capable (intact, left) and FRET-incapable (cleaved, right) KE FRET biosensor in the presence of six unique salts (KCl, LiCl, NaCl, NaBr, NaI, Na_2SO_4). Shown here is the sensitivity of the TCSPC technique to measure the extent of energy transfer in a FRET pair, by comparison of the intact and cleaved decays, as well as the lack of sensitivity of these FRET biosensors to the identity of the salt present.

Figure 4.2 shows the energy transfer efficiency (*E*) of the RD, RE, and KE in the Hofmeister series (KCl, LiCl, NaCl, NaBr, NaI, and Na_2SO_4) using the ensemble averaging approach of the time-resolved fluorescence of the donor. These FRET analyses were also based on the comparative average fluorescence lifetime of the intact sensors and the cleaved counterpart under the same experimental conditions (see Chapters 2 and 3; Equation 2.2) (11, 12). The results show that the energy transfer efficiency (*E*) decreases as the ionic strength of solution increases for all salts investigated. Overall, the biosensors respond to all salt types similarly but with a possible enhanced dynamic range in the presence of NaI or Na_2SO_4 as seen qualitatively (Figure 4.2). In addition, the sensitivity of E6G2 to both the ionic strength and the type of ions seems negligible (Figure 4.2), which we attribute to the neutral α-helices of the linker region and is in

agreement with our findings for KCl-supplemented buffer (Chapter 3). It is worth mentioning that the dotted straight line in Figure 4.2 is simply used for visual guidance and is not based on fitting to any theoretical model. Importantly, KE sensor exhibits a larger dynamic range (1.85 as compared to 1.41 and 1.49) than either RE or RD, respectively, when using ensemble averaged based approaches.

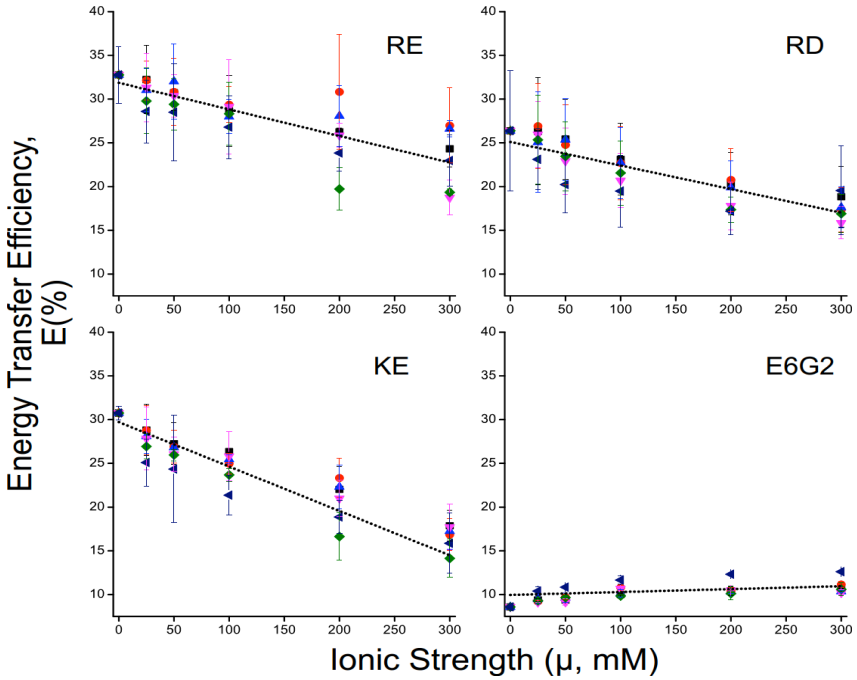

Figure 4.2: The energy transfer efficiency, *E*(%), of all four ionic strength biosensors (RD, RE, KE, and E6G2) acquired from TCSPC measurements in the presence of increasing ionic strength in variety of salts from the Hofmeister series (0, 25, 50, 100, 200, 300 mM) (KCl (black, square), LiCl (red, circle), NaCl (blue, upright triangle), NaBr (pink, inverted triangle), NaI (green, diamond), Na_2SO_4 (dark blue, sideways triangle)) as calculated using the ensemble average based method which is discussed in Chapter 2 of this Thesis (Equation 2.3). The relative donor-acceptor distances were calculated assuming a constant Förster distance of 5.3 ± 0.2 nm under all salt concentrations. Error bars represent the standard error of the mean as calculated from replicate TCSPC measurements. The solid black line represents a linear fit of all six salts as a function of increasing ionic strength and used here only for visual guidance (i.e., not based on a theoretical model).

Next, we calculated the corresponding donor-acceptor distance of RD, RE, and KE as a function of the ionic strength of these Hofmeister series of salts using a Förster

distance of 5.3 ± 0.2 nm (see Chapters 2 and 3). Figure 4.3 shows the donor-acceptor distance of these sensors (RD, RE, and KE) as well as E6G2 (as a control) in the Hofmeister series. These results show that the donor-acceptor distance of RD, RE, and KE increases as the ionic strength of the Hofmeister salt-containing buffer increases. In addition, the dynamic range of R_{DA} is larger for KE and RE than that of RD. Importantly, it seems the type of ions in the Hofmeister salt-containing buffer have negligible effect on the R_{DA} sensitivity.

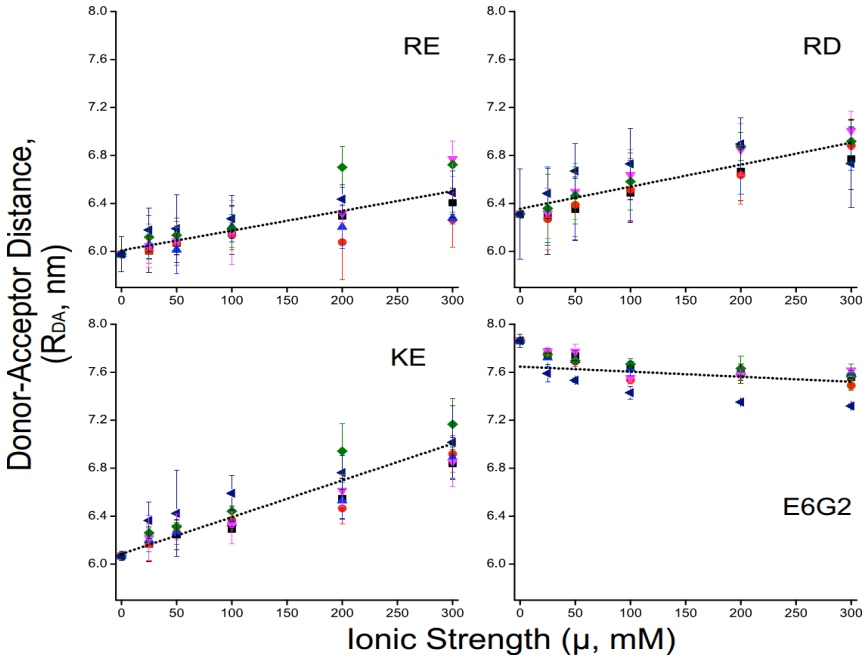

Figure 4.3: The relative donor-acceptor distance, R_{DA}, of all four ionic strength biosensors (RD, RE, KE, and E6G2) acquired from TCSPC measurements in the presence of increasing ionic strength in variety of salts from the Hofmeister series (0, 25, 50, 100, 200, 300 mM) (KCl (black, square), LiCl (red, circle), NaCl (blue, upright triangle), NaBr (pink, inverted triangle), NaI (green, diamond), Na_2SO_4 (dark blue, sideways triangle)) as calculated using the ensemble average based method which is discussed in Chapter 2 of this Thesis (Equation 2.3). The relative donor-acceptor distances were calculated assuming a constant Förster distance of 5.3 ± 0.2 nm under all salt concentrations. Error bars represent the standard error of the mean as calculated from replicate TCSPC measurements. The solid black line represents a linear fit of all six salts as a function of increasing ionic strength and used for a qualitative representation of the trends.

In contrast, E6G2 with the electrostatically neutral α-helices region seems to exhibit slightly different conformational changes as the ionic strength of the Hofmeister salt-containing buffer increases. We observed a negligible reduction of the donor-acceptor distance of E6G2 with the increase in the ionic strength of most of the Hofmeister salt-containing buffer, except $NaSO_4$ under the same range. For example, the reduction of the donor-acceptor distance of E6G2 is more pronounced for NaBr-containing buffer as compared with other salts (Figure 4.3).

As a means of biosensor sensitivity and robustness comparison, the dynamic range of each FRET pair was calculated, simply as the ratio of the maximum to the minimum energy transfer efficiencies (E_{max}/E_{min}), of each sensor averaged across all six salts investigated (KCl, LiCl, NaCl, NaBr, NaI, Na_2SO_4), where no sensitivity would result in a dynamic range of 1 (Table 4.1). Interestingly, KE shows a significantly larger dynamic range in comparison to other sensors.

Table 4.1: Tabulated energy transfer efficiencies, *E*(%), at 0 and 300 mM ionic strength (μ) ($FRET_{max}$ and $FRET_{min}$, respectively) used to calculate the dynamic range of each ionic strength FRET biosensor, where the dynamic range represents a ratio of the maximum FRET to the minimum FRET. The energy transfer efficiencies at 0 and 300 mM ionic strength were averaged across all six salts investigated in Chapter 4 of this Thesis (KCl, LiCl, NaCl, NaBr, NaI, and Na_2SO_4) due to their statistically insignificant difference in their impact on the FRET biosensors. All energy transfer efficiency calculations were performed using the ensemble averaged approach shown in Equation 2.3.

Sensor	**$FRET_{max}$, *E*(%)**	**$FRET_{min}$, *E*(%)**	**Dynamic Range**
RD	26.4	17.7	1.49
RE	32.8	23.2	1.41
KE	30.7	16.6	1.85
E6G2	7.72	8.85	0.81

4.2.2 Energy-transfer Rate dependent approach for calculating the energy transfer efficiency and donor-acceptor distance of the ionic-strength sensors

Using the same set of time-resolved fluorescence measurements (Section 4.2.1) of the ionic strength sensors in the Hofmeister salt-supplemented buffer, we used the energy transfer rate (k_{ET}) approach (Chapters 2 and 3) to calculate the corresponding energy transfer efficiency and the donor-acceptor distance. Our rationale here is that the ensemble-averaging approach (Section 4.2.1) might wash out different populations that undergo FRET at different rates. In addition, the rate-dependent approach for FRET analysis approach exploits the invaluable information provided to us from the time-resolved fluorescence at high temporal resolution. In fact, we argue that this rate-dependent approach allow us, in principle, to calculate the energy transfer efficiency and the donor-acceptor distance without the need for independent measurements of the cleaved counterpart (i.e., donor alone) (11, 26, 59). The estimated energy transfer rate (k_{ET}) was then used to calculate the corresponding energy transfer efficiency (E) of each sensor as described in Equations 2.2–2.3 (Chapter 2 and 3). First, we focus on the rate-dependent approach weighted by the population of the sensors that are undergoing FRET.

Figure 4.4 summarizes the energy transfer efficiency (E) of RE, RD, and KE as a function of the ionic strength of the Hofmeister salt-containing buffer (KCl, LiCl, NaCl, NaBr, NaI, and Na_2SO_4). The rate-dependent FRET analyses also indicate that the energy transfer efficiency of these sensors decreases as the ionic strength increases; in a general agreement with the ensemble averaging approach. In addition, KE exhibits significantly larger dynamic range (1.85) as compared with that of RE (1.41) and RD (1.49) for the ensemble-based approach (Table 4.2). The results also suggest that these sensors exhibit a negligible (i.e., statistically insignificant) ion-specificity in the Hofmeister salt-supplemented buffers used here (KCl, LiCl, NaCl, NaBr, NaI, and Na_2SO_4). This observation implies that once these sensors are genetically encoded in different compartments in living cells, the energy transfer efficiency and the donor-acceptor

distance, as a readout, will depend on the concentration of the compartmentalized ionic strength; regardless the type of the intracellular ions.

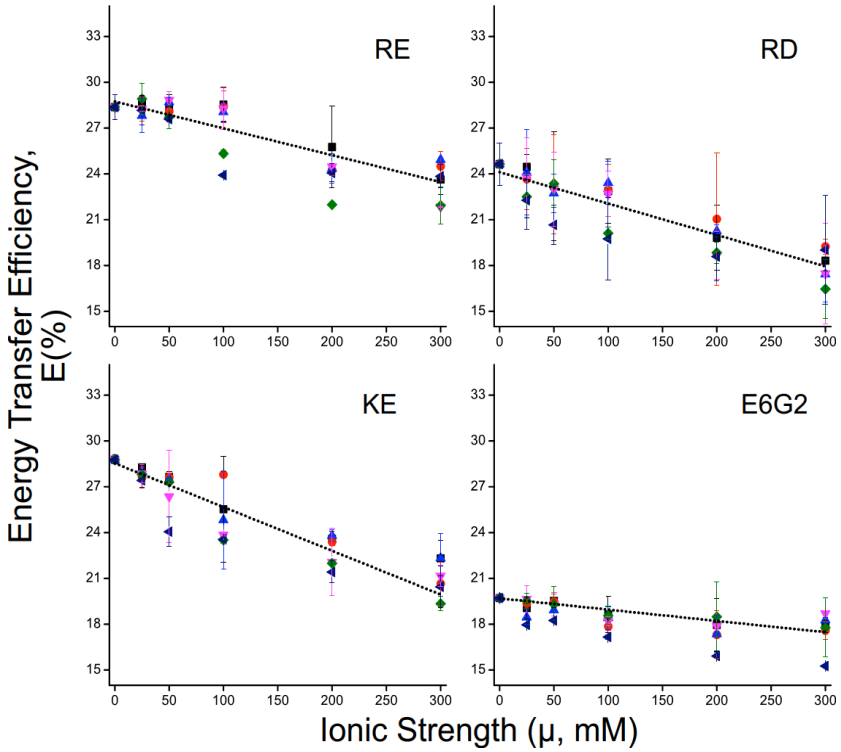

Figure 4.4: The energy transfer efficiency, *E*(%), of all four ionic strength biosensors (RD, RE, KE, and E6G2) acquired from TCSPC measurements in the presence of increasing ionic strength in variety of salts from the Hofmeister series (0, 25, 50, 100, 200, 300 mM) (KCl (black, square), LiCl (red, circle), NaCl (blue, upright triangle), NaBr (pink, inverted triangle), NaI (green, diamond), Na_2SO_4 (dark blue, sideways triangle)) as calculated using the rate determined method which is discussed in Chapter 2 of this Thesis (Equation 2.4). The relative donor-acceptor distances were calculated assuming a constant Förster distance of 5.3 ± 0.2 nm under all salt concentrations. Error bars represent the standard error of the mean as calculated from replicate TCSPC measurements. The solid black line represents a linear fit of all six salts as a function of increasing ionic strength and used for a qualitative representation of the trends.

Interestingly, the energy transfer efficiency of E6G2 slightly decreases as the ionic strength increase (Figure 4.4) even though it has neutral amino acid sequence in the linker region and further experimentation is being conducted to investigated this observed trend.

Using the estimated energy transfer efficiency of RD, RE, KE and E6G2 (control) in the Hofmeister salt-supplemented buffer, we calculated the corresponding donor-acceptor distance as a function of the ionic strength in the buffer supplemented with KCl, LiCl, NaCl, NaBr, NaI, or Na_2SO_4. Figure 4.5 summarizes our findings concerning the ionic-strength dependent donor-acceptor distance (R_{DA}).

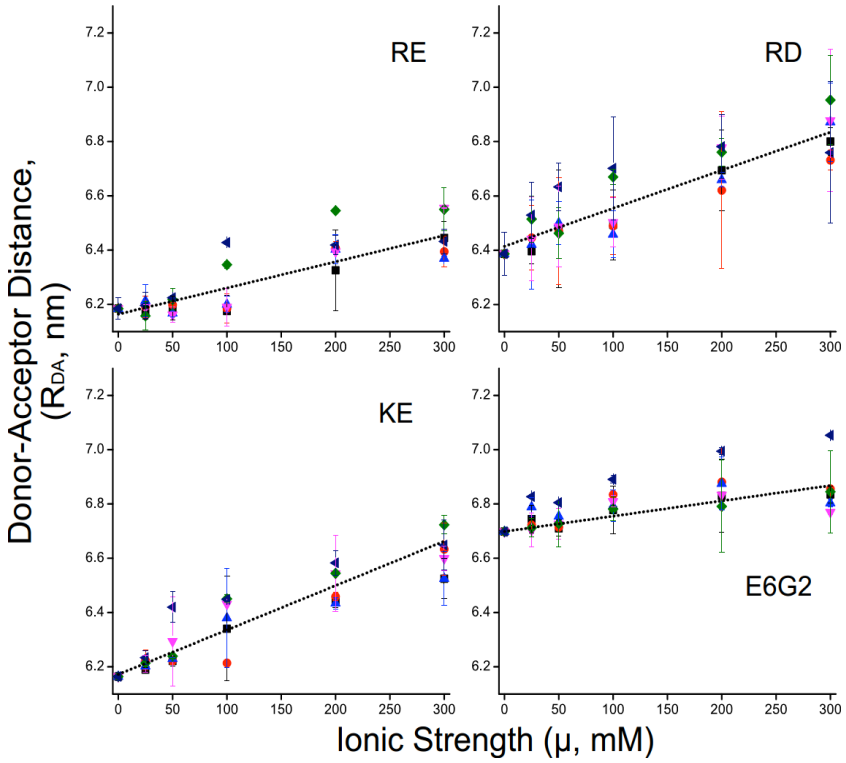

Figure 4.5: The relative donor-acceptor distance, R_{DA}, of all four ionic strength biosensors (RD, RE, KE, and E6G2) acquired from TCSPC measurements in the presence of increasing ionic strength in variety of salts from the Hofmeister series (0, 25, 50, 100, 200, 300 mM) (KCl (black, square), LiCl (red, circle), NaCl (blue, upright triangle), NaBr (pink, inverted triangle), NaI (green, diamond), Na_2SO_4 (dark blue, sideways triangle)) as calculated using the rate determined method which is discussed in Chapter 2 of this Thesis (Equation 2.4). The relative donor-acceptor distances were calculated assuming a constant Förster distance of 5.3 ± 0.2 nm under all salt concentrations. Error bars represent the standard error of the mean as calculated from replicate TCSPC measurements. The solid black line represents a linear fit of all six salts as a function of increasing ionic strength and used for a qualitative representation of the trends.

Our rate-dependent FRET analyses reveal that the donor-acceptor distance increases as the ionic strength sensors (RD, RE, KE) increases (Figure 4.5). Our results

also show that there is no statistically significant difference in the donor-acceptor distance of these sensors concerning the ion-specificity in these Hofmeister salt-containing buffers. In addition, KE exhibits a largest dynamic range compared with RD and RE (Table 4.1–2). Interestingly, the control biosensor, E6G2, which is comprised of a neutral linker region and designed to be insensitive to ionic strength presented minor sensitivity, outside of the bounds of the error, to the level of ionic strength. Specifically for E6G2, in the rate determined and ensemble averaged approach the energy transfer efficiency decreases and increases approximately by 2% and 1%, respectively. Although these changes are minor, they may suggest that the linker region itself, when absent of charge, contains a slightly inversed sensitivity, as compared to ionic strength sensing, to the hydration of ions and therefore local water ordering (35, 36, 61). We proposed that this response may arise from the water ordering acting as a macromolecular crowder forcing the biosensor to adopt a more compact confirmation and increasing its energy transfer efficiency (11, 12).

Similarly to the ensemble average based approach, the dynamic range of each sensor was compared by averaging the maximum and minimum energy transfer efficiency of all four biosensors at 0 and 300 mM for all six of the Hofmeister salts investigated (KCl, LiCl, NaCl, NaBr, NaI, and Na_2SO_4) (Table 4.2). Interestingly, the dynamic range of KE is reduced in comparison to the ensemble average approach and equal to the dynamic range of RD but the overall dynamic range of the control, E6G2, is diminished and approaches unity. Therefore, using the rate-determined approach may dampen the dynamic range of the sensors but produces a more reliable and consistent analysis result and therefore interpretation of the linker design and ion sensing mechanism.

Table 4.2: Tabulated energy transfer efficiencies, E(%), at 0 and 300 mM ionic strength (μ) ($FRET_{max}$ and $FRET_{min}$, respectively) used to calculate the dynamic range of each ionic strength FRET biosensor, where the dynamic range represents a ratio of the maximum FRET to the minimum FRET. The energy transfer efficiencies at 0 and 300 mM ionic strength were averaged across all six salts investigated in Chapter 4 of this Thesis (KCl, LiCl, NaCl, NaBr, NaI, and Na_2SO_4) due to their statistically insignificant difference in their impact on the FRET biosensors. All energy transfer efficiency calculations were performed using the rate determined approach shown in Equation 2.4.

Sensor	$FRET_{max}$, E(%)	$FRET_{min}$, E(%)	Dynamic Range
RD	24.6	18.0	1.37
RE	28.4	23.4	1.21
KE	28.8	21.0	1.37
E6G2	19.7	17.6	1.12

4.3 Conclusions

In this Chapter, we measured the time-resolved fluorescence of RD, RE, and KE sensors as a function of the ionic strength of the Hofmeister salt-supplemented buffers (KCl, LiCl, NaCl, NaBr, NaI, and Na_2SO_4). As a control, we also carried out similar measurements on the cleaved counterpart (i.e., mCerulean3 alone) of these sensors, as well as E6G2 with the electrostatically neutral amino acid sequence in the linker region.

Our results, regardless the model used for FRET analysis, do not support the hypothesis that the sensitivity of the RD, RE, and KE sensors will be ion-specific as the ionic strength varied in the Hofmeister salt-containing buffer (KCl, LiCl, NaCl, NaBr, NaI, and Na_2SO_4). In other words, our results suggest that the energy transfer efficiency and the donor-acceptor distance of these sensors are not specifically dependent of the type of dissolved ions; but rather dependent of the environmental ionic strength.

As the ionic strength increases, the energy transfer efficiency decreases regardless the type of ions dissolved in the Hofmeister salt-supplemented buffers. In addition, the donor-acceptor distance (R_{DA}) of RE, RD, and KE increases as the ionic strength increases in the Hofmeister salt-supplemented buffers, independent of the type of ions dissolved.

Therefore, the FRET biosensors are unable to distinguish between different ions in solution or living cells but are robust to fluctuations in the ionic strength, such as those that are experienced in living cells. These results are beneficial for future live cell studies because the levels of ionic strength of specific salts varies of different magnitudes and thus there is a need for a general and robust ionic strength sensor (24, 62).

The bottom line is that is not clear to us how to interpret the observed trends of E6G2 as a function of the ionic strength. Because the β-barrel is known to be protective of the embedded chromophore in both mCerulean3 and mCitrine in E6G2, it is unlikely that these ions may penetrate the barrel to get closer to the chromophore leading to the observed sensitivity of R_{DA} to the ionic strength. In addition, the α-helices in the linker region are neutral and therefore unlikely to be affected by the changes in ionic strength and the type of dissolved ions. On the other hand, one may argue that at higher ionic strength, the ions may electrostatically interacts with the exterior amino acids of both mCerulean3 and mCitrine in E6G2, which may lead to some type of a long-range electrostatic interactions among the donor and acceptor and therefore a reduced R_{DA}.

To test these arguments of ion hydration and the electrostatic interaction of dissolved ions with the exterior amino acids of mCitrine and mCerulean3, we carried out time-resolved fluorescence polarization anisotropy of RD, RE, KE, and E6G2 in the presence of KCl at different ionic strengths. These results are outlined in Chapter 5.

Chapter 5:

Rotational-Dynamics Approach for FRET Analysis of Ionic-Strength Biosensors to the Presence of Potassium Chloride (KCl)

5.1 Rationale

Time-resolved fluorescence and the excited-state dynamics of hetero-FRET pairs are sensitive to many environmental parameters such pH, viscosity, charge transfer, conformational changes, photophysical processes, association reactions, and oxygen (63). These environmental parameters may complicate data interpretation and FRET analysis towards the assessment of the energy transfer efficiency and the donor-acceptor distance. This in return may skew the assessment of the sensitivity of these biosensors to the environmental ionic strength. As a result, there is a need for a new FRET analysis approach that would complement the traditional methods employed for energy transfer energy measurements such as steady-state spectroscopy and fluorescence lifetime.

Here we employed a new approach (Figure 5.1) developed in our laboratory (11, 26, 59) to investigate the energy transfer efficiency and the donor-acceptor distance of these ionic-strength sensors in KCl-supplemented buffer. In this approach, we used time-resolved fluorescence polarization anisotropy to quantify the rotational dynamics of the donor in the presence and absence of the acceptor in RD, RE, and KE. As a reminder, in time-resolved fluorescence approach (Chapters 3 & 4), the donor was excited (425 nm) and its emission was detected (475/50 nm) in the presence and absence of the acceptor as a function of the environmental ionic strength. In contrast, time-resolved anisotropy was carried out where the donor (mCerulean3) is excited using 425 nm while the fluorescence depolarization (i.e., parallel and perpendicular emission) of the acceptor (mCitrine) was detected at 530/40 nm as described in Figure 5.1 and in Chapter 2. Because the MCP detectors do not recognize whether the polarization-analyzed fluorescence photons are emitted by the donor or the acceptor, this experimental design provides an opportunity to determine the energy transfer rate (k_{ET}) as described in Chapter 2 (Section 5.3). Here we assume that the sampled FRET probes will consist of two subpopulations, one undergoing FRET and another that does not. Such assumption is supported by our

experimental observations. The underlying fitting model in this rotational-dynamic approach is valid when there is no spectral overlap of the donor and acceptor fluorescence emissions as well as negligible direct excitation of the acceptor at 425 nm (11, 12).

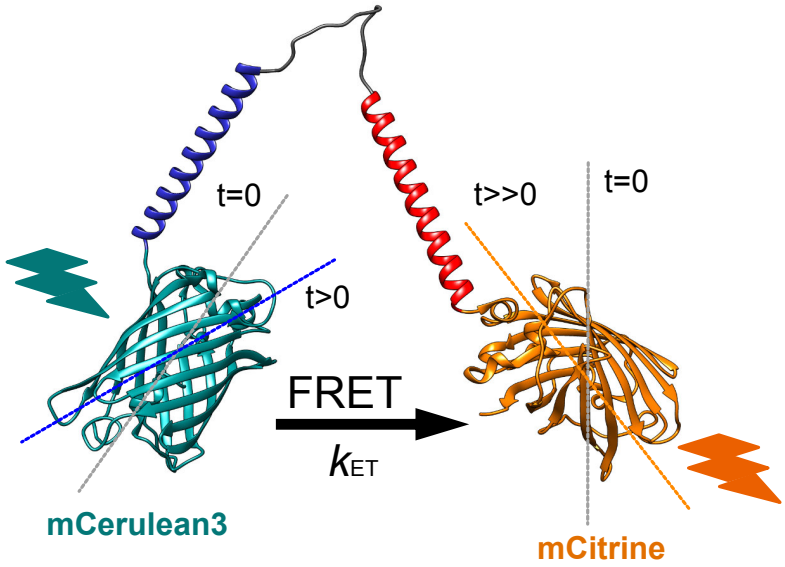

Figure 5.1: Illustration of the ionic strength protein-based hetero-FRET sensors and schematic of the time-resolved polarized fluorescence anisotropy detection and excitation conditions where one-photon laser pulses (425 nm) were generated to excite the donor fluorophore and the polarization analysis was performed on the acceptors fluorescence emission using a 530/40 nm band pass filter. Importantly, this illustrates the rapid depolarization of the fluorescence emission, in comparison to the polarized laser excitation pulse, due to the ability of the donor and acceptor fluorophores to rotate freely from one another.

In this rotational dynamics approach using the ionic strength FRET sensors, time-resolved anisotropy was calculated using the time-resolved fluorescence at parallel and perpendicular polarizations, which are detected simultaneously to avoid any artifacts due to laser instability. The corresponding anisotropy decays were acquired for both intact and cleaved FRET sensors in buffer (10 mM NaPi, pH 7.4) and as a function of the ionic strength in KCl-supplemented buffer (0–500 mM). Comparative time-resolved anisotropy

measurements on E6G2 were carried out under the same experimental conditions as a control due to its neutral amino acids in the linker region. These rotational dynamics approach would enable us to test the hypothesis that the electrostatic interaction between the charged α-helices in the flexible linker region would be reduced at high ionic strength due to the ionic screening, which would lead to reduced energy transfer efficiency and increased donor-acceptor distance. All nonlinear regression FRET analysis was carried out as described in Section 5.2 and calculations for energy transfer efficiency and donor-acceptor distances are outlined in Section 2.5.1.

We anticipate that a number of fast photophysical processes (i.e., molecular blinking, triplet dark states, or multiple FRET populations) may be at play in these FRET sensors. As a result, we used a robust method of nonlinear regression model based on the Akaike information criterion (64, 65) in our time-resolved anisotropy analysis. The results of this statistical model selection indicated that the biexponential model best represents the anisotropy decays of the intact ionic strength FRET pairs and therefore all energy transfer efficiency and donor-acceptor distance calculations were carried out as described in Chapter 2.

5.2 Results and Discussion

5.2.1 The intact and cleaved biosensors have distinct anisotropy decays and rotational dynamics

To test the sensitivity of rotational dynamics approach for FRET analysis, we measured time-resolved anisotropy of cleaved and intact of the ion-stregnth sensors in sodium phosphate buffer. Figure 5.2 shows a representative time-resolved anisotropy of cleaved and intact RD in buffer at room temperature, where the donor was excited at 425 nm and the acceptor's emission was polarization analysed and detected at 530/40 nm. The results show that the cleaved RD decays as a single exponential with a rotational time of ~27 ns, which is consistent with its molecular wight of 61 kDa. In contrast, the intact RD decays as a biexponental with a faster component (~1 ns, amplitude fraction = 0.106, Table S1.2) and a slow rotation time constant of 29 ns (amplitude fraction = 0.096, Table S1.2). The time-constant of the fast decay component of the time-resolved

anisotropy of the intact RD equals to the sum of both the rotational rate (1/rotational time constant) of the overall protein plus the energy tansfer rate (k_{ET}) as described in Chapter 2 (Equations 2.11–2.12).

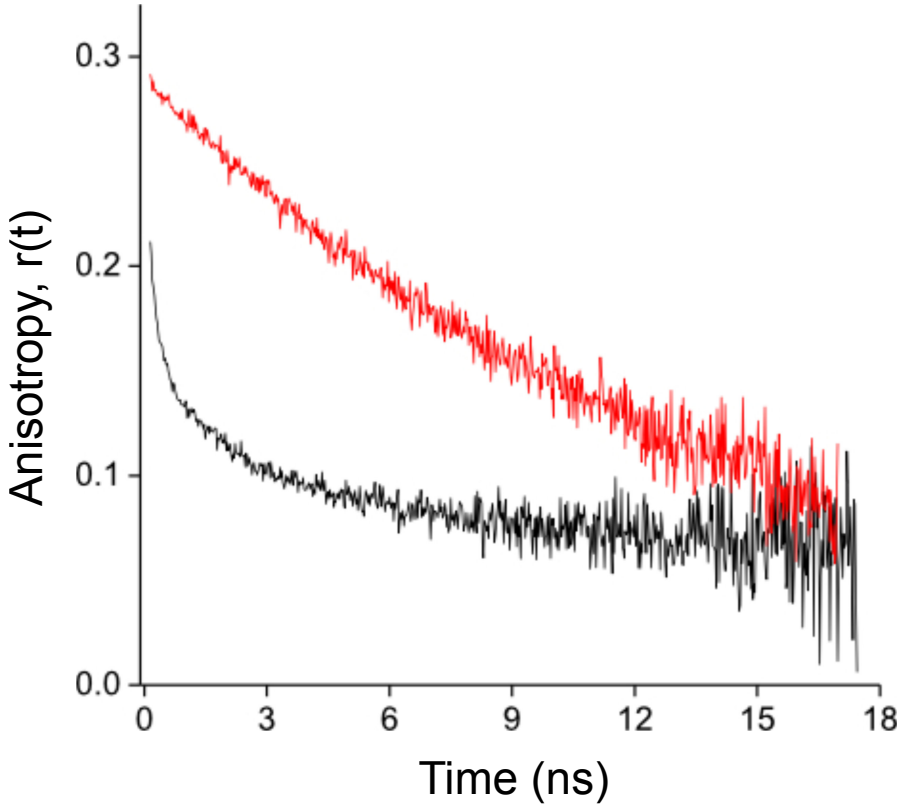

Figure 5.2: Representative anisotropy decays of the intact (black) and cleaved (red) biosensor, RD, in a 10 mM sodium phosphate (NaPi) buffer solution, pH 7.4. The diminished initial anisotropy, $r_o(t)$, (magnitude of the signal at t=0) of the intact sample was attribute to the signal acquisition approach of exciting the donor and monitoring the depolarization analysis of the fluorescence emission of the acceptor fluorophore. The cleaved and intact samples decayed according to a single and double exponential function, respectively. The cleaved rotational time (ϕ_{DA}) and amplitude fraction were determined via nonlinear regression to be 27 ns and 0.294, respectively and the anisotropy decay fitting parameters of the intact RD can be found in Table S1.2 of the appendix.

In the remaining Sections of this Chapter, the fast comonent of the time-resolved anisotropy of FRET biosensors will be used to calculate the corresponding energy transfer efficiency (E) and the donor-acceptor distance in a given KCl solution and an ionic strength. In addition, the intial anisotropy (r_o) at time-zero of the anisotropy decay

of the intact RD is significantly smaller that of the cleaved counterpart, which is attributed to nonradiative energy transfer from the donor to the acceptor.

5.2.2 Examining the effects of ion hydration on the rotational dynamics of the ionic strength sensor

To examine whether the hydrated ions in the buffer solution impacts the electrostatic interaction between the mCerulean3 (or mCitrine) or how the disolved ion may influence the rotational dynamics of the FRET biosensor, we conducted a time-resolved anisotropy on cleaved and intact RD in both the presence and absence of 500 mM KCl at room remperature.

Figure 5.3 shows a representative time-resolved anisotropy of cleaved RD both the presence and absence of 500 mM KCl at room temperature. The results show that the anisotropy of cleaved RD in both buffer and 500 mM KCl decays as a single exponential with rotational times of 14.3 ns and 14.4 ns, respectively.

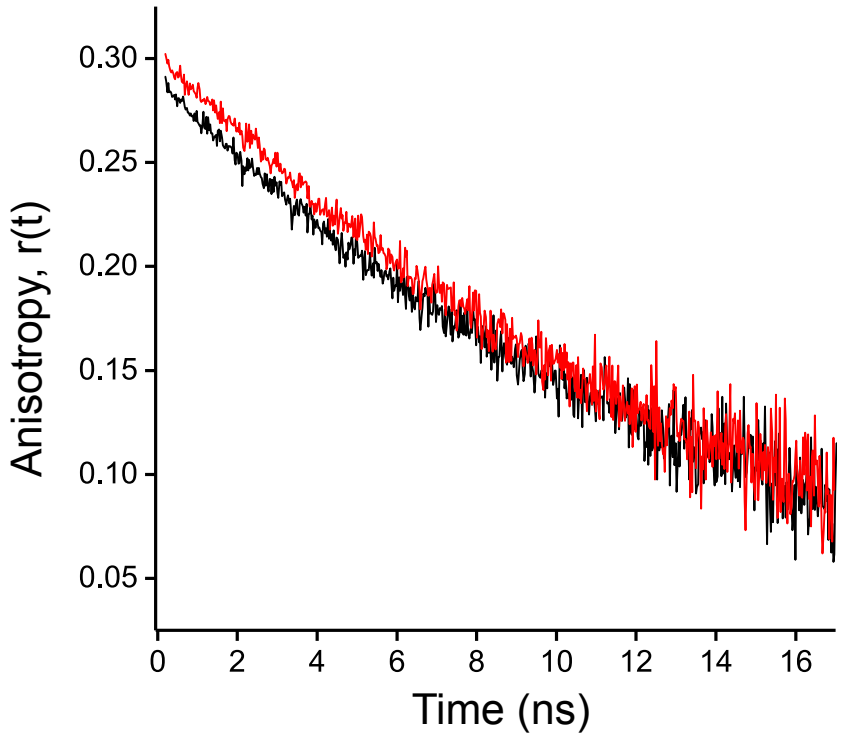

Figure 5.3: Representative anisotropy decays of the cleaved biosensor, RD, in a 10 mM sodium phosphate (NaPi) buffer solution, pH 7.4, at both 0 mM (black) and 500 mM (red) KCl. The small deviation in the initial anisotropy is likely due to minor fluctuations in sample preparation and overall the FRET-incapable (donor alone) species indicated no sensitivity to the presence of KCl ions on the range of 0–500 mM. The cleaved rotational time (ϕ_{DA}) and amplitude fraction at both 0 and 500 mM were determined via nonlinear regression to be 14.3 ns and 0.291, and 14.4 ns and 0.303, respectively.

Assuming that the cleavage reaction is complete and without any segment of the charged α-helices remained attached to the β barrel of mCerulean3, these results suggest minor ion-mCerulean3 interactions. Such interaction may involve some ions being attached to the exterior of the β-barrel where polar or charged amino acids will be found. Another possibility could be that some of the K^+ or Cl^- ions in the KCl solution may penetrate the β-barrel towards the embedded chromophore, where the spectroscopy of the mCerulean3 is likely to be affected.

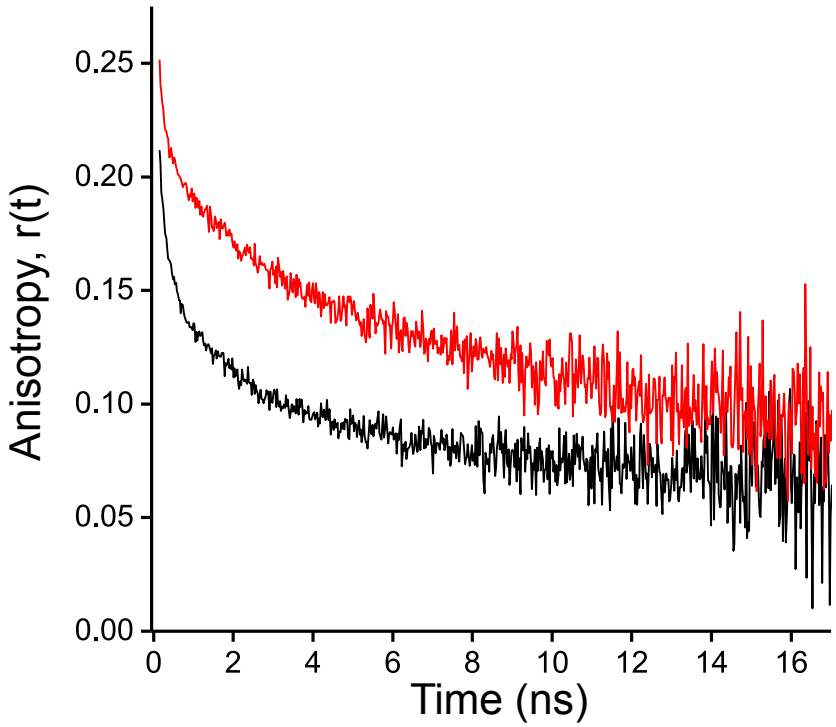

Figure 5.4: Representative anisotropy decays of the intact biosensor, RD, in a 10 mM sodium phosphate (NaPi) buffer solution, pH 7.4, at both 0 mM (black) and 500 mM (red) KCl. The small deviation in the initial anisotropy is likely due to minor fluctuations in sample preparation and overall the FRET-capable species indicated a strong sensitivity to the presence of KCl ions on the range of 0–500 mM. In both the 0 and 500 mM samples, the anisotropy decayed was modeled using a biexponential model (Equation 2.11), where the rapid decay at early time steps is attributed to the presence of FRET. The fitting parameters of the 0 and 500 mM KCl RD anisotropy decays were determined to be (β_{slow} = 0.096, ϕ_{DA} = 29 ns, β_{fast} = 0.106, k_{ET} = 0.96 ns^{-1}) and (β_{slow} = 0.140, ϕ_{DA} = 29 ns, β_{fast} = 0.059, k_{ET} = 0.5 ns^{-1}), respectively (Table S1.2).

When we repeated similar time-resolved anisotropy measurements of intact RD in both buffer and 500 mM KCl solution, we observed a drastic difference as shown in Figure 5.4. The time-resolved anisotropy of intact RD in buffer decays as a biexponential (Equations 2.11–2.12), where the rate constant (k_{ET} = 0.96 ns^{-1}) and amplitude fraction (52 %, Table S1.2) of the fast decay component is significantly larger than that in 500 mM KCl solution. This can be interpretded in terms of enhanced energy transfer efficiency in buffer due to the electrostatic interactions between the charged α-helices in the linker region. This is in line with our stated hypothesis where such interactions

decrease as the ionic strength increases due to ion screening. Our fitting parameters of the slow anisotropy decay components in other biosensors, KE for example, in buffer (19.7 ns) and buffer containing 500 mM KCl (23.7 ns) can be interpreted in terms of the rotational motion of a folded versus stretched (open confirmation) biosensor, respectively (Table S1.2).

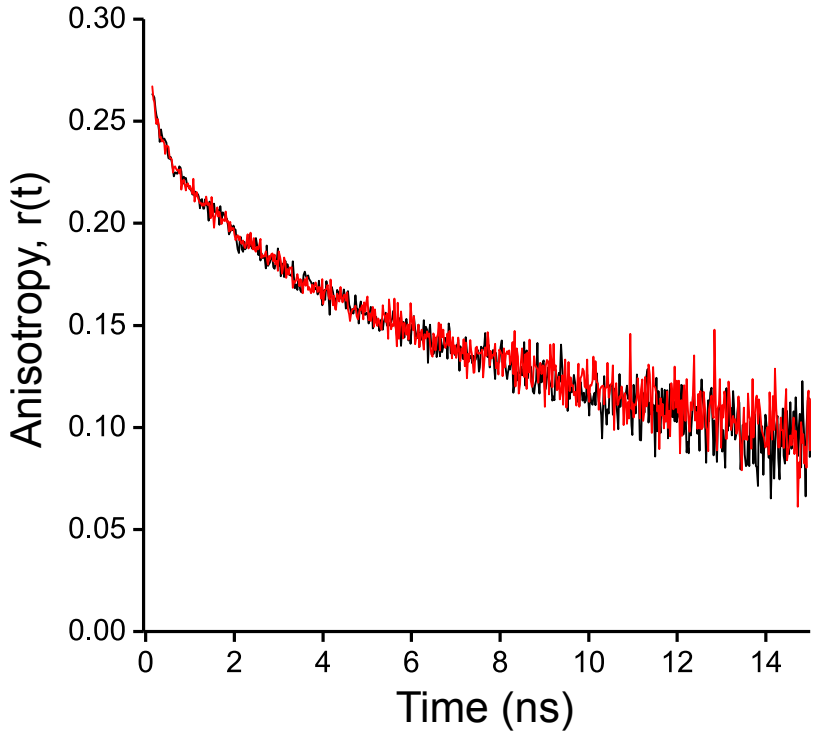

Figure 5.5: Representative anisotropy decays of the intact biosensor, E6G2, in a 10 mM sodium phosphate (NaPi) buffer solution, pH 7.4, at both 0 mM (black) and 500 mM (red) KCl. In both the 0 and 500 mM samples, the anisotropy decayed was modeled using a biexponential model (Equation 2.11), where the rapid decay at early time steps is attributed to the presence of FRET. The fitting parameters of the 0 and 500 mM KCl E6G2 anisotropy decays were determined to be (β_{slow} = 0.195, ϕ_{DA} = 20.9 ns, β_{fast} = 0.059, k_{ET} = 0.40 ns^{-1}) and (β_{slow} = 0.192, ϕ_{DA} = 21.4 ns, β_{fast} = 0.060, k_{ET} = 0.50 ns^{-1}), respectively (Table S1.2).

Interestingly, the anisotropy decays of intact E6G2, in both the presence and absence of 500 mM KCl, are perfectly overlapping (Figure 5.5). The time-resolved anisotropy measurements of intact E6G2 decays in 0 and 500 mM KCl as a biexponential

(β_{slow} = 0.195, ϕ_{DA} = 20.9 ns, β_{fast} = 0.059, k_{ET} = 0.40 ns^{-1}) and (β_{slow} = 0.192, ϕ_{DA} = 21.4 ns, β_{fast} = 0.060, k_{ET} = 0.50 ns^{-1}), respectively (Table S1.2), where the fast component is assigned to a subpopulation of E6G2 undergoing FRET between mCerulean3 and mCitrine (see below). In our model, we assign the slow rotational component of these anisotropy decays are assigned to the subpoulation of E6G2 that do not undergo FRET.

5.2.3 The energy transfer efficiency of KE sensor as a function of the ionic strength in KCl solution as measured using time-resolved anisotropy

To test the sensitivity of the rotational dynamics-based model for FRET analysis, we carried out time-resolved anisotropy of intact and cleaved KE and E6G2 (as a control) as a function of the ionic strength of KCl-supplemented buffer (0–500 mM). The corresponding energy transfer efficiency of KE, in each ionic-strength solution, was then calculated as described in Chapter 2 (Equations 2.8–2.9) and the results are shown in Figure 5.6 below.

Using the energy transfer rate approach, weighted by the population fraction of undergoing FRET (Equation 2.9), KE exhibits ~43 % energy transfer efficiency in buffer. The observed large *E*-value in buffer is attributed to the electrostatic interaction between the α-helices of the linker region and therefore a smaller donor-acceptor distance (see below). In addition, the energy transfer efficiency KE decreases as the ionic strength of the KCl solution increases, which support our stated hypothesis above. In contrast, the energy transfer efficiency of E6G2, calculated using the same approach, exhibits a smaller *E*-value (~21 %) due to the neutral amino acids sequence of the linker. In addition, the energy transfer efficiency of E6G2 remains the same with a negligible increase as the ionic strength of the KCl solution increases. It is worth mentioning that the anisotropy-based energy transfer efficiency of both KE and E6G2 in buffer is significantly larger (~15 and 10 % difference in magnitude, respectively) than that estimated using the fluorescence lifetime of the donor in the presence and absence of the acceptor. This observation can be attributed to the multiple environmental parameters that

may influence the excited-state dynamics probed using time-resolved fluorescence using magic-angle detection.

When the time-resolved anisotropy were analyzed using the k_{ET}-value based on the fast decay component, without being weighted using the subpopulation fraction undergoing FRET, the calculated energy transfer efficiency is almost twice the *E*-value calculated using the weighted approach mentioned above and as shown in Figure 5.6 (Bottom). As a reminder, these large *E*-values is only for the population of KE undergoing FRET, which is expected to be larger than that using an ensemble-averaged or weighted rate approach (Figure 5.6, Top) as shown previously (Chapter 3). The observed large *E*-value using this approach may also be due to the possibility of direct observation of acceptor under 425-nm excitation as well as the spectral overlap between the fluorescence emission of both the donor and acceptor in these FRET sensors.

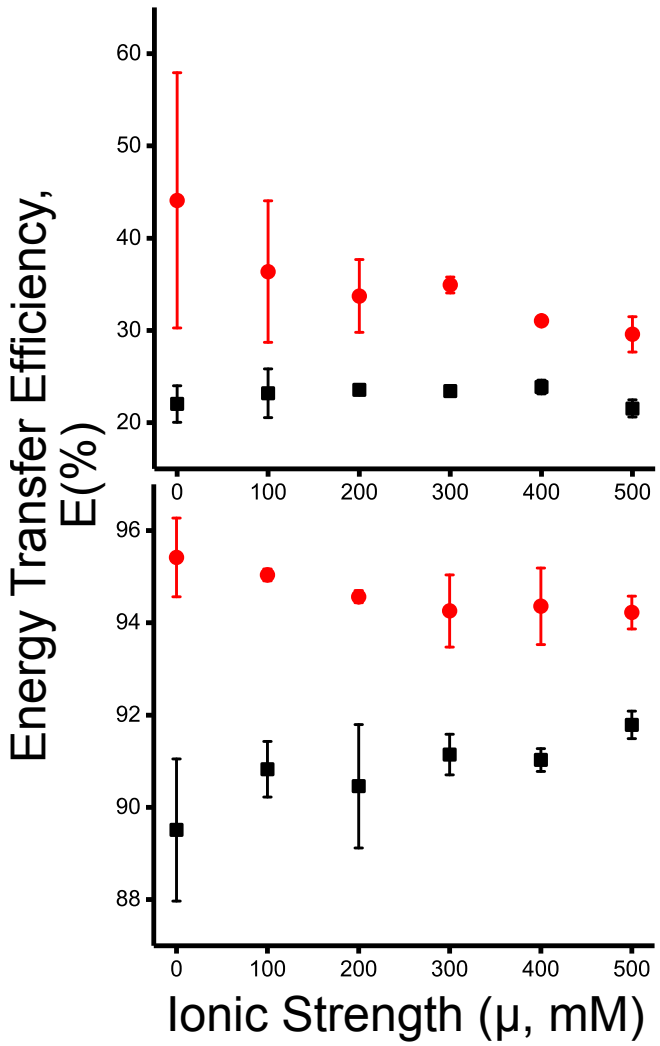

Figure 5.6: The energy transfer efficiency, *E*(%) of the ionic strength biosensor KE (red, circles) and the control biosensor E6G2 (black, squares) as a function of increasing ionic strength (μ) due to the presence of KCl ions over a range of 0–500 mM (0, 100, 200, 300, 400, and 500 mM). The top panel (A) displays the weighted energy transfer efficiency (Equation 2.9) and the bottom panel (B) displayed the unweighted energy transfer efficiency (Equation 2.8), which does not consider the fractional population of excited fluorophores undergoing FRET.

5.2.4 The effects of the amino acid sequence in the linker region on the energy transfer efficiency of the FRET sensors as a function of the ionic strength in KCl solution

Thus far, we have established that the time-resolved anisotropy approach provides a means to assess the energy transfer efficiency of KE and E6G2 as a function of the ionic strength in KCl solution. Now, we want to examine the sensitivity of this approach to the difference in the amino acid sequence of the linker region of these probes. Towards this objective, similar time-resolved anisotropy measurements on intact and cleaved RD and RE sensors were carried out as a function of the ionic strength in KCl-supplemented buffer.

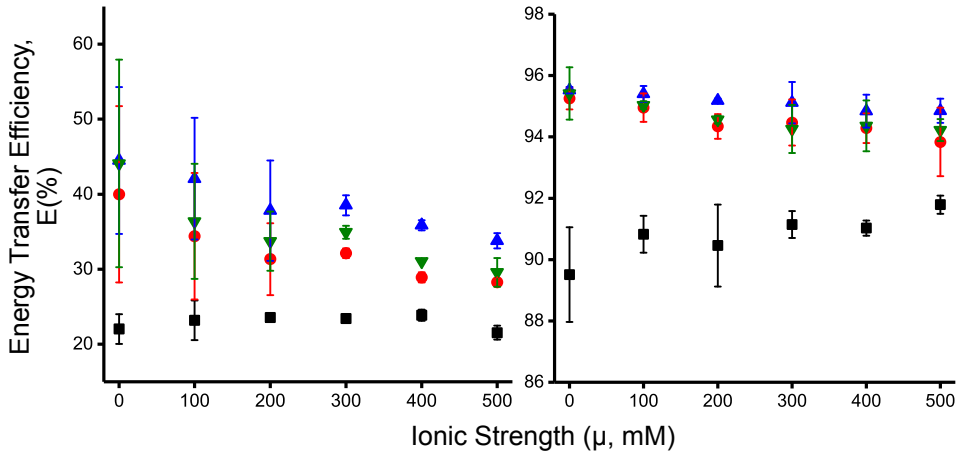

Figure 5.7: The energy transfer efficiency, *E*(%), from time-resolved polarized fluorescence anisotropy measurements of the protein-based hetero-FRET biosensors RD (red, circle), RE (blue, upright triangle), KE (green, inverted triangle), and E6G2 (black, square) in the presence of increasing ionic strength (0, 100, 200, 300, 400, 500 mM) as calculated using the two approaches for the rate determined method (Left=weighted, Right=unweighted) discussed in Chapter 2 of this Thesis. Error bars represent the standard error of the mean as calculated from replicate anisotropy measurements.

Figure 5.7 shows a summary of the energy transfer efficiency of RE, KE, RD, and E6G2 as a function of the ionic strength in KCl-containing buffer at room temperature. The figure also shows two approaches for calculating the energy transfer efficiency using weighted (Figure 5.7, Left) and unweighted (Figure 5.7, Right) energy transfer rate (k_{ET})

as described in Chapter 2. While the energy transfer efficiency (E) using time-resolved anisotropy is relatively larger than that calculated using time-resolved fluorescence, the observed trends remain the same. For example, the E-value of RE, RD, and KE decreases as the ionic strength increase due to the electrostatic screening in support of our hypothesis. In addition, the KE sensor exhibit a relatively larger dynamic range than RE and RD counterparts. In contrast, the energy transfer efficiency of E6G2 exhibits negligible sensitivity to the environmental ionic strength in KCl-containing buffer. The weighted energy transfer rate (k_{ET}) approach (Figure 5.7, Left) yields an energy transfer efficiency that is approximately half of the corresponding value using the unweighted approach (Figure 5.7, Right) due to the ensemble averaging for both subpopulations of excited sensors, where a fraction of the excited molecules are simply undergoing fluorescence decay rather than FRET.

5.2.5 The effect of the amino acid sequence in the linker region on the donor-acceptor distance the FRET sensors as a function of the ionic strength in KCl solution

Using the estimated energy transfer efficiency using time-resolved anisotropy measurements (Section 5.3.4), we calculated the corresponding donor-acceptor distance (R_{DA}) for RE, RD, KE and E6G2 as a function of the ionic strength in KCl-supplemented buffer (Figure 5.8) as outlined in Chapter 2. These R_{DA} was calculated using two different approaches based on the corresponding E-values estimated using weighted (Figure 5.8, Left) and unweighted (Figure 5.8, Right) energy transfer efficiency shown in Figure 5.7.

The results suggest in the absence of KCl, the FRET biosensor (RE, RD, and KE) adapts a compact (folded) configuration with the smallest donor-acceptor distance due to the electrostatic interactions between the charged α-helices. In addition, such electrostatic interactions seem stronger in both KE and RE than that of RD in buffer. As the ionic strength increases, the donor-acceptor distance increases in KE, RE, and RD regardless of the method of calculation (i.e., weighted versus unweighted energy transfer rate, k_{ET}). It is worth mentioning that KE exhibit a relatively larger dynamic range concerning the conformational changes (R_{DA}) than that of RE and RD (Figure 5.8). By comparison, the donor-acceptor distance in E6G2 seems larger than that of these ionic-strength sensors

due to the both the lack of electrostatic interaction between neutral α-helices and the relatively stiff (less flexible) linker. The sensitivity of R_{DA}-values in E6G2 to the ionic strength in KCl-supplmented buffer seems negligible (Figure 5.8, solid squares).

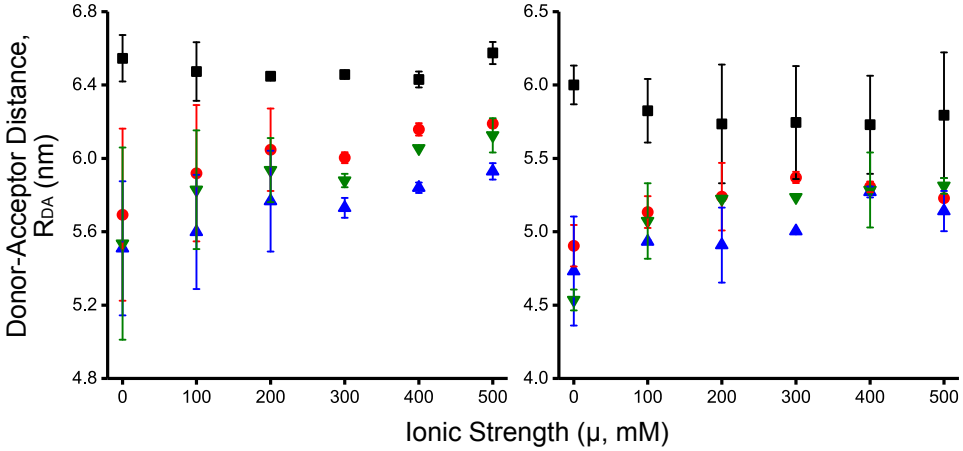

Figure 5.8: The donor-acceptor distance, R_{DA}, from time-resolved polarized fluorescence anisotropy measurements of the protein-based hetero-FRET biosensors RD (red, circle), RE (blue, upright triangle), KE (green, inverted triangle), and E6G2 (black, square) in the presence of increasing ionic strength (0, 100, 200, 300, 400, 500 mM) as calculated using the two approaches for the rate determined method (Left=weighted, Right=unweighted) discussed in Chapter 2 of this Thesis. The relative donor-acceptor distances were calculated assuming a constant Förster distance of 5.3 ± 0.2 nm under all KCl concentrations. Error bars represent the standard error of the mean as calculated from replicate anisotropy measurements.

Taken together, these results are in general agreement with our findings using time-resolved fluorescence as described in Chapters 3 and 4. In addition, our anisotropy-based findings support our stated hypothesis that the dissolved ions in KCl solution screen the electrostatic interaction between the charged α-helices in these ionic sensors, which lead to enhanced donor-acceptor distance and therefore reduced energy transfer efficiency between mCerulean3 and mCitrine.

5.3 Conclusions

We carried out time-resolved anisotropy on a set of hetero-FRET sensors as a means to develop a new, complementary rotational dynamics approach for FRET analysis, where the donor was excited at 425 nm and the emission of the acceptor was detected at 530/40 nm. Our rationale is that the overall depolarization of the epifluorescence, measured using time-resolved polarization anisotropy, would provide valuable information on both the rotational dynamics of these FRET sensors (RE, RD, and KE) and the energy transfer rate (k_{ET}) that can be used to calculate the energy transfer efficiency as well as the donor-acceptor distance in a given environment.

Our results demonstrate that the rotational dynamics of both the cleaved and intact FRET sensor such as RD are distinct in buffer at room temperature. The fast component in the time-resolved anisotropy depends on both the rotational diffusion rate of the construct and the energy transfer rate (k_{ET}). In contrast, the slow rotational decay component is assigned to the overall rotational diffusion rate of the intact FRET sensor.

We also examined whether the ion hydration, protein-ion, and linker-ion interactions may influence the rotational dynamics of these hetero-FRET sensors. Towards this goal, we carried out time-resolved anisotropy of both cleaved and intact RD sensor in both the presence and absence of 500 mM KCl at room temperature. For the cleaved RD, we observed minor difference in the rotational dynamics that can be attributed to some ions penetrating the β-barrel of mCerulean3. Based on Figure 2.1, SDS-PAGE gel, we believe the possibility of incomplete cleavage with a small segment of the linker remaining attached to the mCerulean3 seems negligible.

Interestingly, when the same measurements were repeated on intact RD, a distinguishable difference in the rotational dynamics in both the presence and absence of 500 mM KCl was observed. Such rotational behavior was attributed to the stretched structural conformation of RD due to the ionic screening of the charged α-helices, which leads to a reduced electrostatic interactions and larger donor-acceptor distance. In contrast, the rotational dynamics of intact E6G2 is exactly the same in both the presence

and absence of 500 mM KCl. This confirms that the dissolved ions (K^+ and Cl^-)do interact with the neutral amino acid residues in the linker region, as compared with that in RE, RD, and KE.

We also examined whether time-resolved anisotropy approach is sensitive to the conformational changes and sensitivity of these sensors to the ionic strength in KCl-supplemented buffer due to the difference in the charged amino acid sequences in the linker regions. Our results indicate that the energy transfer efficiency (E) in RE, RD, and KE decreases as the ionic strength of KCl solution increase; independent of the way we employed the measured energy transfer rate (k_{ET}). Assuming Förster distance of 5.3 nm for these FRET pairs, we also calculate the corresponding donor-acceptor distance as a function of both the amino acid sequence and the ionic strength. Our results indicate that the donor-acceptor distance of RE, RD, and KE increases as the ionic strength of KCl solution increase. This is in a general agreement with our previous findings time-resolved fluorescence of the donor in these ionic sensors (Chapters 3 and 4). In contrast to these ionic sensors, the sensitivity of both the energy transfer efficiency and the donor-acceptor distance of E6G2 to the environmental ionic strength are negligible in KCl-containing buffer. These results are attributed to the neutral αhelices in E6G2 as compared with the charged counterparts in RE, RD, and KE.

Overall, these results validate our newly developed time-resolved anisotropy approach for FRET analysis for these ionic strength sensors, while complementing the other traditional time-resolved fluorescence and steady-state spectroscopy approaches. Importantly, these results support our stated hypothesis concerning the structural conformational changes in response to environmental ionic strength as the underlying mechanism for their ionic sensitivity.

Chapter 6:

Conclusions and Future Directions

In this Thesis project, we investigated the sensitivity of newly developed genetically encoded mCerulean3–linker–mCitrine constructs (namely, KE, RD, and RE) using integrated fluorescence spectroscopy. In these ionic-strength sensors, mCerulean3 (donor) to mCitrine (acceptor) constitute a FRET pair where the energy transfer efficiency and donor-acceptor distances are sensitive to the environmental ionic strength. The rationale here is that the linker consists of two charged α-helices that undergo a strong electrostatic interaction in 10 mM sodium phosphate (i.e., a reduced donor-acceptor distance and therefore enhanced FRET in the absence of salt). As the environmental ionic strength increases, the dissolved ions screen the charged α-helices in the linker region, which reduces the strength of their electrostatic interactions and therefore increases donor-acceptor distances (i.e., reduced energy transfer efficiency).

To date, these sensors have been characterized in a cuvette using steady-state spectroscopy, where the relative fluorescence intensity of the donor and acceptor was used for qualitative assessment of the energy transfer efficiency as a function of ionic strength. However, this approach suffers from some disadvantages and incompatible with live cell imaging, inherently hindering the ultimate goal of using these sensors to quantify the compartmentalized ionic strength in living cells noninvasively. Towards this goal, we employed time-resolved fluorescence measurements as a means to determine the fluorescence lifetime of the first excited electronic state of these sensors as a function of ionic strength. Here, the donor (mCerulean3) was excited using 425-nm laser pulses and its fluorescence emission was detected at 475/50 nm. In addition of using the average fluorescence lifetime of the donor in the presence and absence of the acceptor, we have developed a new model for FRET analysis using the directly measureable energy transfer rate. To mimic the environmental ionic strength of living cells, we investigated these sensors in buffer supplemented with the Hofmeister series of salts (KCl, LiCl, NaCl, NaBr, NaI, or Na_2SO_4).

Because the fluorescence lifetime of a given fluorophore is sensitive to other environmental parameters, we also used a complementary approach to monitor the excited-state rotational dynamics for FRET analysis. In this new approach, we used time-resolved fluorescence polarization anisotropy of these sensors as a function of the ionic strength. Here, the donor (mCerulean3) was excited using 425-nm laser pulses and the fluorescence depolarization of the acceptor (mCitrine) was detected at 531/40 nm.

In either time-resolved fluorescence or time-resolved anisotropy of the intact RE, RD, and KE, biexponential decays were observed regardless the environmental ionic strength. In some of the models used for FRET analysis, we used the time-constant of the fast decay component to calculate the energy transfer rate (k_{ET}) from the donor to the acceptor. The estimated rates were then used to calculate the corresponding energy transfer efficiency (E) and the donor-acceptor distance (R_{DA}) of each sensor as a function of the environmental ionic strength.

Our results indicate that the fluorescence lifetime of the donor in these sensors is sensitive to the presence of the acceptor in close proximity (<10 nm). In addition, the fluorescence lifetime of the donor in the intact sensors (RD, RE, and KE) is sensitive to both the amino acid sequence of the linker region as well as the environmental ionic strength. In contrast, the fluorescence lifetime of E6G2 (control) with the neutral amino acids in the linker region exhibit negligible sensitivity to the environmental ionic strength. In addition, the fluorescence lifetime of the donor in the cleaved sensors is also constant, independent of the environmental ionic strength. Our results also support the hypothesis that as the ionic strength increases (0–500 mM KCl), the energy transfer efficiency, E(%), decreases and the donor-acceptor distance, R_{DA}, increases, regardless of the model used for FRET analysis using these fluorescence lifetime measurements. This observation is attributed to ionic screening of the charged α-helices in the linker region in KCl solution with larger ionic strength, which leads to a reduced electrostatic interaction and therefore enhanced donor-acceptor distance. While the trends are similar in the three methods used for FRET analysis, the estimate energy transfer efficiency and donor-acceptor distance of each sensor population that undergo FRET was significantly different the ensemble-averaged estimates.

Because the intracellular ionic strength contains different types of ions, it is important to examine the sensitivity of these sensors to different types of ions or salts. As a result, we used time-resolved fluorescence measurements of RD, RE, and KE sensors as a function of the ionic strength of the Hofmeister salt (KCl, LiCl, NaCl, NaBr, NaI, and Na_2SO_4). As a control, we also carried out similar measurements on the cleaved counterpart (i.e., mCerulean3 alone) of these sensors as well as E6G2 with the neutral amino acid sequence in the linker region. Regardless the model used for FRET analysis, our results do not support the hypothesis that the sensitivity of the RD, RE, and KE sensors will be ion-specific as the ionic strength varied in buffers supplemented with the Hofmeister salt series (KCl, LiCl, NaCl, NaBr, NaI, or Na_2SO_4). In other words, our results suggest that the energy transfer efficiency and the donor-acceptor distance of these sensors are not specifically dependent of the type of dissolved ions; but rather dependent of the environmental ionic strength. As the ionic strength increases, the energy transfer efficiency decreases regardless the type of ions dissolved. In addition, the donor-acceptor distance (R_{DA}) of RE, RD, and KE increases as the ionic strength increases, independent of the type of ions dissolved. Therefore, the FRET biosensors are unable to distinguish between different ions in solution or living cells but are robust to fluctuations in the ionic strength, such as those that are experienced in living cells. This is beneficial to live cell studies as the levels of ionic strength of specific salts varies of different magnitudes and therefore there is a need for a general and robust ionic strength sensor (24, 62).

To test these arguments of ion hydration and the electrostatic interaction of dissolved ions with the exterior amino acids of mCitrine and mCerulean3, we carried out complementary time-resolved fluorescence polarization anisotropy of RD, RE, KE, and E6G2 for FRET analysis at different ionic strength of KCl-supplemented buffer. Our results demonstrate that the rotational dynamics of both the cleaved and intact FRET sensor, such as RD, are distinct in buffer at room temperature. The fast component in the time-resolved anisotropy depends on both the rotational diffusion rate of the construct and the energy transfer rate (k_{ET}). In contrast, the slow rotational decay component is assigned to the overall rotational diffusion rate of the intact FRET sensor. We also examined whether the ions hydration, protein-ion, and linker-ion interactions may

influence the rotational dynamics of these hetero-FRET sensors. Towards this goal, we carried out time-resolved anisotropy of both cleaved and intact RD sensor in both the presence and absence of 500 mM KCl at room temperature. For the cleaved RD, we observed minor difference in the rotational dynamics that can be attributed to some ions penetrating the β-barrel of mCerulean3. We believe the possibility of incomplete cleavage with a small segment of the linker remaining attached to the mCerulean3 seems negligible. Interestingly, when the same measurements were repeated on intact RD, a drastic difference in the rotational dynamics in both the presence and absence of 500 mM KCl was observed. Such rotational behavior was attributed to the stretched structural conformation of RD due to the ionic screening of the charged α-helices, which leads to a reduced electrostatic interactions and larger donor-acceptor distance. In contrast, the rotational dynamics of intact E6G2 is exactly the same in both the presence and absence of 500 mM KCl. This confirms that the dissolved ions (K^+ and Cl^-) do interact with the neutral amino acid residues in the linker region, as compared with that in RE, RD, and KE.

We also examined whether time-resolved anisotropy approach is sensitive to the conformational changes and sensitivity of these sensors to the ionic strength in KCl-containing buffer due to the difference in the charged amino acid sequences in the linker regions. Our results indicate that the energy transfer efficiency (E) in RE, RD, and KE decreases as the ionic strength increases, independent of the way we employed the measured energy transfer rate (k_{ET}). Assuming Förster distance of 5.3 nm for these FRET pairs, we also calculated the corresponding donor-acceptor distance as a function of both the amino acid sequence and the ionic strength. Our results show that the donor-acceptor distance of RE, RD, and KE increases as the ionic strength increases. This is in general agreement with our previous findings of the time-resolved fluorescence of the donor in these ionic sensors. In contrast to these ionic sensors, the sensitivity of both the energy transfer efficiency and the donor-acceptor distance of E6G2 to the environmental ionic strength are negligible in KCl-containing buffer. These results are attributed to the neutral α-helices in E6G2 as compared with the charged counterparts in RE, RD, and KE. Overall, these results validate the newly developed time-resolved anisotropy approach for

FRET analysis for these ionic strength sensors, while complementing the other traditional time-resolved fluorescence and steady-state spectroscopy approaches. Importantly, these results support our stated hypothesis concerning the structural conformational changes in response to environmental ionic strength as the underlying mechanism for their ionic sensitivity.

Moving forward, we are currently developing a novel approach for quantifying the energy transfer efficiency of these sensors at a single-molecule level using fluorescence correlation spectroscopy (FCS). In new single-molecule approach, the molecular brightness (number of fluorescent photons/molecule) of mCerulean3 (donor) is directly measured, both in the presence and absence of mCitrine (acceptor). The measured molecular brightness of RD is then used to calculate the energy transfer efficiency and the corresponding donor-acceptor distance at the single-molecule level. This portion of the project is currently in preparation and will be published elsewhere. We are planning to examine the dynamic range and sensitivity of FCS-based approach to both the ionic strength and the amino acid sequence of the linker region.

Finally, we already have access to the DNA plasmid of some of these sensors and are in the process of expressing them in living eukaryotic cells. Our objective is to employ these integrated fluorescence methods for noninvasive and quantitative mapping of the ionic strength throughout the cell. The ultimate goal is to correlate the compartmentalized ionic strength with cell pathophysiology using fluorescence lifetime imaging microscopy (FLIM).

References

1. Warshel, A., and S. T. Russell. 1984. Calculations of electrostatic interactions in biological systems and in solutions. Quarterly reviews of biophysics 17:283-422.
2. Honig, B., and A. Nicholls. 1995. Classical electrostatics in biology and chemistry. Science 268:1144-1149.
3. Nørby, J. G., and M. Esmann. 1997. The effect of ionic strength and specific anions on substrate binding and hydrolytic activities of Na, K-ATPase. The Journal of general physiology 109:555-570.
4. Mikhailov, A., and B. Hess. 1995. Fluctuations in living cells and intracellular traffic. Journal of theoretical biology 176:185-192.
5. Ellis, R. J., and A. P. Minton. 2003. Cell biology: Join the crowd. Nature 425:27-28. 10.1038/425027a.
6. Minton, A. P. 1992. Confinement as a determinant of macromolecular structure and reactivity. Biophys. J. 63:1090-1100.
7. Minton, A. P. 1995. Confinement as a determinant of macromolecular structure and reactivity. II. Effects of weakly attractive interactions between confined macrosolutes and confining structures. Biophys. J. 68:1311-1322.
8. Minton, A. P. 2001. The influence of macromolecular crowding and macromolecular confinement on biochemical reactions in physiological media. J. Biol. Chem. 276:10577-10580. Review.
9. König, I., A. Zarrine-Afsar, M. Aznauryan, A. Soranno, B. Wunderlich, F. Dingfelder, J. C. Stüber, A. Plückthun, D. Nettels, and B. Schuler. 2015. Single-molecule spectroscopy of protein conformational dynamics in live eukaryotic cells. Nature methods 12:773.
10. Straub, M., P. Lodemann, P. Holroyd, R. Jahn, and S. W. Hell. 2000. Live cell imaging by multifocal multiphoton microscopy. European journal of cell biology 79:726-734.
11. Leopold, H. J., R. Leighton, J. Schwarz, A. J. Boersma, E. D. Sheets, and A. A. Heikal. 2018. Crowding effects on energy-transfer efficiencies of hetero-FRET probes as measured using time-resolved fluorescence anisotropy. The Journal of Physical Chemistry B 123:379-393.
12. Schwarz, J., H. J. Leopold, R. Leighton, R. C. Miller, C. P. Aplin, A. J. Boersma, A. A. Heikal, and E. D. Sheets. 2019. Macromolecular crowding effects on energy transfer efficiency and donor-acceptor distance of hetero-FRET sensors using time-resolved fluorescence. Methods and applications in fluorescence 7:025002.
13. Biemans-Oldehinkel, E., N. A. Mahmood, and B. Poolman. 2006. A sensor for intracellular ionic strength. Proceedings of the National Academy of Sciences 103:10624-10629.
14. Syeda, R., Z. Qiu, A. E. Dubin, S. E. Murthy, M. N. Florendo, D. E. Mason, J. Mathur, S. M. Cahalan, E. C. Peters, and M. Montal. 2016. LRRC8 proteins form volume-regulated anion channels that sense ionic strength. Cell 164:499-511.
15. Berezhkovskii, A. M., and A. Szabo. 2016. Theory of crowding effects on bimolecular reaction rates. J. Phys. Chem. B 120:5998-6002.

16. Loo, S., and J. E. Erman. 1975. Kinetic study of the reaction between cytochrome c peroxidase and hydrogen peroxide. Dependence on pH and ionic strength. Biochemistry 14:3467-3470.
17. Cohen-Saidon, C., A. A. Cohen, A. Sigal, Y. Liron, and U. Alon. 2009. Dynamics and variability of ERK2 response to EGF in individual living cells. Molecular cell 36:885-893.
18. Wu, P., and L. Brand. 1994. Resonance energy transfer: Methods and applications. Analytical biochemistry 218:1-13.
19. Stryer, L. 1978. Fluorescence energy transfer as a spectroscopic ruler. Annu Rev Biochem 47:819-846.
20. Gopich, I. V., and A. Szabo. 2012. Theory of the energy transfer efficiency and fluorescence lifetime distribution in single-molecule FRET. Proc. Natl. Acad. Sci. U. S. A. 109:7747-7752.
21. Weiss, S. 1999. Fluorescence spectroscopy of single biomolecules. Science 283:1676-1683.
22. Censullo, R., J. C. Martin, and H. C. Cheung. 1992. The use of the isotropic orientation factor in fluorescence resonance energy transfer (FRET) studies of the actin filament. Journal of fluorescence 2:141-155.
23. Weiss, S. 2000. Measuring conformational dynamics of biomolecules by single molecule fluorescence spectroscopy. Nature Structural & Molecular Biology 7:724.
24. Liu, B., B. Poolman, and A. J. Boersma. 2017. Ionic strength sensing in living cells. ACS Chemical Biology 12:2510-2514.
25. Boersma, A. J., I. S. Zuhorn, and B. Poolman. 2015. A sensor for quantification of macromolecular crowding in living cells. Nat. Meth. 12:227-229.
26. Currie, M., H. Leopold, J. Schwarz, A. J. Boersma, E. D. Sheets, and A. A. Heikal. 2017. Fluorescence dynamics of a FRET probe designed for crowding studies. J. Phys. Chem. B 121:5688-5698.
27. Heikal, A. A., S. T. Hess, G. S. Baird, R. Y. Tsien, and W. W. Webb. 2000. Molecular spectroscopy and dynamics of intrinsically fluorescent proteins: Coral red (dsRed) and yellow (Citrine). Proc. Natl. Acad. Sci. U. S. A. 97:11996 - 12001.
28. Goedhart, J., D. Von Stetten, M. Noirclerc-Savoye, M. Lelimousin, L. Joosen, M. A. Hink, L. Van Weeren, T. W. Gadella Jr, and A. Royant. 2012. Structure-guided evolution of cyan fluorescent proteins towards a quantum yield of 93%. Nature communications 3:751.
29. Liu, Y., H.-R. Kim, and A. A. Heikal. 2006. Structural basis of fluorescence fluctuation dynamics of green fluorescent proteins in acidic environments. The Journal of Physical Chemistry B 110:24138-24146.
30. Müller, S. M., H. Galliardt, J. Schneider, B. G. Barisas, and T. Seidel. 2013. Quantification of Förster resonance energy transfer by monitoring sensitized emission in living plant cells. Front. Plant Sci. 4.
31. Jares-Erijman, E. A., and T. M. Jovin. 2003. FRET imaging. Nature Biotechnology 21:1387 - 1395.

32. Dickson, R. M., A. B. Cubitt, R. Y. Tsien, and W. E. Moerner. 1997. On/off blinking and switching behaviour of single molecules of green fluorescent protein. Nature 388:355-358.
33. Swaminathan, R., C. P. Hoang, and A. S. Verkman. 1997. Photobleaching recovery and anisotropy decay of green fluorescent protein GFP-S65T in solution and cells: cytoplasmic viscosity probed by green fluorescent protein translational and rotational diffusion. Biophysical Journal 72:1900-1907.
34. Oancea, E., M. N. Teruel, A. F. Quest, and T. Meyer. 1998. Green fluorescent protein (GFP)-tagged cysteine-rich domains from protein kinase C as fluorescent indicators for diacylglycerol signaling in living cells. The Journal of cell biology 140:485-498.
35. Shimizu, S., W. M. McLaren, and N. Matubayasi. 2006. The Hofmeister series and protein-salt interactions. The Journal of chemical physics 124:234905.
36. Zhang, Y., and P. S. Cremer. 2006. Interactions between macromolecules and ions: the Hofmeister series. Current opinion in chemical biology 10:658-663.
37. Cacace, M., E. Landau, and J. Ramsden. 1997. The Hofmeister series: salt and solvent effects on interfacial phenomena. Quarterly reviews of biophysics 30:241-277.
38. Peter, M., and S. M. Ameer‐Beg. 2004. Imaging molecular interactions by multiphoton FLIM. Biology of the Cell 96:231-236.
39. Yu, Q., M. Proia, and A. A. Heikal. 2008. Integrated biophotonics approach for noninvasive and multiscale studies of biomolecular and cellular biophysics. J. Biomed. Optics 13:041315. Evaluation Studies
40. Harms, G., M. Sonnleitner, G. Schütz, H. Gruber, and T. Schmidt. 1999. Single-molecule anisotropy imaging. Biophysical journal 77:2864-2870.
41. Heikal, A. A. 2014. Time-resolved fluorescence anisotropy and fluctuation correlation analysis of major histocompatibility complex class I proteins in fibroblast cells. Methods 66:283-291.
42. Grinvald, A., J. Schlessinger, I. Pecht, and I. Steinberg. 1975. Homogeneity and variability in the structure of azurin molecules studied by fluorescence decay and circular polarization. Biochemistry 14:1921-1929.
43. Pecht, I., E. Ortega, and T. M. Jovin. 1991. Rotational dynamics of the Fc. ε-receptor on mast cells monitored by specific monoclonal antibodies and IgE. Biochemistry 30:3450-3458.
44. Rahman, N., I. Pecht, D. Roess, and B. Barisas. 1992. Rotational dynamics of type I Fc ε-receptors on individually-selected rat mast cells studied by polarized fluorescence depletion. Biophysical journal 61:334-346.
45. Ameloot, M., M. vandeVen, A. U. Acuña, and B. Valeur. 2013. Fluorescence anisotropy measurements in solution: Methods and reference materials (IUPAC Technical Report). Pure & Applied Chemistry 85:589-608. Article.
46. Padilla‐Parra, S., and M. Tramier. 2012. FRET microscopy in the living cell: different approaches, strengths and weaknesses. Bioessays 34:369-376.
47. Kinosita Jr, K., A. Ikegami, and S. Kawato. 1982. On the wobbling-in-cone analysis of fluorescence anisotropy decay. Biophysical journal 37:461-464.

48. Cross, A. J., and G. R. Fleming. 1984. Analysis of time-resolved fluorescence anisotropy decays. Biophysical journal 46:45-56.
49. Balbo, J., P. Mereghetti, D.-P. Herten, and Rebecca C. Wade. 2013. The shape of protein crowders is a major determinant of protein diffusion. Biophysical Journal 104:1576-1584.
50. Girard, C., O. J. Martin, and A. Dereux. 1995. Molecular lifetime changes induced by nanometer scale optical fields. Physical review letters 75:3098.
51. Kapusta, P., R. Erdmann, U. Ortmann, and M. Wahl. 2003. Time-resolved fluorescence anisotropy measurements made simple. Journal of Fluorescence 13:179-183.
52. Ihaka, R., and R. Gentleman. 1996. R: a language for data analysis and graphics. Journal of computational and graphical statistics 5:299-314.
53. Miller, C. C. 1924. The Stokes-Einstein law for diffusion in solution. Proceedings of the Royal Society of London. Series A, Containing Papers of a Mathematical and Physical Character 106:724-749.
54. Kratky, O., H. Leopold, and H. Stabinger. 1973. The determination of the partial specific volume of proteins by the mechanical oscillator technique. Methods in enzymology. Elsevier, pp. 98-110.
55. Miller, H. C., and D. C. Darrow. 1940. Relation of muscle electrolyte to alterations in serum potassium and to the toxic effects of injected potassium chloride. American Journal of Physiology-Legacy Content 130:747-758.
56. Koushik, S. V., and S. S. Vogel. 2008. Energy migration alters the fluorescence lifetime of Cerulean: implications for fluorescence lifetime imaging Forster resonance energy transfer measurements. J Biomed Opt 13:031204-031204-031209.
57. Markwardt, M. L., G. J. Kremers, C. A. Kraft, K. Ray, P. J. C. Cranfill, K. A. Wilson, R. N. Day, R. M. Wachter, M. W. Davidson, and M. A. Rizzo. 2011. An improved Cerulean fluorescent protein with enhanced brightness and reduced Reversible photoswitching. PLoS One 6:1 - 10.
58. Heikal, A. A., S. T. Hess, and W. W. Webb. 2001. Multiphoton molecular spectroscopy and excited-state dynamics of enhanced green fluorescent protein (EGFP): Acid–base specificity. Chem. Phys. 274:37-55.
59. Schwarz, J., R. Leighton, H. J. Leopold, M. Currie, A. J. Boersma, E. D. Sheets, and A. A. Heikal. 2017. Kinetics model for the wavelength-dependence of excited-state dynamics of hetero-FRET sensors. Proceedings of SPIE 10380(103800S).
60. Ebeling, W., N. Hennrich, M. Klockow, H. Metz, H. D. Orth, and H. Lang. 1974. Proteinase K from Tritirachium album limber. European Journal of Biochemistry 47:91-97.
61. Zhang, Y., S. Furyk, D. E. Bergbreiter, and P. S. Cremer. 2005. Specific ion effects on the water solubility of macromolecules: PNIPAM and the Hofmeister series. Journal of the American Chemical Society 127:14505-14510.
62. Liu, B., S. N. Mavrova, J. van den Berg, S. K. Kristensen, L. Mantovanelli, L. M. Veenhoff, B. Poolman, and A. J. Boersma. 2018. Influence of fluorescent protein maturation on fret measurements in living cells. ACS sensors 3:1735-1742.

63. Heikal, A. A., S. T. Hess, and W. W. Webb. 2001. Multiphoton molecular spectroscopy and excited-state dynamics of enhanced green fluorescent protein (EGFP): Acid-base specificity. Chem. Phys. 274:37 - 55.
64. Sakamoto, Y., M. Ishiguro, and G. Kitagawa. 1986. Akaike information criterion statistics. Dordrecht, The Netherlands: D. Reidel 81.
65. Wagenmakers, E.-J., and S. Farrell. 2004. AIC model selection using Akaike weights. Psychonomic bulletin & review 11:192-196.
66. Jennrich, R. I., and P. Sampson. 1976. Newton-Raphson and related algorithms for maximum likelihood variance component estimation. Technometrics 18:11-17.
67. Volkmer, A., V. Subramaniam, D. J. Birch, and T. M. Jovin. 2000. One-and two-photon excited fluorescence lifetimes and anisotropy decays of green fluorescent proteins. Biophysical journal 78:1589-1598.
68. Grothendieck, G. 2013. Non-linear regression with brute force. R package nls2. contact: ggrothendieck@ gmail. com 20.
69. Beale, E. 1960. Confidence regions in non‐linear estimation. Journal of the Royal Statistical Society: Series B (Methodological) 22:41-76.
70. von Ende, C. N. 2001. Repeated-measures analysis. Design and analysis of ecological experiments 8:134-157.
71. Heffner, R. A., M. J. Butler, and C. K. Reilly. 1996. Pseudoreplication revisited. Ecology 77:2558-2562.

Appendices

Appendix 1: Fitting Parameters of both Time-Resolved Fluorescence and Anisotropy

Table S1.1: Nonlinear regression fitting parameters resulting from the analysis of duplicate TCSPC decays of protein-based hetero-FRET biosensors in the presence and absence of KCl (μ = 0–500 mM). One-photon laser pulses (425 nm) were generated to excite the donor fluorophore and. for detection of the acceptor a 531 filter with a FWHM of 40 was used. The resultant fluorescence lifetime decays were regressed with a biexponential model, Equation 2.13, from which the average lifetime of the donor in the presence of the acceptor (τ_{DA}) and rate of energy transfer (k_{ET}) were calculated as discussed in Chapter [2.4.1–2.4.3]. The chi-squared statistic used to evaluate the quality of the resultant fit under all experimental conditions. The error is shown in parenthesis following the fitting values and represents the standard error of the mean.

Cleaved/Intact	**Sensor**	**μ (mM)**	**α_{slow} (%)**	**τ_{DA} (ns)**	**α_{fast} (%)**	**τ_{fast} (ns)**	**χ^2**
Cleaved	**RD**	0	—	—	100	4.00 (2)	1.47
		100	—	—	100	4.01 (9)	1.40
		200	—	—	100	4.00 (5)	1.37
		300	—	—	100	4.00 (1)	1.51
		400	—	—	100	3.99 (1)	1.50
		500	—	—	100	3.99 (9)	1.49
Intact	**RD**	0	46.3 (3)	1.5 (2)	53.7 (4)	3.85 (9)	1.44
		100	43 (1)	1.8 (1)	57 (1)	4.04 (8)	1.47
		200	41 (4)	2.0 (3)	59 (4)	4.1 (2)	1.41
		300	40.3 (2)	2.12 (5)	59.7 (2)	4.14 (4)	1.38
		400	35.3 (5)	2.02 (5)	64.7 (5)	4.08 (4)	1.24
		500	32 (1)	1.93 (1)	68 (1)	4.03 (2)	1.21
Cleaved	**RE**	0	—	—	100	4.04 (2)	1.66
		100	—	—	100	4.03 (3)	1.35
		200	—	—	100	4.03 (4)	1.28
		300	—	—	100	4.03 (3)	1.49
		400	—	—	100	4.02 (2)	1.43
		500	—	—	100	4.02 (3)	1.32
		0	46 (2)	—	54 (2)	3.8 (3)	1.33

Intact	**RE**	100	44 (5)	—	56 (5)	3.95 (3)	1.30
		200	38.6 (5)	—	61.4 (5)	3.9 (2)	1.21
		300	39 (3)	1.66 (2)	61 (3)	3.98 (2)	1.42
		400	44 (2)	2.01 (5)	56 (2)	4.15 (3)	1.47
		500	36.8 (9)	1.8 (2)	63.2 (9)	4.01 (8)	1.24
Cleaved	**KE**	0	—	—	100	4.03 (2)	1.46
		100	—	—	100	4.03 (3)	1.45
		200	—	—	100	4.03 (4)	1.41
		300	—	—	100	4.02 (3)	1.50
		400	—	—	100	4.02 (3)	1.45
		500	—	—	100	4.00 (2)	1.39
Intact	**KE**	0	42.3 (7)	1.10 (8)	57.7 (7)	3.59 (8)	1.32
		100	45 (9)	1.7 (3)	55 (9)	4.0 (1)	1.56
		200	43 (3)	1.95 (1)	57 (3)	4.14 (2)	1.49
		300	39 (2)	1.96 (2)	61 (2)	4.11 (4)	1.41
		400	40 (4)	2.0 (4)	60 (4)	4.1 (2)	1.33
		500	38 (8)	2.07 (5)	62 (8)	4.15 (6)	1.42
Cleaved	**E6G2**	0	—	—	100	4.02 (2)	1.43
		100	—	—	100	4.01 (2)	1.6
		200	—	—	100	4.00 (1)	1.54
		300	—	—	100	4.00 (2)	1.68
		400	—	—	100	4.00 (1)	1.56
		500	—	—	100	3.98 (1)	1.66
Intact	**E6G2**	0	56 (7)	2.9 (2)	44 (7)	4.5 (1)	1.24
		100	43 (7)	2.7 (3)	57 (7)	4.3 (1)	1.33
		200	42 (9)	2.6 (5)	57 (7)	4.3 (2)	1.25
		300	44 (9)	2.6 (5)	56 (9)	4.3 (2)	1.23
		400	41 (9)	2.6 (4)	59 (9)	4.2 (2)	1.28
		500	45 (9)	2.6 (5)	55 (9)	4.3 (2)	1.24

Table S1.2: Nonlinear regression fitting parameters resulting from the global analysis of duplicate time-resolved polarized fluorescence anisotropy decays of protein-based hetero-FRET biosensors in the presence and absence of KCl (μ = 0–500 mM). One-photon laser pulses (425 nm) were generated to excite the donor fluorophore and. for detection of the acceptor a 531 filter with a FWHM of 40 was used. The resultant anisotropy decays were regressed with a biexponential model, Equation 2.11, from which the rotational constant (ϕ_{DA}) and rate of energy transfer (k_{ET}) were calculated as discussed in Chapter [2.5.1–2.5.3]. All nonlinear regression and minimization was performed in the statistical programming language R (52) and the chi-squared (χ^2) values represent a manually calculated reduced Pearson's chi-squared statistic. The chi-squared statistic, as well as the Akaike information criterion, was used to evaluate the quality of the resultant fit under all experimental conditions. The error is shown in parenthesis following the fitting values and represents the standard error of the mean as calculated from the eigenvalues of the minimization matrix generated by the nonlinear regression algorithm ("Newton-Raphson") (66).

Sensor	**μ (mM)**	**β_{slow}**	**ϕ_{DA} (ns)**	**β_{fast}**	**k_{ET} (ns^{-1})**	**χ^2**
RD	0	0.0956 (2)	29 (1)	0.106 (4)	0.96 (7)	1.75
	100	0.119 (2)	27.2 (9)	0.087 (3)	0.85 (5)	2.77
	200	0.137 (2)	27.1 (9)	0.078 (2)	0.69 (5)	3.16
	300	0.149 (2)	27 (1)	0.076 (3)	0.63 (5)	2.28
	400	0.159 (2)	25.2 (7)	0.071 (3)	0.65 (3)	3.36
	500	0.140 (4)	29 (2)	0.059 (4)	0.5 (1)	0.98
RE	0	0.094 (2)	26 (1)	0.097 (4)	0.89 (6)	1.84
	100	0.106 (2)	27 (1)	0.098 (3)	0.84 (5)	2.71
	200	0.122 (2)	25.1 (8)	0.091 (3)	0.80 (6)	2.43
	300	0.131 (2)	25.8 (8)	0.088 (2)	0.75 (5)	3

	400	0.137 (2)	27.6 (9)	0.082 (3)	0.62 (5)	3.55
	500	0.140 (2)	28.3 (8)	0.084 (2)	0.65 (4)	4.83
KE	0	0.089 (1)	19.7 (5)	0.121 (2)	1.31 (6)	4.42
	100	0.109 (1)	24.1 (7)	0.089 (3)	0.85 (5)	3.9
	200	0.129 (1)	24.8 (6)	0.083 (2)	0.79 (5)	4.14
	300	0.136 (2)	26.4 (8)	0.079 (2)	0.62 (4)	4.73
	400	0.148 (2)	24.3 (6)	0.072 (2)	0.69 (5)	4.69
	500	0.154 (2)	23.7 (6)	0.070 (2)	0.69 (5)	3.73
E6G2	0	0.195 (3)	20.9 (6)	0.059 (3)	0.40 (5)	3.18
	100	0.191 (2)	19.6 (4)	0.061 (2)	0.54 (5)	4.32
	200	0.184 (2)	21.3 (5)	0.064 (2)	0.44 (4)	4.47
	300	0.189 (2)	21.4 (5)	0.064 (2)	0.49 (4)	4.15
	400	0.186 (3)	22.6 (6)	0.066 (2)	0.43 (4)	4.21
	500	0.192 (2)	21.4 (5)	0.060 (2)	0.50 (5)	4.22

Appendix 2: Time-Resolved Anisotropy Analysis using R-Studio

Chapter 2.5.1 describes the theoretical and mathematical approach for the analysis of time-resolved polarized fluorescence anisotropy data. However, a well-established protocol and description of the mechanics of the analysis is not yet largely known. The lack of a universal methodology for the analysis of this type of data may lead to different results and interpretations from a number of trials, which diminishes the strength and purpose of the experimental approach. Therefore, we developed a globally accessible analysis platform that is capable of all forms of nonlinear regression analysis and robust statistical testing (52). This platform was generated in the statistical programming language, R, due to its statistical power. R and R-Studio are open source languages that are free to download (https://www.r-project.org) and operate to any users with open access to the internet.

Briefly, the individual parallel and perpendicular fluorescence decay signals were imported into the programming environment separately and overlaid to visualize a difference in the initial time step ($t = 0$). The difference in this initial time step arises from the minor difference in the distance travelled by both the parallel and perpendicularly polarized photons, where the data acquisition system is unable to correct for this simultaneously (Fig 5.1) (51). It is important to note that aligning the time steps using other statistical data softwares, such as OriginPro or Microsoft Excel, is time consuming, whereas the R-based analysis platform requires less than a second and is not susceptible to user bias or error.

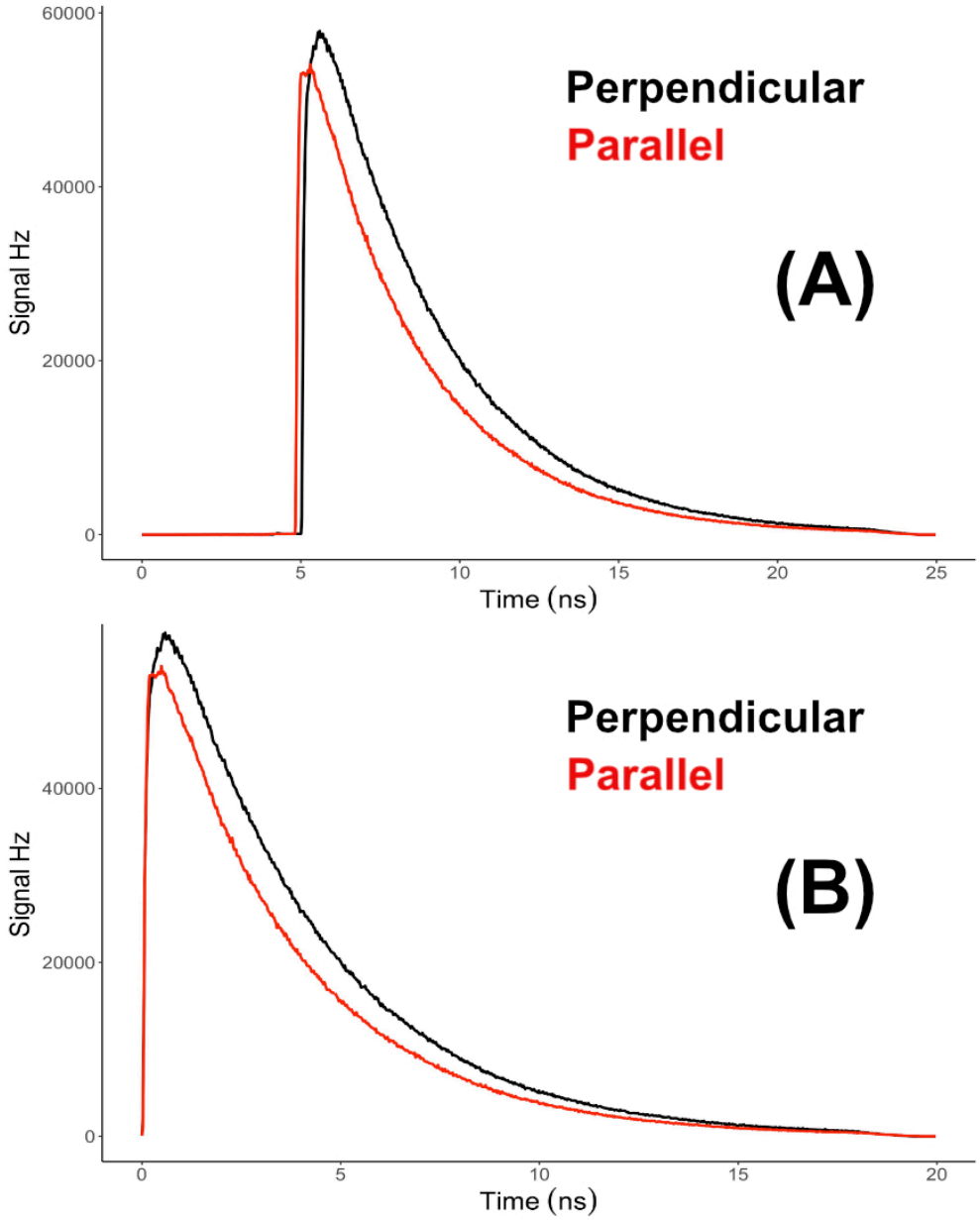

Figure S2.1: Illustration of the initial time step alignment of the parallel and perpendicularly polarized fluorescent emission signals of RD in 10 mM PBS, pH 7.4. The time step for both signals was selected by a two-point differential calculation with a threshold of 40 Hz. The time delay (A) arises from the difference in distance traveled by the parallel and perpendicularly polarized fluorescence emission and the alignment point is treated as time-zero (B).

Following the initial time step alignment the standard anisotropy signal shown in Equation 2.10 was used to calculate the anisotropy decay (Figure S2.1–2). The fluctuation in the signal prior to time-zero is due to the background (baseline) signal,

which at later time generates variance in the anisotropy signal due to low signal near the tail-end of the parallel and perpendicular polarization analysis. This process was done step-wise using basic minimum and maximum functions as shown below. Also, this process ensures the modeling of the maximum amount of the data, regardless of the quality of the data, by removing human bias and the ability to manually "trim" the data.

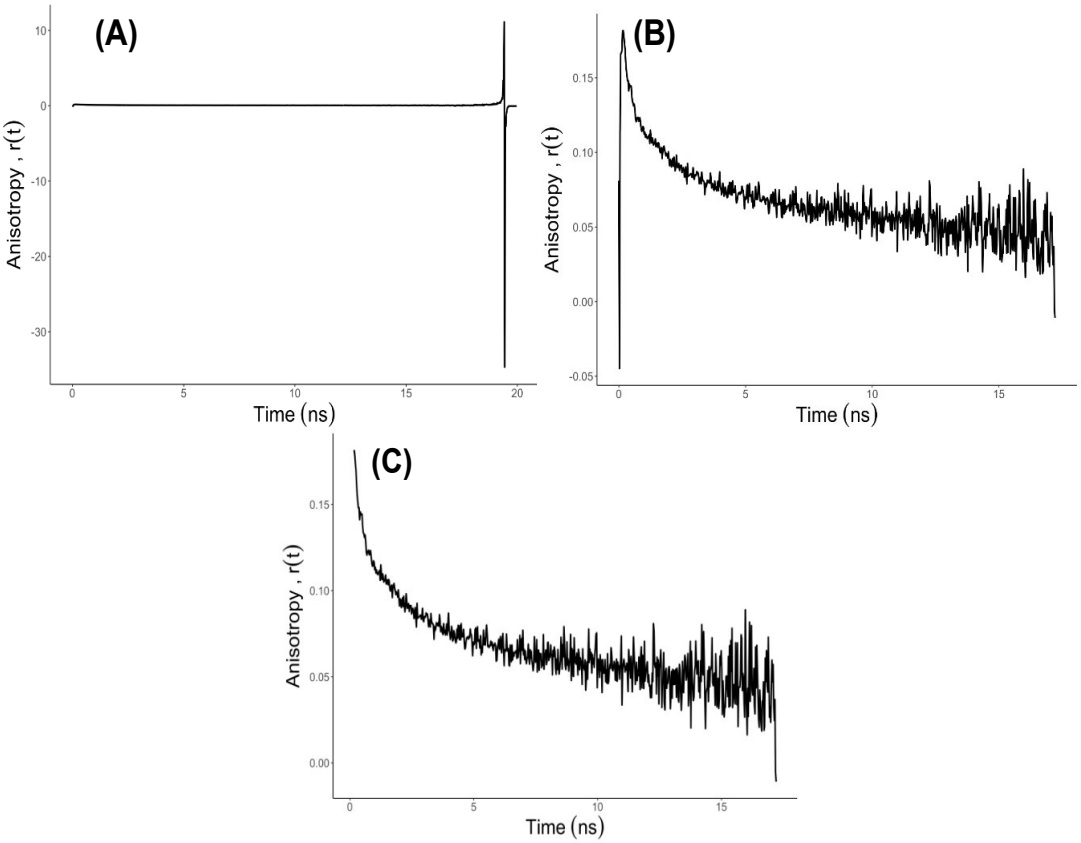

Figure S2.2: The step-wise "trimming" of the raw anisotropy signal obtained from the parallel and perpendicularly polarized fluorescence emission of the FRET biosensor RD as performed by the R-based analysis platform. (A) The raw "untrimmed" signal, (B) The partially "trimmed" signal, (C) The anisotropy signal used for modeling.

Upon "trimming" the data by removing the undesirable components not included in the nonlinear regression, a series of parameter estimates was made for both the biexponential and triexponential model shown in Equation 2.13. The rotational time constant (ϕ_{DA}) of the excited molecules was determined in a similar manner to the

fluorescence lifetime as describe in Chapter 3 of this Thesis. The raw anisotropy signal shown in Figure 5.2C was analyzed to determine the time step at which the anisotropy signal was equal to one half of the initial anisotropy, $r_o(t)$, and this time step was used as an approximation and initial seeding parameter for the rotational constant in the nonlinear regression (NLS) analysis. The rate of energy transfer (k_{ET}) of the biexponential model was then approximated by assuming, only for the parameter estimation, that the rate was minimally five times faster than the rotational rate due to both the size of the FRET pair and the known time constant of FRET (67). A similar procedure was used for the triexponential model, where the second two exponential terms were assumed to be due to two distinct FRET populations undergoing energy transfer at different rates. Therefore, for the initial parameter estimation the rates of energy transfer ($k_{ET,1,2}$) between the two FRET populations was approximated to be different by a minimum of 50%. The approximation of relatively large differences in the exponential decay constants lends itself to more successful nonlinear regression model minim. The quality of the model, based off of the automated parameter approximations, is represented visually below (Fig 5.3).

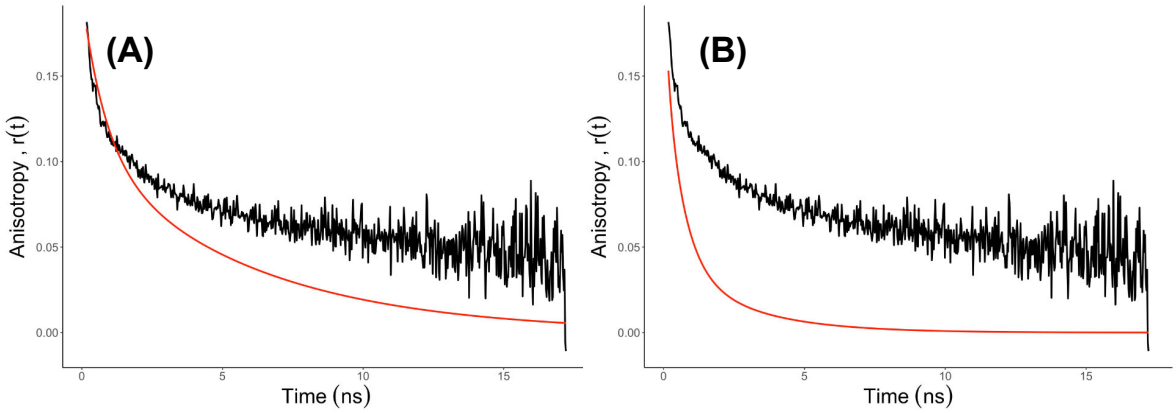

Figure S2.3: Representation of the resultant fit of the time-resolved polarized fluorescence anisotropy decay from the geometric parameter approximations for the bi and triexponential model (A and B, respectively) of the ionic strength FRET sensor RD (10 mM sodium phosphate, pH 7.4).

It is important to note that the apparent enhanced quality of the fit using a biexponential model as compared to a triexponential model is a function of the parameter estimation. As the difference in the rate of energy transfer efficiency between the two FRET populations, as well as the rotational constant, increases the quality of the triexponential approximations increases.

The results of the parameter approximation of the two exponential decay constants were used as initial parameters guesses in the nonlinear regression, which was performed identically for both the bi and triexponential models. Initially, a grid or n-dimensional hypercube was generated, where the number of dimensions is equal to the number of independent fitting parameters, spanning one order of magnitude symmetrically around each parameter estimate. The hypercube was passed into a nonlinear regression minimization algorithm, brute-force, which tests each pairwise combination of fitting parameters within the hypercube and reports the set of parameters that best minimizes the sum of squares of the residuals between the model and the anisotropy signal (68). The results of this minimization were reported, tabulated, and passed into a more robust minimization algorithm, the Newton-Raphson minimization algorithm, which was used to calculate the final fitting parameters and the representative quality of model plot shown below (Fig 5.4) (66).

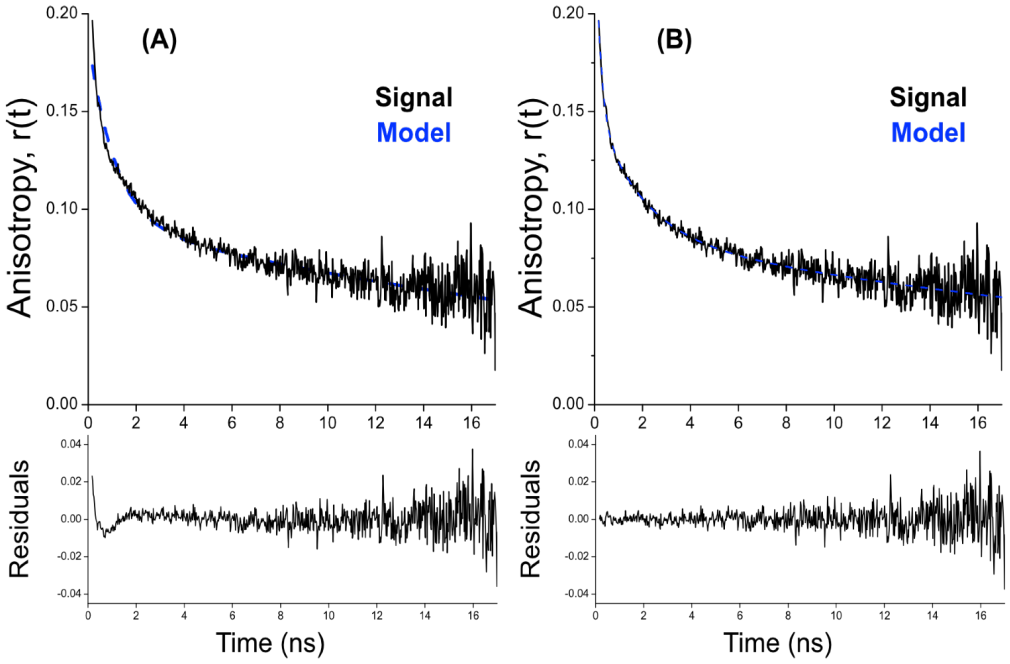

Figure S2.4: A representative final model (dashed line, blue) result of both the bi and triexponential model (A and B, respectively) with their corresponding residual plots of the time-resolved polarized fluorescence anisotropy decay (solid line, black) of RD (10 mM sodium phosphate buffer, pH 7.4).

Following the visualization of the final modeling results, both a global analysis and series of robust statistical tests are used to evaluate the most accurate fitting parameters, such as a series of rigorously fitting parameter evaluations and a statistical criterion to compare nested and non-nested nonlinear regression models (i.e., double and triple exponential decay) in a manner that penalizes for complexity while simultaneously rewarding for the goodness-of-fit (64).

In addition to the increased efficiency and reproducibility of the data analysis process already discussed the R-based analysis platform also offers extensive statistical tests, two of which that are applied to the anisotropy analysis are the Beale 95% confidence criterion and so-called confidence contour plots that may be used to visualize how well defined fitting parameters are in all pairwise combination of independent parameters (69). If the error of each fitting parameter is normally distributed and well defined with respect to the other fitting parameters each pairwise Beale criterion and confidence contour plot should resemble an ellipse. The confidence contour plots may be

interpreted as a 3-dimensional heat map and offer a more readily interpreted result of the quality of the model and individual fit parameters (69).

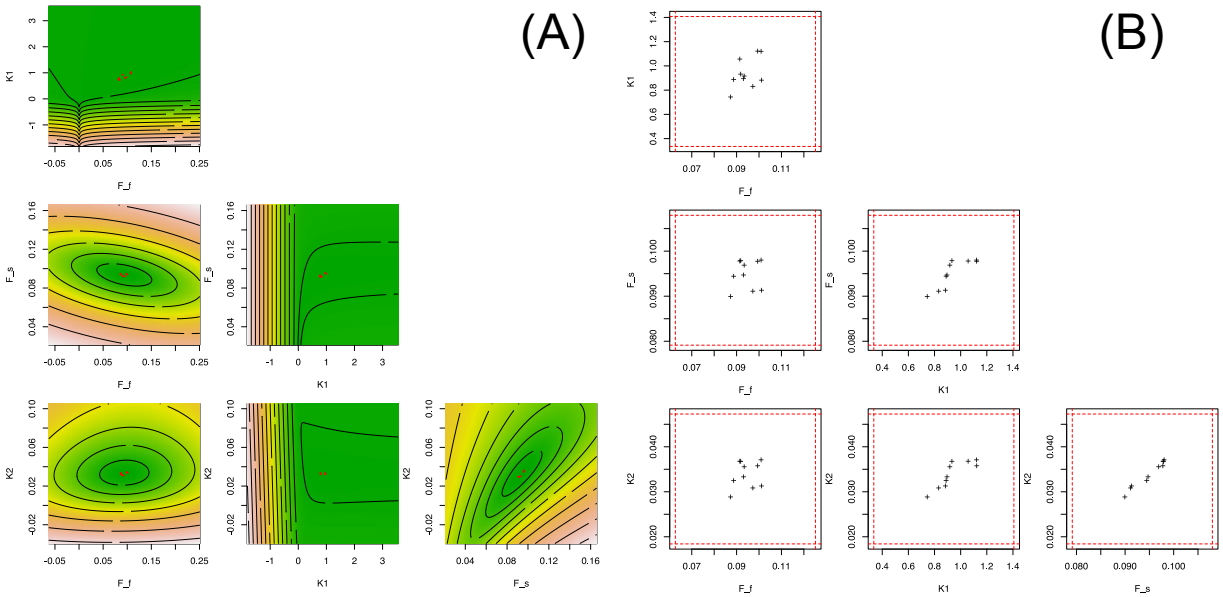

Figure S2.5: The statistical analysis of the resultant fit parameters from the Newton-Raphson minimization. F_s corresponds to the exponential fractional amplitude term describing only molecular rotation, K1 corresponds to the rate of molecular rotation which is equal to the inverse of the rotational constant (ϕ_{DA}), F_f corresponds to the exponential fractional amplitude term describing the population undergoing energy transfer from a donor to an acceptor molecule, and K2 is the corresponding sum of the rate of energy transfer and inverse rotational constant (ϕ_{DA}). (A) The confidence contour plot of all pairwise fit parameter combinations of the biexponential model (2.7) and (B) and the 95% Beale criterion confidence interval of all pairwise fit parameter combinations of the biexponential model (2.7). The color scale shown in the contour plots (A) represent a measure of the regression minimum and quality of fit of each pairwise set of fitting parameters, where green to red represents a minimum to maximum error, respectively.

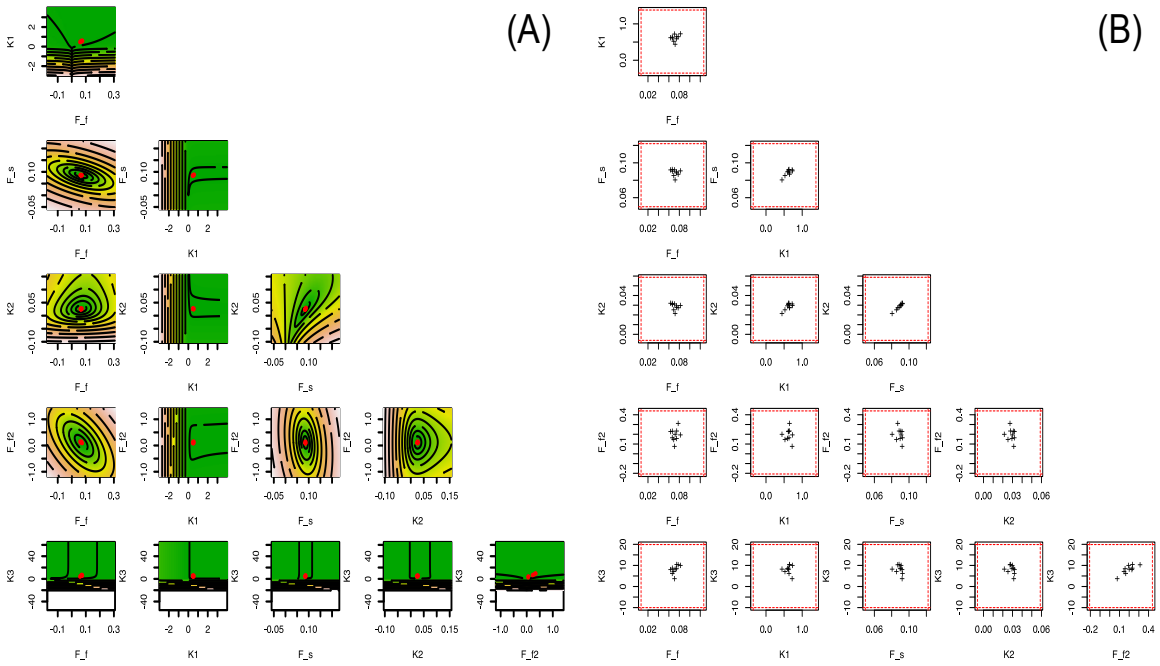

Figure S2.6: The statistical analysis of the resultant fit parameters from the Newton-Raphson minimization. F_s corresponds to the exponential fractional amplitude term describing only molecular rotation, K1 corresponds to the rate of molecular rotation which is equal to the inverse of the rotational constant (ϕ_{DA}), F_f and F_f2 correspond to the exponential fractional amplitude term describing the two populations undergoing energy transfer from a donor to an acceptor molecule, and K2 and K3 is the corresponding sum of the rate of energy transfer and inverse rotational constant (ϕ_{DA}). (A) The confidence contour plot of all pairwise fit parameter combinations of the triexponential model (2.13) and (B) and the 95% Beale criterion confidence interval of all pairwise fit parameter combinations of the triexponential model (2.13). The color scale shown in the contour plots (A) represent a measure of the regression minimum and quality of fit of each pairwise set of fitting parameters, where green to red represents a minimum to maximum error, respectively.

Preceding the evaluation of the quality of the nonlinear regression minimization as determined from the confidence contour and Beale criterion plots (69) in Figure 5.6, we performed a global analysis . As an example, the global analysis of two separate scans will be discussed here but this approach may be extended to any number of scans, although with each additional anisotropy decay added to the global analysis the computational time of analysis will increase slightly. Briefly, the global analysis of any number of replicate measurements was carried out in a similar manner to the nonlinear regression analysis described for individual scans. The power of the global analysis

resides primarily in the increased number of data points available to the minimization algorithm used to determine the fitting parameters and their relative certainty or standard error (70). The global analysis approach takes advantage of this by simultaneously minimizing the sum of the square of the residuals between the model and all anisotropy signals, where the number of scans in the global analysis must be equal to or greater than two, and due to the R-based analysis platform, it is not limited by an upper limit of the number of scans although this can generate "pseudoreplication" (71). Pseudoreplication can cause statistical significance in tests that would otherwise be insignificant and create a false sense of confidence in conclusions about any statistical tests because of the decrease apparent error in the measurement. When available, the results of the global analysis are preferential to any form of averaging approaches across individual replicates or modeling. Below is a representative plot illustrating the results of the global analysis of two scans (black and grey signal, respectively.), applying both the bi (A) and triexponential (B) models.

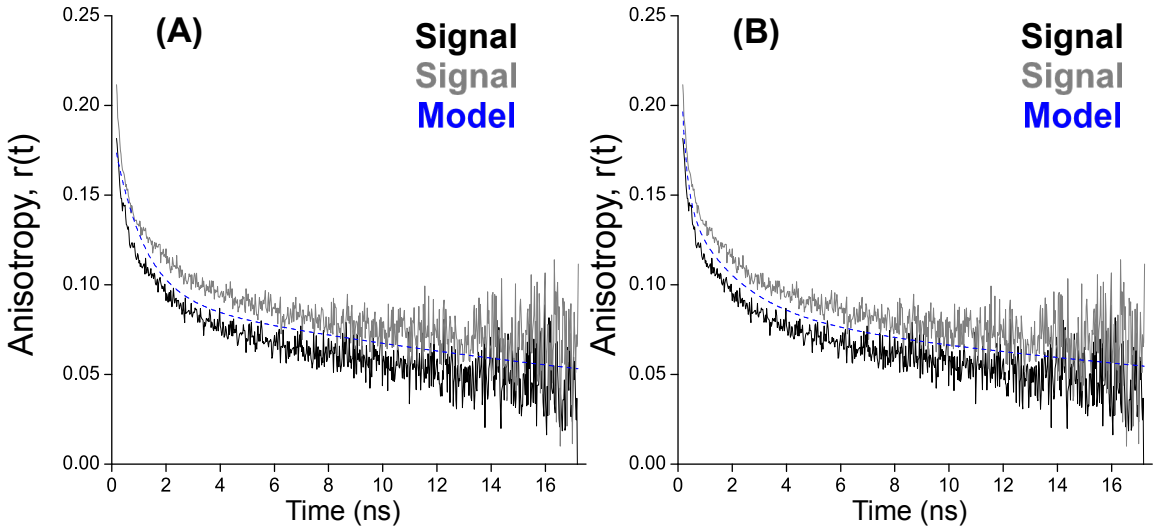

Figure S2.7: Representative global nonlinear regression analysis of two RD (10 mM PBS, pH 7.4) anisotropy signals and the subsequent model (Solid black/gray and blue dashed lines, respectively) for both the biexponential and triexponential model (A and B, respectively).

The magnitude of the information content described by each model, generally determined by the goodness-of-fit, was then evaluated using the Akaike and Bayesian

information criterion (AIC, BIC) scores (65) rather than the classical approached of the adjusted chi-squared (χ^2) analysis which is extremely insensitive to "over-fitting" or selecting overly complex models with a high number of fitting parameters (64). Although the statistical approach itself is complex, it is now a commonly used method for model selection and has the advantage of being able to compare "non-nested models" (i.e., comparing a complex polynomial and exponential model) whereas most goodness-of-fits require the models to be "nested". In addition, most model selection techniques such as Pearsons R-squared and the chi-squared (χ^2) goodness-of-fit analysis lack the ability to account for the issue of increase complexity. Simply stated, as the number of independent fitting parameters increase the apparent quality of the fit increases proportionally but the information obtained from the analysis simultaneously decreases proportionally. Therefore, the AIC and BIC were developed to address the need for a robust statistical test for selecting the "best" model that appropriately balances the complexity of the model with the goodness-of-fit (64). The AIC achieves this by estimating the information loss when the probability distribution associated with the "true" model, which experimentally cannot be obtained, is approximated with the model to be evaluated. This information loss is approximated using the Kullback-Leibler information quantity, which is equivalent to the negative of Boltzmann's generalized entropy. It has been shown in other works that selecting a proposed model that minimizes the Kullback-Leibler discrepancy is asymptotically equivalent to selecting a model that has the lowest AIC score (65). The AIC score is evaluated in the R-based analysis platform using the following function.

$$\mathrm{AIC}_i = -2\log L_i + 2V_i \tag{5.1}$$

Where L_i is the maximum likelihood for a proposed model, which is determined by adjusting the independent fitting parameters (V_i) to maximize the probability that the proposed model generated the observed data. Table 5.1 shows representative AIC and BIC scores for the FRET sensor RD in 10 mM sodium phosphate at pH 7.4, as determined from the global analysis.

Table S2.1: Results of the AIC and BIC evaluation of the global nonlinear regression for the bi and triexponential models of the model FRET sensor RD (10 mM PBS, pH 7.4) (2.7).

Model (Bi/Tri)	**AIC Score**	ω_{AIC}	**BIC Score**	ω_{BIC}
Biexponential	11.35	0.51	11.31	0.50
Triexponential	11.39	0.49	11.33	0.50

Appendix 3: Plasmid Maps and DNA Sequences of the Ionic Strength Biosensors RE, RD, KE, and E6G2

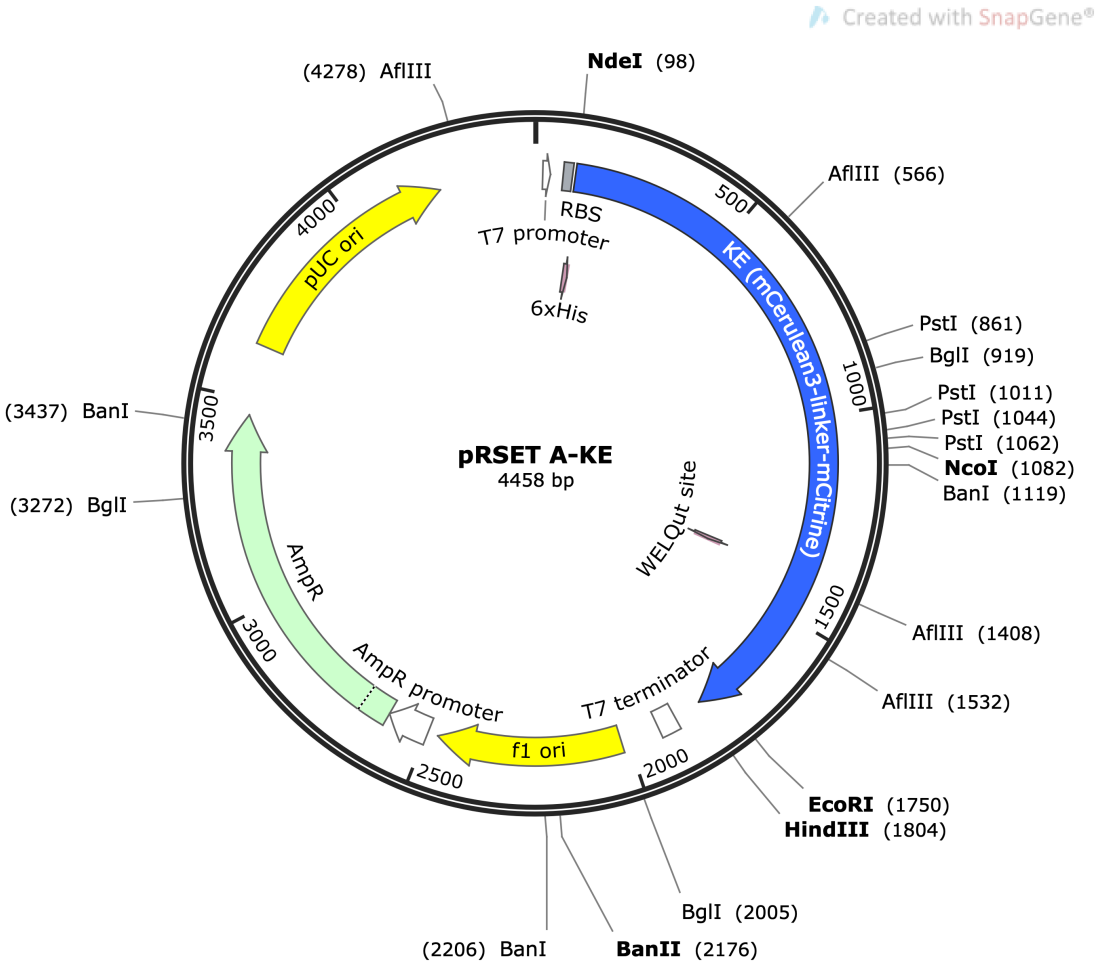

Figure S3.1: Ionic strength biosensor, KE, DNA plasmid map in pRSET A used for the bacterial expression and purification of the FRET pair. The plasmid consists of 4458 base pairs and contains ampicillin resistance for selective growth of desired bacterial colonies.

Table S3.1: Ionic strength biosensor, KE, DNA sequence in pRSET A used for the bacterial expression and purification of the FRET pair. The plasmid consists of 4458 base pairs and contains ampicillin resistance for selective growth of desired bacterial colonies.

GATCTCGATCCCGCGAAATTAATACGACTCACTATAGGGAGACCACAACGGT
TTCCCTCTAGAAATAATTTTGTTTAACTTTAAGAAGGAGATATACATATGCAT
CATCATCACCATCATGTGAGCAAAGGTGAAGAACTGTTTACCGGTGTTGTTCC
GATTCTGGTTGAACTGGATGGTGACGTTAATGGTCACAAATTTTCAGTTAGCG
GTGAAGGCGAAGGTGATGCAACCTATGGTAAACTGACCCTGAAATTTATCTG
TACCACCGGCAAACTGCCGGTTCCGTGGCCGACCCTGGTTACCACCCTGAGC
TGGGGTGTTCAGTGTTTTGCACGTTATCCGGATCACATGAAACAGCACGATTT
TTTCAAAAGCGCAATGCCGGAAGGTTATGTTCAAGAACGTACCATCTTCTTCA
AAGATGACGGCAACTATAAAACCCGTGCCGAAGTTAAATTTGAAGGTGATAC
CCTGGTGAATCGCATTGAACTGAAAGGCATCGATTTTAAAGAGGATGGTAAT
ATCCTGGGCCACAAACTGGAATATAATGCCATTCATGGCAACGTGTATATCA
CCGCAGATAAACAGAAAAACGGCATCAAAGCAAATTTTGGCCTGAACTGCAA
TATTGAAGATGGTTCAGTTCAGCTGGCAGATCATTATCAGCAGAATACCCCG
ATTGGTGATGGTCCGGTTCTGCTGCCGGATAATCATTATCTGAGCACCCAGAG
CAAACTGAGCAAAGATCCGAATGAAAAACGTGATCACATGGTGCTGCTGGAA
TTTGTTACCGCAGCAGGTATTACCCTGGGTATGGATGAACTGTATAAAGCAG
CAGCAGCCGCAAAAGCCGCTGCAGCAAAAGCGGCAGCTGCGAAAGCTGCCG
CAGCCAAAGCAGCGGCAGCTAAAGCCGCAGCGGCTAAAGCAGGTAGCGGTG
GTAGTGGTGGTTCAGGTGGCAGCGGTGGCTCTGGTGGCTCAGGCGCAGAGGC
AGCCGCTGCTGAAGCTGCAGCCGCAGAAGCGGCAGCAGCCGAGGCAGCTGC
AGCCGAAGCAGCCGCTGCAGAGGCAGCAGCAGCTGCATCCATGGTGTCAAA
AGGTGAGGAACTGTTTACAGGCGTGGTGCCGATCCTGGTAGAGCTGGACGGG
GATGTGAATGGCCATAAATTCAGCGTTTCAGGTGAAGGTGAGGGCGACGCCA
CGTACGGAAAACTGACACTGAAATTCATTTGCACAACAGGTAAACTGCCTGT
GCCTTGGCCTACACTGGTGACCACCTTTGGTTATGGTCTGATGTGCTTTGCTC
GCTATCCTGACCACATGAAACAACATGATTTCTTTAAATCTGCCATGCCTGAA
GGCTACGTGCAAGAGCGCACCATTTTTTTCAAAGACGATGGGAATTACAAAA
CACGTGCGGAGGTGAAATTCGAGGGCGATACACTGGTTAACCGTATCGAGCT
GAAAGGTATCGACTTCAAAGAGGACGGAAACATTCTGGGTCATAAACTGGAA
TACAACTACAACAGCCATAACGTGTACATCATGGCCGACAAACAAAAAAAC
GGGATTAAAGTGAACTTCAAAATCCGCCACAACATCGAAGATGGCAGCGTGC
AGCTGGCCGACCACTATCAACAAAACACACCGATCGGCGACGGTCCTGTACT
GCTGCCTGACAACCACTATCTGTCATATCAGAGCGCACTGTCAAAAGATCCT
AACGAGAAACGCGACCACATGGTTCTGCTGGAATTCGTGACAGCCGCTGGCA
TTACACTGGGCATGGACGAGCTGTACAAATAAAAGCTTGATCCGGCTGCTAA
CAAAGCCCGAAAGGAAGCTGAGTTGGCTGCTGCCACCGCTGAGCAATAACTA
GCATAACCCCTTGGGGCCTCTAAACGGGTCTTGAGGGGTTTTTTGCTGAAAGG
AGGAACTATATCCGGATCTGGCGTAATAGCGAAGAGGCCCGCACCGATCGCC
CTTCCCAACAGTTGCGCAGCCTGAATGGCGAATGGGACGCGCCCTGTAGCGG
CGCATTAAGCGCGGCGGGTGTGGTGGTTACGCGCAGCGTGACCGCTACACTT
GCCAGCGCCCTAGCGCCCGCTCCTTTCGCTTTCTTCCCTTCCTTTCTCGCCACG
TTCGCCGGCTTTCCCCGTCAAGCTCTAAATCGGGGGCTCCCTTTAGGGTTCCG

ATTTAGTGCTTTACGGCACCTCGACCCCAAAAAACTTGATTAGGGTGATGGTT
CACGTAGTGGGCCATCGCCCTGATAGACGGTTTTTCGCCCTTTGACGTTGGAG
TCCACGTTCTTTAATAGTGGACTCTTGTTCCAAACTGGAACAACACTCAACCC
TATCTCGGTCTATTCTTTTGATTTATAAGGGATTTTGCCGATTTCGGCCTATTG
GTTAAAAAATGAGCTGATTTAACAAAAATTTAACGCGAATTTTAACAAAATA
TTAACGCTTACAATTTAGGTGGCACTTTTCGGGGAAATGTGCGCGGAACCCCT
ATTTGTTTATTTTTCTAAATACATTCAAATATGTATCCGCTCATGAGACAATA
ACCCTGATAAATGCTTCAATAATATTGAAAAAGGAAGAGTATGAGTATTCAA
CATTTCCGTGTCGCCCTTATTCCCTTTTTTGCGGCATTTTGCCTTCCTGTTTTTG
CTCACCCAGAAACGCTGGTGAAAGTAAAAGATGCTGAAGATCAGTTGGGTGC
ACGAGTGGGTTACATCGAACTGGATCTCAACAGCGGTAAGATCCTTGAGAGT
TTTCGCCCCGAAGAACGTTTTCCAATGATGAGCACTTTTAAAGTTCTGCTATG
TGGCGCGGTATTATCCCGTATTGACGCCGGGCAAGAGCAACTCGGTCGCCGC
ATACACTATTCTCAGAATGACTTGGTTGAGTACTCACCAGTCACAGAAAAGC
ATCTTACGGATGGCATGACAGTAAGAGAATTATGCAGTGCTGCCATAACCAT
GAGTGATAACACTGCGGCCAACTTACTTCTGACAACGATCGGAGGACCGAAG
GAGCTAACCGCTTTTTTGCACAACATGGGGGATCATGTAACTCGCCTTGATCG
TTGGGAACCGGAGCTGAATGAAGCCATACCAAACGACGAGCGTGACACCAC
GATGCCTGTAGCAATGGCAACAACGTTGCGCAAACTATTAACTGGCGAACTA
CTTACTCTAGCTTCCCGGCAACAATTAATAGACTGGATGGAGGCGGATAAAG
TTGCAGGACCACTTCTGCGCTCGGCCCTTCCGGCTGGCTGGTTTATTGCTGAT
AAATCTGGAGCCGGTGAGCGTGGGTCTCGCGGTATCATTGCAGCACTGGGGC
CAGATGGTAAGCCCTCCCGTATCGTAGTTATCTACACGACGGGGAGTCAGGC
AACTATGGATGAACGAAATAGACAGATCGCTGAGATAGGTGCCTCACTGATT
AAGCATTGGTAACTGTCAGACCAAGTTTACTCATATATACTTTAGATTGATTT
AAAACTTCATTTTTAATTTAAAAGGATCTAGGTGAAGATCCTTTTTGATAATC
TCATGACCAAAATCCCTTAACGTGAGTTTTCGTTCCACTGAGCGTCAGACCCC
GTAGAAAAGATCAAAGGATCTTCTTGAGATCCTTTTTTTCTGCGCGTAATCTG
CTGCTTGCAAACAAAAAAACCACCGCTACCAGCGGTGGTTTGTTTGCCGGAT
CAAGAGCTACCAACTCTTTTTCCGAAGGTAACTGGCTTCAGCAGAGCGCAGA
TACCAAATACTGTTCTTCTAGTGTAGCCGTAGTTAGGCCACCACTTCAAGAAC
TCTGTAGCACCGCCTACATACCTCGCTCTGCTAATCCTGTTACCAGTGGCTGC
TGCCAGTGGCGATAAGTCGTGTCTTACCGGGTTGGACTCAAGACGATAGTTA
CCGGATAAGGCGCAGCGGTCGGGCTGAACGGGGGGTTCGTGCACACAGCCC
AGCTTGGAGCGAACGACCTACACCGAACTGAGATACCTACAGCGTGAGCTAT
GAGAAAGCGCCACGCTTCCCGAAGGGAGAAAGGCGGACAGGTATCCGGTAA
GCGGCAGGGTCGGAACAGGAGAGCGCACGAGGGAGCTTCCAGGGGGAAACG
CCTGGTATCTTTATAGTCCTGTCGGGTTTCGCCACCTCTGACTTGAGCGTCGA
TTTTTGTGATGCTCGTCAGGGGGGCGGAGCCTATGGAAAAACGCCAGCAACG
CGGCCTTTTTACGGTTCCTGGCCTTTTGCTGGCCTTTTGCTCACATGTTCTTTC
CTGCGTTATCCCCTGATTCTGTGGATAACCGTATTACCGCCTTTGAGTGAGCT
GATACCGCTCGCCGCAGCCGAACGACCGAGCGCAGCGAGTCAGTGAGCGAG
GAAGCGGAAGAGCGCCCAATACGCAAACCGCCTCTCCCCGCGCGTTGGCCGA
TTCATTAATGCAG

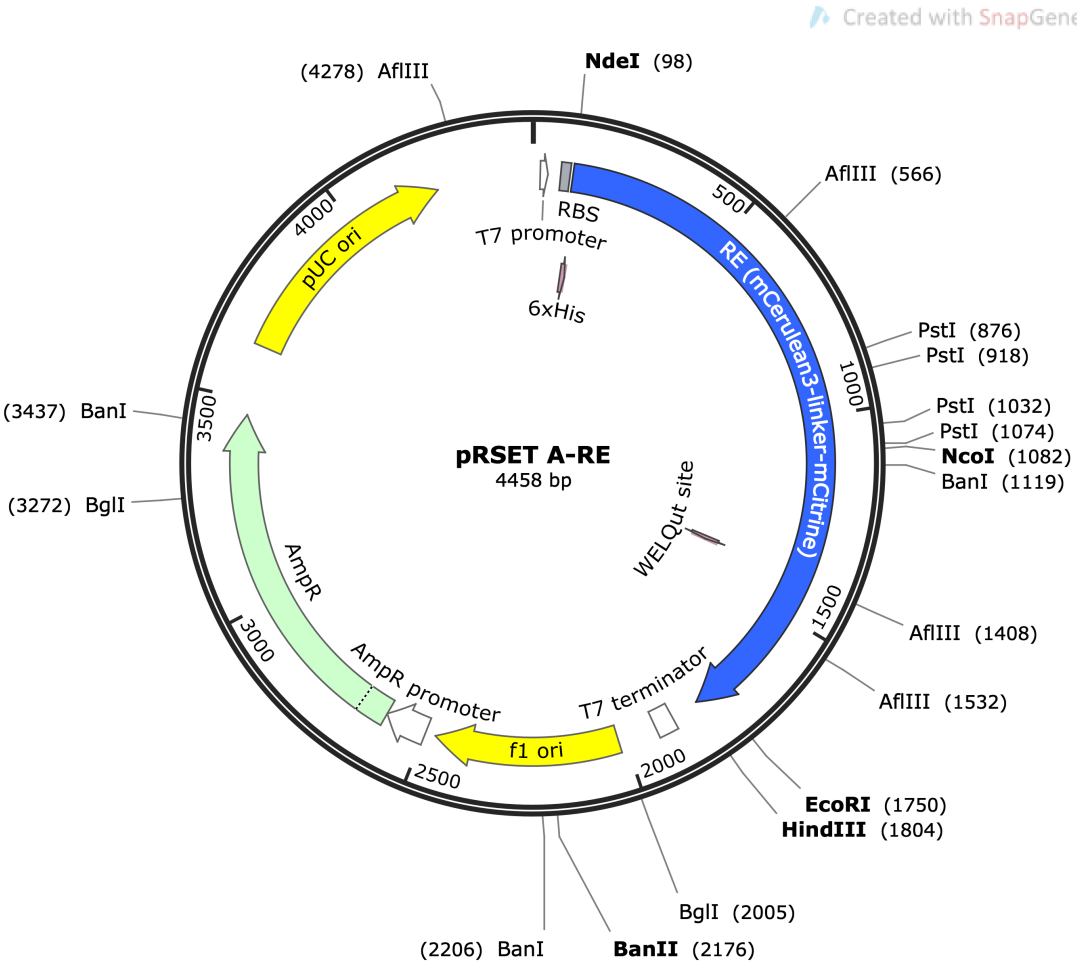

Figure S3.2: Ionic strength biosensor, RE, DNA plasmid map in pRSET A used for the bacterial expression and purification of the FRET pair. The plasmid consists of 4458 base pairs and contains ampicillin resistance for selective growth of desired bacterial colonies.

Table S3.2: Ionic strength biosensor, RE, DNA sequence in pRSET A used for the bacterial expression and purification of the FRET pair. The plasmid consists of 4458 base pairs and contains ampicillin resistance for selective growth of desired bacterial colonies.

GATCTCGATCCCGCGAAATTAATACGACTCACTATAGGGAGACCACAACGGT
TTCCCTCTAGAAATAATTTTGTTTAACTTTAAGAAGGAGATATACATATGCAT
CATCATCACCATCATGTGAGCAAAGGTGAAGAACTGTTTACCGGTGTTGTTCC
GATTCTGGTTGAACTGGATGGTGACGTTAATGGTCACAAATTTTCAGTTAGCG
GTGAAGGCGAAGGTGATGCAACCTATGGTAAACTGACCCTGAAATTTATCTG
TACCACCGGCAAACTGCCGGTTCCGTGGCCGACCCTGGTTACCACCCTGAGC
TGGGGTGTTCAGTGTTTTGCACGTTATCCGGATCACATGAAACAGCACGATTT
TTTCAAAAGCGCAATGCCGGAAGGTTATGTTCAAGAACGTACCATCTTCTTCA

AAGATGACGGCAACTATAAAACCCGTGCCGAAGTTAAATTTGAAGGTGATAC
CCTGGTGAATCGCATTGAACTGAAAGGCATCGATTTTAAAGAGGATGGTAAT
ATCCTGGGCCACAAACTGGAATATAATGCCATTCATGGCAACGTGTATATCA
CCGCAGATAAACAGAAAAACGGCATCAAAGCAAATTTTGGCCTGAACTGCAA
TATTGAAGATGGTTCAGTTCAGCTGGCAGATCATTATCAGCAGAATACCCCG
ATTGGTGATGGTCCGGTTCTGCTGCCGGATAATCATTATCTGAGCACCCAGAG
CAAACTGAGCAAAGATCCGAATGAAAAACGTGATCACATGGTGCTGCTGGAA
TTTGTTACCGCAGCAGGTATTACCCTGGGTATGGATGAACTGTATAAAGCAG
CAGCAGCCGCACGTGCAGCCGCAGCCCGTGCCGCTGCAGCTCGTGCGGCAGC
AGCACGCGCAGCTGCTGCTCGCGCTGCAGCAGCTCGTGCAGGTAGCGGTGGT
AGTGGTGGTTCAGGTGGCAGCGGTGGCTCTGGTGGCTCAGGCGCAGAAGCCG
CAGCAGCGGAAGCTGCCGCAGCTGAAGCGGCAGCTGCAGAAGCAGCAGCGG
CTGAGGCAGCGGCAGCTGAAGCAGCTGCAGCAGCCTCCATGGTGAGTAAAG
GCGAGGAACTGTTCACAGGCGTGGTGCCGATCCTGGTAGAGCTGGACGGGGA
TGTGAATGGCCATAAATTCAGCGTTTCAGGTGAAGGTGAGGGCGACGCCACG
TACGGAAAACTGACACTGAAATTCATTTGCACAACAGGTAAACTGCCTGTGC
CTTGGCCTACACTGGTGACCACCTTTGGTTATGGTCTGATGTGCTTTGCTCGCT
ATCCTGACCACATGAAACAACATGATTTCTTTAAATCTGCCATGCCTGAAGGC
TACGTGCAAGAGCGCACCATTTTTTTCAAAGACGATGGGAATTACAAAACAC
GTGCGGAGGTGAAATTCGAGGGCGATACACTGGTTAACCGTATCGAGCTGAA
AGGTATCGACTTCAAAGAGGACGGAAACATTCTGGGTCATAAACTGGAATAC
AACTACAACAGCCATAACGTGTACATCATGGCCGACAAACAAAAAAACGGG
ATTAAAGTGAACTTCAAAATCCGCCACAACATCGAAGATGGCAGTGTGCAGC
TGGCCGACCACTATCAACAAAACACACCGATCGGCGACGGTCCTGTACTGCT
GCCTGACAACCACTATCTGTCATATCAGAGCGCACTGTCAAAAGATCCTAAC
GAGAAACGCGACCACATGGTTCTGCTGGAATTCGTGACAGCCGCTGGCATTA
CACTGGGCATGGACGAGCTGTACAAATAAAAGCTTGATCCGGCTGCTAACAA
AGCCCGAAAGGAAGCTGAGTTGGCTGCTGCCACCGCTGAGCAATAACTAGCA
TAACCCCTTGGGGCCTCTAAACGGGTCTTGAGGGGTTTTTTGCTGAAAGGAG
GAACTATATCCGGATCTGGCGTAATAGCGAAGAGGCCCGCACCGATCGCCCT
TCCCAACAGTTGCGCAGCCTGAATGGCGAATGGGACGCGCCCTGTAGCGGCG
CATTAAGCGCGGCGGGTGTGGTGGTTACGCGCAGCGTGACCGCTACACTTGC
CAGCGCCCTAGCGCCCGCTCCTTTCGCTTTCTTCCCTTCCTTTCTCGCCACGTT
CGCCGGCTTTCCCCGTCAAGCTCTAAATCGGGGGCTCCCTTTAGGGTTCCGAT
TTAGTGCTTTACGGCACCTCGACCCCAAAAAACTTGATTAGGGTGATGGTTCA
CGTAGTGGGCCATCGCCCTGATAGACGGTTTTTCGCCCTTTGACGTTGGAGTC
CACGTTCTTTAATAGTGGACTCTTGTTCCAAACTGGAACAACACTCAACCCTA
TCTCGGTCTATTCTTTTGATTTATAAGGGATTTTGCCGATTTCGGCCTATTGGT
TAAAAAATGAGCTGATTTAACAAAAATTTAACGCGAATTTTAACAAAATATT
AACGCTTACAATTTAGGTGGCACTTTTCGGGGAAATGTGCGCGGAACCCCTA
TTTGTTTATTTTTCTAAATACATTCAAATATGTATCCGCTCATGAGACAATAA
CCCTGATAAATGCTTCAATAATATTGAAAAAGGAAGAGTATGAGTATTCAAC
ATTTCCGTGTCGCCCTTATTCCCTTTTTTGCGGCATTTTGCCTTCCTGTTTTTGC
TCACCCAGAAACGCTGGTGAAAGTAAAAGATGCTGAAGATCAGTTGGGTGCA
CGAGTGGGTTACATCGAACTGGATCTCAACAGCGGTAAGATCCTTGAGAGTT

TTCGCCCCGAAGAACGTTTTCCAATGATGAGCACTTTTAAAGTTCTGCTATGT
GGCGCGGTATTATCCCGTATTGACGCCGGGCAAGAGCAACTCGGTCGCCGCA
TACACTATTCTCAGAATGACTTGGTTGAGTACTCACCAGTCACAGAAAAGCA
TCTTACGGATGGCATGACAGTAAGAGAATTATGCAGTGCTGCCATAACCATG
AGTGATAACACTGCGGCCAACTTACTTCTGACAACGATCGGAGGACCGAAGG
AGCTAACCGCTTTTTTGCACAACATGGGGGATCATGTAACTCGCCTTGATCGT
TGGGAACCGGAGCTGAATGAAGCCATACCAAACGACGAGCGTGACACCACG
ATGCCTGTAGCAATGGCAACAACGTTGCGCAAACTATTAACTGGCGAACTAC
TTACTCTAGCTTCCCGGCAACAATTAATAGACTGGATGGAGGCGGATAAAGT
TGCAGGACCACTTCTGCGCTCGGCCCTTCCGGCTGGCTGGTTTATTGCTGATA
AATCTGGAGCCGGTGAGCGTGGGTCTCGCGGTATCATTGCAGCACTGGGGCC
AGATGGTAAGCCCTCCCGTATCGTAGTTATCTACACGACGGGGAGTCAGGCA
ACTATGGATGAACGAAATAGACAGATCGCTGAGATAGGTGCCTCACTGATTA
AGCATTGGTAACTGTCAGACCAAGTTTACTCATATATACTTTAGATTGATTTA
AAACTTCATTTTTAATTTAAAAGGATCTAGGTGAAGATCCTTTTTGATAATCT
CATGACCAAAATCCCTTAACGTGAGTTTTCGTTCCACTGAGCGTCAGACCCCG
TAGAAAAGATCAAAGGATCTTCTTGAGATCCTTTTTTTCTGCGCGTAATCTGC
TGCTTGCAAACAAAAAAACCACCGCTACCAGCGGTGGTTTGTTTGCCGGATC
AAGAGCTACCAACTCTTTTTCCGAAGGTAACTGGCTTCAGCAGAGCGCAGAT
ACCAAATACTGTTCTTCTAGTGTAGCCGTAGTTAGGCCACCACTTCAAGAACT
CTGTAGCACCGCCTACATACCTCGCTCTGCTAATCCTGTTACCAGTGGCTGCT
GCCAGTGGCGATAAGTCGTGTCTTACCGGGTTGGACTCAAGACGATAGTTAC
CGGATAAGGCGCAGCGGTCGGGCTGAACGGGGGGTTCGTGCACACAGCCCA
GCTTGGAGCGAACGACCTACACCGAACTGAGATACCTACAGCGTGAGCTATG
AGAAAGCGCCACGCTTCCCGAAGGGAGAAAGGCGGACAGGTATCCGGTAAG
CGGCAGGGTCGGAACAGGAGAGCGCACGAGGGAGCTTCCAGGGGGAAACGC
CTGGTATCTTTATAGTCCTGTCGGGTTTCGCCACCTCTGACTTGAGCGTCGATT
TTTGTGATGCTCGTCAGGGGGGCGGAGCCTATGGAAAAACGCCAGCAACGCG
GCCTTTTTACGGTTCCTGGCCTTTTGCTGGCCTTTTGCTCACATGTTCTTTCCT
GCGTTATCCCCTGATTCTGTGGATAACCGTATTACCGCCTTTGAGTGAGCTGA
TACCGCTCGCCGCAGCCGAACGACCGAGCGCAGCGAGTCAGTGAGCGAGGA
AGCGGAAGAGCGCCCAATACGCAAACCGCCTCTCCCCGCGCGTTGGCCGATT
CATTAATGCAG

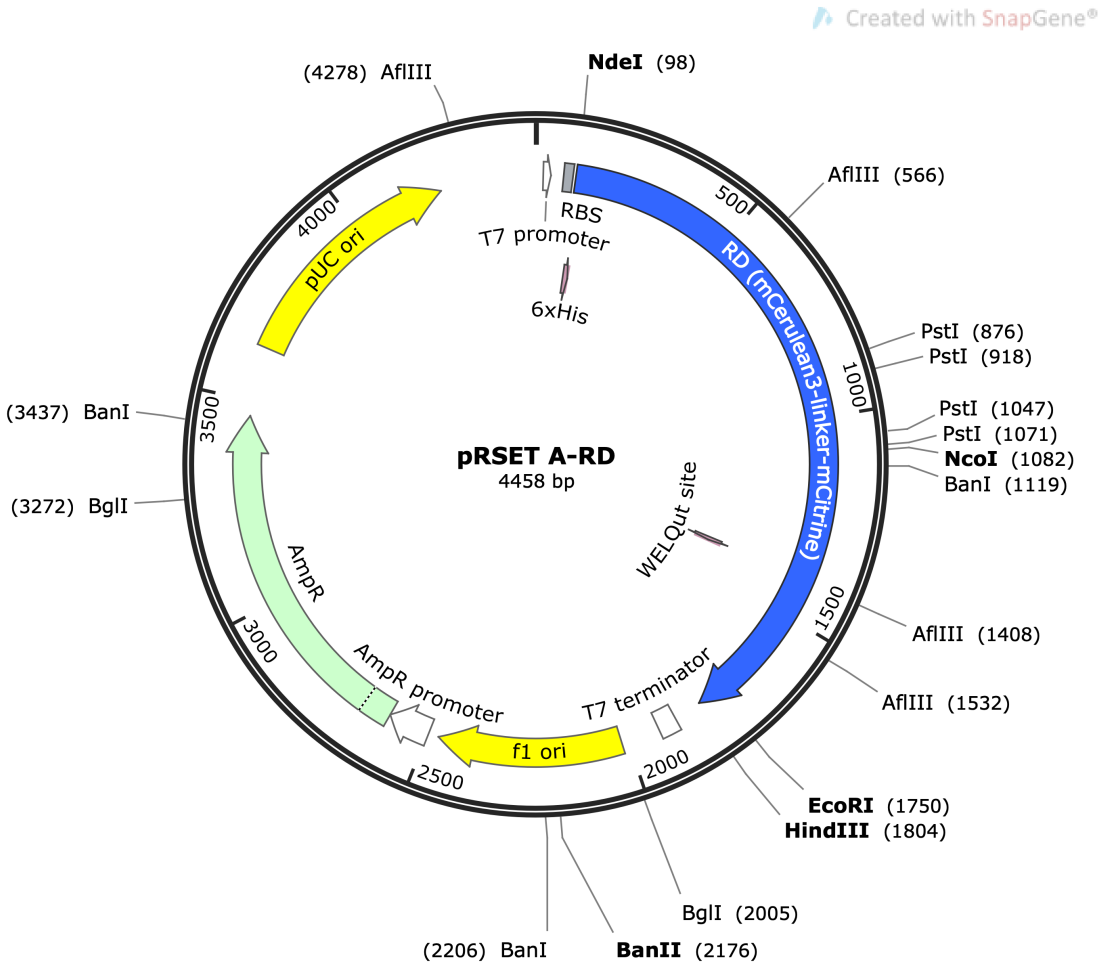

Figure S3.3: Ionic strength biosensor, RD, DNA plasmid map in pRSET A used for the bacterial expression and purification of the FRET pair. The plasmid consists of 4458 base pairs and contains ampicillin resistance for selective growth of desired bacterial colonies.

Table S3.3: Ionic strength biosensor, RD, DNA sequence in pRSET A used for the bacterial expression and purification of the FRET pair. The plasmid consists of 4458 base pairs and contains ampicillin resistance for selective growth of desired bacterial colonies.

GATCTCGATCCCGCGAAATTAATACGACTCACTATAGGGAGACCACAACGGT

TTCCCTCTAGAAATAATTTTGTTTAACTTTAAGAAGGAGATATACATATGCAT
CATCATCACCATCATGTGAGCAAAGGTGAAGAACTGTTTACCGGTGTTGTTCC
GATTCTGGTTGAACTGGATGGTGACGTTAATGGTCACAAATTTTCAGTTAGCG
GTGAAGGCGAAGGTGATGCAACCTATGGTAAACTGACCCTGAAATTTATCTG
TACCACCGGCAAACTGCCGGTTCCGTGGCCGACCCTGGTTACCACCCTGAGC
TGGGGTGTTCAGTGTTTTGCACGTTATCCGGATCACATGAAACAGCACGATTT
TTTCAAAAGCGCAATGCCGGAAGGTTATGTTCAAGAACGTACCATCTTCTTCA
AAGATGACGGCAACTATAAAACCCGTGCCGAAGTTAAATTTGAAGGTGATAC
CCTGGTGAATCGCATTGAACTGAAAGGCATCGATTTTAAAGAGGATGGTAAT
ATCCTGGGCCACAAACTGGAATATAATGCCATTCATGGCAACGTGTATATCA
CCGCAGATAAACAGAAAAACGGCATCAAAGCAAATTTTGGCCTGAACTGCAA
TATTGAAGATGGTTCAGTTCAGCTGGCAGATCATTATCAGCAGAATACCCCG
ATTGGTGATGGTCCGGTTCTGCTGCCGGATAATCATTATCTGAGCACCCAGAG
CAAACTGAGCAAAGATCCGAATGAAAAACGTGATCACATGGTGCTGCTGGAA
TTTGTTACCGCAGCAGGTATTACCCTGGGTATGGATGAACTGTATAAAGCAG
CAGCAGCCGCACGTGCAGCCGCAGCCCGTGCCGCTGCAGCTCGTGCGGCAGC
AGCACGCGCAGCTGCTGCTCGCGCTGCAGCAGCTCGTGCAGGTAGCGGTGGT
AGTGGTGGTTCAGGTGGCAGCGGTGGCTCTGGTGGCTCAGGCGCAGATGCAG
CAGCGGCTGATGCCGCTGCCGCTGACGCAGCTGCCGCAGATGCCGCAGCTGC
AGATGCAGCCGCAGCGGATGCTGCAGCCGCAGCTTCCATGGTGTCAAAAGGC
GAGGAACTGTTCACAGGCGTGGTGCCGATCCTGGTAGAGCTGGACGGGGATG
TGAATGGCCATAAATTCAGCGTTTCAGGTGAAGGTGAGGGCGACGCCACGTA
CGGAAAACTGACACTGAAATTCATTTGCACAACAGGTAAACTGCCTGTGCCT
TGGCCTACACTGGTGACCACCTTTGGTTATGGTCTGATGTGCTTTGCTCGCTA
TCCTGACCACATGAAACAACATGATTTCTTTAAATCTGCCATGCCTGAAGGCT
ACGTGCAAGAGCGCACCATTTTTTTCAAAGACGATGGGAATTACAAAACACG
TGCGGAGGTGAAATTCGAGGGCGATACACTGGTTAACCGTATCGAGCTGAAA
GGTATCGACTTCAAAGAGGACGGAAACATTCTGGGTCATAAACTGGAATACA
ACTACAACAGCCATAACGTGTACATCATGGCCGACAAACAAAAAAACGGGA
TTAAAGTGAACTTCAAAATCCGCCACAACATCGAAGATGGCAGCGTGCAGCT
GGCCGACCACTATCAACAAAACACACCGATCGGCGACGGTCCTGTACTGCTG
CCTGACAACCACTATCTGTCATATCAGAGCGCACTGTCAAAAGATCCTAACG
AGAAACGCGACCACATGGTTCTGCTGGAATTCGTGACAGCCGCTGGCATTAC
ACTGGGCATGGACGAGCTGTACAAATAAAAGCTTGATCCGGCTGCTAACAAA
GCCCGAAAGGAAGCTGAGTTGGCTGCTGCCACCGCTGAGCAATAACTAGCAT
AACCCCTTGGGGCCTCTAAACGGGTCTTGAGGGGTTTTTTGCTGAAAGGAGG
AACTATATCCGGATCTGGCGTAATAGCGAAGAGGCCCGCACCGATCGCCCTT
CCCAACAGTTGCGCAGCCTGAATGGCGAATGGGACGCGCCCTGTAGCGGCGC
ATTAAGCGCGGCGGGTGTGGTGGTTACGCGCAGCGTGACCGCTACACTTGCC
AGCGCCCTAGCGCCCGCTCCTTTCGCTTTCTTCCCTTCCTTTCTCGCCACGTTC
GCCGGCTTTCCCCGTCAAGCTCTAAATCGGGGGCTCCCTTTAGGGTTCCGATT
TAGTGCTTTACGGCACCTCGACCCCAAAAAACTTGATTAGGGTGATGGTTCAC
GTAGTGGGCCATCGCCCTGATAGACGGTTTTTCGCCCTTTGACGTTGGAGTCC
ACGTTCTTTAATAGTGGACTCTTGTTCCAAACTGGAACAACACTCAACCCTAT
CTCGGTCTATTCTTTTGATTTATAAGGGATTTTGCCGATTTCGGCCTATTGGTT

AAAAAATGAGCTGATTTAACAAAAATTTAACGCGAATTTTAACAAAATATTA
ACGCTTACAATTTAGGTGGCACTTTTCGGGGAAATGTGCGCGGAACCCCTATT
TGTTTATTTTTCTAAATACATTCAAATATGTATCCGCTCATGAGACAATAACC
CTGATAAATGCTTCAATAATATTGAAAAAGGAAGAGTATGAGTATTCAACAT
TTCCGTGTCGCCCTTATTCCCTTTTTTGCGGCATTTTGCCTTCCTGTTTTTGCTC
ACCCAGAAACGCTGGTGAAAGTAAAAGATGCTGAAGATCAGTTGGGTGCAC
GAGTGGGTTACATCGAACTGGATCTCAACAGCGGTAAGATCCTTGAGAGTTT
TCGCCCCGAAGAACGTTTTCCAATGATGAGCACTTTTAAAGTTCTGCTATGTG
GCGCGGTATTATCCCGTATTGACGCCGGGCAAGAGCAACTCGGTCGCCGCAT
ACACTATTCTCAGAATGACTTGGTTGAGTACTCACCAGTCACAGAAAAGCAT
CTTACGGATGGCATGACAGTAAGAGAATTATGCAGTGCTGCCATAACCATGA
GTGATAACACTGCGGCCAACTTACTTCTGACAACGATCGGAGGACCGAAGGA
GCTAACCGCTTTTTTGCACAACATGGGGGATCATGTAACTCGCCTTGATCGTT
GGGAACCGGAGCTGAATGAAGCCATACCAAACGACGAGCGTGACACCACGA
TGCCTGTAGCAATGGCAACAACGTTGCGCAAACTATTAACTGGCGAACTACT
TACTCTAGCTTCCCGGCAACAATTAATAGACTGGATGGAGGCGGATAAAGTT
GCAGGACCACTTCTGCGCTCGGCCCTTCCGGCTGGCTGGTTTATTGCTGATAA
ATCTGGAGCCGGTGAGCGTGGGTCTCGCGGTATCATTGCAGCACTGGGGCCA
GATGGTAAGCCCTCCCGTATCGTAGTTATCTACACGACGGGGAGTCAGGCAA
CTATGGATGAACGAAATAGACAGATCGCTGAGATAGGTGCCTCACTGATTAA
GCATTGGTAACTGTCAGACCAAGTTTACTCATATATACTTTAGATTGATTTAA
AACTTCATTTTTAATTTAAAAGGATCTAGGTGAAGATCCTTTTTGATAATCTC
ATGACCAAAATCCCTTAACGTGAGTTTTCGTTCCACTGAGCGTCAGACCCCGT
AGAAAAGATCAAAGGATCTTCTTGAGATCCTTTTTTTCTGCGCGTAATCTGCT
GCTTGCAAACAAAAAAACCACCGCTACCAGCGGTGGTTTGTTTGCCGGATCA
AGAGCTACCAACTCTTTTTCCGAAGGTAACTGGCTTCAGCAGAGCGCAGATA
CCAAATACTGTTCTTCTAGTGTAGCCGTAGTTAGGCCACCACTTCAAGAACTC
TGTAGCACCGCCTACATACCTCGCTCTGCTAATCCTGTTACCAGTGGCTGCTG
CCAGTGGCGATAAGTCGTGTCTTACCGGGTTGGACTCAAGACGATAGTTACC
GGATAAGGCGCAGCGGTCGGGCTGAACGGGGGGTTCGTGCACACAGCCCAG
CTTGGAGCGAACGACCTACACCGAACTGAGATACCTACAGCGTGAGCTATGA
GAAAGCGCCACGCTTCCCGAAGGGAGAAAGGCGGACAGGTATCCGGTAAGC
GGCAGGGTCGGAACAGGAGAGCGCACGAGGGAGCTTCCAGGGGGAAACGCC
TGGTATCTTTATAGTCCTGTCGGGTTTCGCCACCTCTGACTTGAGCGTCGATTT
TTGTGATGCTCGTCAGGGGGGCGGAGCCTATGGAAAAACGCCAGCAACGCGG
CCTTTTTACGGTTCCTGGCCTTTTGCTGGCCTTTTGCTCACATGTTCTTTCCTGC
GTTATCCCCTGATTCTGTGGATAACCGTATTACCGCCTTTGAGTGAGCTGATA
CCGCTCGCCGCAGCCGAACGACCGAGCGCAGCGAGTCAGTGAGCGAGGAAG
CGGAAGAGCGCCCAATACGCAAACCGCCTCTCCCCGCGCGTTGGCCGATTCA
TTAATGCAG

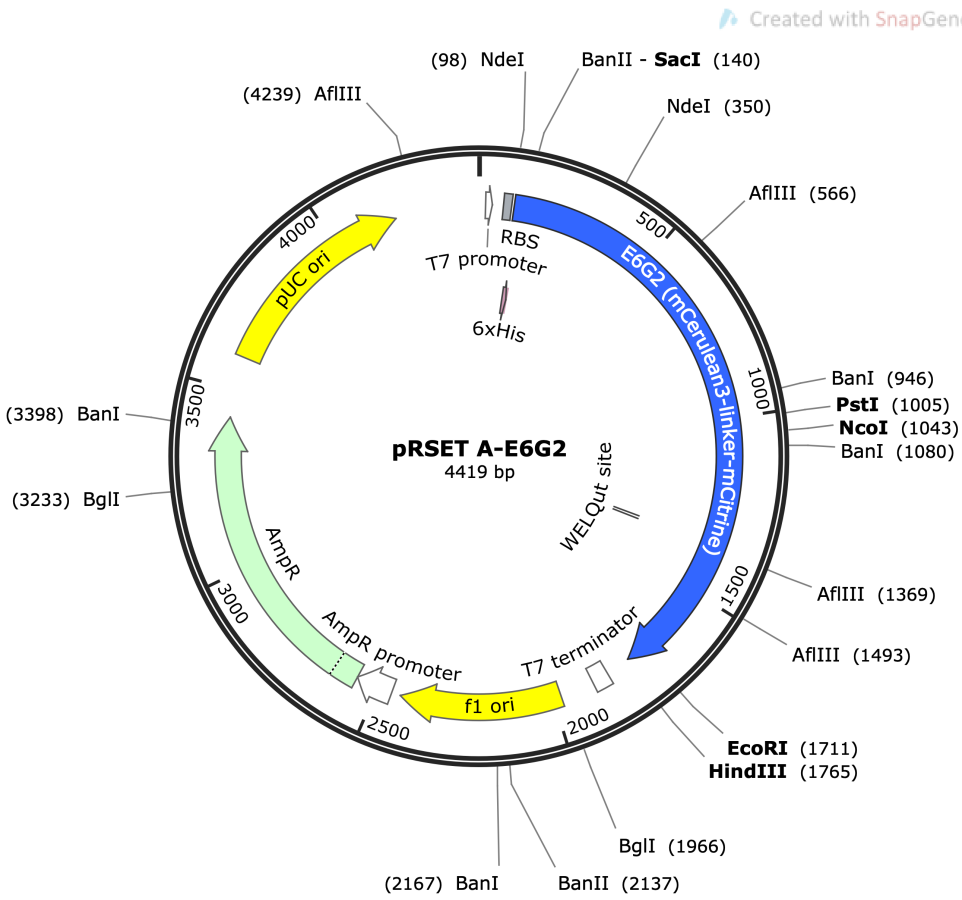

Figure S3.4: Ionic strength biosensor, E6G2, DNA plasmid map in pRSET A used for the bacterial expression and purification of the FRET pair. The plasmid consists of 4458 base pairs and contains ampicillin resistance for selective growth of desired bacterial colonies.

Table S3.4: Ionic strength biosensor, E6G2, DNA sequence in pRSET A used for the bacterial expression and purification of the FRET pair. The plasmid consists of 4458 base pairs and contains ampicillin resistance for selective growth of desired bacterial colonies.

GATCTCGATCCCGCGAAATTAATACGACTCACTATAGGGAGACCACAACGGT
TTCCCTCTAGAAATAATTTTGTTTAACTTTAAGAAGGAGATATACATATGCAT
CATCATCACCATCATGTGAGCAAAGGTGAAGAGCTCTTTACCGGTGTTGTTCC
GATTCTGGTTGAACTGGATGGTGACGTTAATGGTCACAAATTTTCAGTTAGCG
GTGAAGGCGAAGGTGATGCAACCTATGGTAAACTGACCCTGAAATTTATCTG
TACCACCGGCAAACTGCCGGTTCCGTGGCCGACCCTGGTTACCACCCTGAGC
TGGGGTGTTCAGTGTTTTGCACGTTATCCGGATCATATGAAACAGCACGATTT
TTTCAAAAGCGCAATGCCGGAAGGTTATGTTCAAGAACGTACCATCTTCTTCA
AAGATGACGGCAACTATAAAACCCGTGCCGAAGTTAAATTTGAAGGTGATAC
CCTGGTGAATCGCATTGAACTGAAAGGCATCGATTTTAAAGAGGATGGTAAT
ATCCTGGGCCACAAACTGGAATATAATGCCATTCATGGCAACGTGTATATCA
CCGCAGATAAACAGAAAAACGGCATCAAAGCAAATTTTGGCCTGAACTGCAA
TATTGAAGATGGTTCAGTTCAGCTGGCAGATCATTATCAGCAGAATACCCCG

ATTGGTGATGGTCCGGTTCTGCTGCCGGATAATCATTATCTGAGCACCCAGAG
CAAACTGAGCAAAGATCCGAATGAAAAACGTGATCACATGGTTCTGCTCGAG
TTTGTTACCGCAGCAGGTATTACCCTGGGTATGGATGAACTGTATAAAGCAG
AAGCAGCAGCAAAAGAAGCCGCTGCCAAAGAAGCGGCAGCGAAAGAGGCTG
CCGCAAAAGAGGCAGCAGCGAAAGAAGCAGCGGCTAAAGCAGGTAGCGGTG
GTAGTGGTGCCGAGGCAGCCGCTAAAGAAGCTGCGGCAAAAGAAGCAGCGG
CAAAAGAGGCTGCAGCTAAAGAAGCCGCAGCAAAAGAGGCAGCAGCAAAA
GCCATGGTGAGTAAAGGTGAGGAACTGTTTACAGGCGTGGTGCCGATCCTGG
TAGAGCTGGACGGGGATGTGAATGGCCATAAATTCAGCGTTTCAGGTGAAGG
TGAGGGCGACGCCACATACGGAAAACTGACACTGAAATTCATTTGCACAACA
GGTAAACTGCCTGTGCCTTGGCCTACACTGGTGACCACCTTTGGTTATGGTCT
GATGTGCTTTGCTCGCTATCCTGACCACATGAAACAACATGATTTCTTTAAAT
CTGCCATGCCTGAAGGCTACGTGCAAGAGCGCACCATTTTTTTCAAAGACGA
TGGGAATTACAAAACACGTGCGGAGGTGAAATTCGAGGGCGATACACTGGTT
AACCGTATCGAGCTGAAAGGTATCGACTTCAAAGAGGACGGAAACATTCTGG
GTCATAAACTGGAATACAACTACAACAGCCATAACGTGTACATCATGGCCGA
CAAACAAAAAAACGGGATTAAAGTGAACTTCAAAATCCGCCACAACATCGA
AGATGGCAGCGTGCAGCTGGCCGACCACTATCAACAAAACACACCGATCGGC
GACGGTCCTGTACTGCTGCCTGACAACCACTATCTGTCATATCAGAGCGCACT
GTCAAAAGATCCTAACGAGAAACGCGACCACATGGTGCTGCTGGAATTCGTG
ACAGCCGCTGGCATTACACTGGGCATGGACGAGCTGTACAAATAAAAGCTTG
ATCCGGCTGCTAACAAAGCCCGAAAGGAAGCTGAGTTGGCTGCTGCCACCGC
TGAGCAATAACTAGCATAACCCCTTGGGGCCTCTAAACGGGTCTTGAGGGGT
TTTTTGCTGAAAGGAGGAACTATATCCGGATCTGGCGTAATAGCGAAGAGGC
CCGCACCGATCGCCCTTCCCAACAGTTGCGCAGCCTGAATGGCGAATGGGAC
GCGCCCTGTAGCGGCGCATTAAGCGCGGCGGGTGTGGTGGTTACGCGCAGCG
TGACCGCTACACTTGCCAGCGCCCTAGCGCCCGCTCCTTTCGCTTTCTTCCCTT
CCTTTCTCGCCACGTTCGCCGGCTTTCCCCGTCAAGCTCTAAATCGGGGGCTC
CCTTTAGGGTTCCGATTTAGTGCTTTACGGCACCTCGACCCCAAAAAACTTGA
TTAGGGTGATGGTTCACGTAGTGGGCCATCGCCCTGATAGACGGTTTTTCGCC
CTTTGACGTTGGAGTCCACGTTCTTTAATAGTGGACTCTTGTTCCAAACTGGA
ACAACACTCAACCCTATCTCGGTCTATTCTTTTGATTTATAAGGGATTTTGCC
GATTTCGGCCTATTGGTTAAAAAATGAGCTGATTTAACAAAAATTTAACGCG
AATTTTAACAAAATATTAACGCTTACAATTTAGGTGGCACTTTTCGGGGAAAT
GTGCGCGGAACCCCTATTTGTTTATTTTTCTAAATACATTCAAATATGTATCC
GCTCATGAGACAATAACCCTGATAAATGCTTCAATAATATTGAAAAAGGAAG
AGTATGAGTATTCAACATTTCCGTGTCGCCCTTATTCCCTTTTTTGCGGCATTT
TGCCTTCCTGTTTTTGCTCACCCAGAAACGCTGGTGAAAGTAAAAGATGCTGA
AGATCAGTTGGGTGCACGAGTGGGTTACATCGAACTGGATCTCAACAGCGGT
AAGATCCTTGAGAGTTTTCGCCCCGAAGAACGTTTTCCAATGATGAGCACTTT
TAAAGTTCTGCTATGTGGCGCGGTATTATCCCGTATTGACGCCGGGCAAGAG
CAACTCGGTCGCCGCATACACTATTCTCAGAATGACTTGGTTGAGTACTCACC
AGTCACAGAAAAGCATCTTACGGATGGCATGACAGTAAGAGAATTATGCAGT
GCTGCCATAACCATGAGTGATAACACTGCGGCCAACTTACTTCTGACAACGA
TCGGAGGACCGAAGGAGCTAACCGCTTTTTTGCACAACATGGGGGATCATGT

AACTCGCCTTGATCGTTGGGAACCGGAGCTGAATGAAGCCATACCAAACGAC
GAGCGTGACACCACGATGCCTGTAGCAATGGCAACAACGTTGCGCAAACTAT
TAACTGGCGAACTACTTACTCTAGCTTCCCGGCAACAATTAATAGACTGGATG
GAGGCGGATAAAGTTGCAGGACCACTTCTGCGCTCGGCCCTTCCGGCTGGCT
GGTTTATTGCTGATAAATCTGGAGCCGGTGAGCGTGGGTCTCGCGGTATCATT
GCAGCACTGGGGCCAGATGGTAAGCCCTCCCGTATCGTAGTTATCTACACGA
CGGGGAGTCAGGCAACTATGGATGAACGAAATAGACAGATCGCTGAGATAG
GTGCCTCACTGATTAAGCATTGGTAACTGTCAGACCAAGTTTACTCATATATA
CTTTAGATTGATTTAAAACTTCATTTTTAATTTAAAAGGATCTAGGTGAAGAT
CCTTTTTGATAATCTCATGACCAAAATCCCTTAACGTGAGTTTTCGTTCCACTG
AGCGTCAGACCCCGTAGAAAAGATCAAAGGATCTTCTTGAGATCCTTTTTTTC
TGCGCGTAATCTGCTGCTTGCAAACAAAAAAACCACCGCTACCAGCGGTGGT
TTGTTTGCCGGATCAAGAGCTACCAACTCTTTTTCCGAAGGTAACTGGCTTCA
GCAGAGCGCAGATACCAAATACTGTTCTTCTAGTGTAGCCGTAGTTAGGCCA
CCACTTCAAGAACTCTGTAGCACCGCCTACATACCTCGCTCTGCTAATCCTGT
TACCAGTGGCTGCTGCCAGTGGCGATAAGTCGTGTCTTACCGGGTTGGACTCA
AGACGATAGTTACCGGATAAGGCGCAGCGGTCGGGCTGAACGGGGGGTTCGT
GCACACAGCCCAGCTTGGAGCGAACGACCTACACCGAACTGAGATACCTACA
GCGTGAGCTATGAGAAAGCGCCACGCTTCCCGAAGGGAGAAAGGCGGACAG
GTATCCGGTAAGCGGCAGGGTCGGAACAGGAGAGCGCACGAGGGAGCTTCC
AGGGGGAAACGCCTGGTATCTTTATAGTCCTGTCGGGTTTCGCCACCTCTGAC
TTGAGCGTCGATTTTTGTGATGCTCGTCAGGGGGGCGGAGCCTATGGAAAAA
CGCCAGCAACGCGGCCTTTTTACGGTTCCTGGCCTTTTGCTGGCCTTTTGCTCA
CATGTTCTTTCCTGCGTTATCCCCTGATTCTGTGGATAACCGTATTACCGCCTT
TGAGTGAGCTGATACCGCTCGCCGCAGCCGAACGACCGAGCGCAGCGAGTCA
GTGAGCGAGGAAGCGGAAGAGCGCCCAATACGCAAACCGCCTCTCCCCGCG
CGTTGGCCGATTCATTAATGCAG